Experimental and Theoretical Investigation of Signaling in Quorum Sensing of Pseudomonas Aeruginosa

Claussen, Anetta; Givskov, Michael Christian; Sams, Thomas

Publication date:
2013

Document Version
Publisher's PDF, also known as Version of record

Experimental and Theoretical Investigation of Signaling in Quorum Sensing of *Pseudomonas Aeruginosa*

Anetta Claussen

Technical University of Denmark

A thesis submitted for the degree of Doctor of Philosophy

Supervisors: Thomas Sams
Michael Givskov

Kongens Lyngby 2012
DTU Elektro-Ph.D.

Technical University of Denmark
Department of Electrical Engineering
Ørsteds Plads, Building 349
DK-2800 Kongens Lyngby, Denmark

ISBN 978-87-92465-60-3

Preface

This thesis was prepared at Department of Electrical Engineering, the Technical University of Denmark in partial fulfillment of the requirements for acquiring the Ph.D. degree in engineering. Part of the project was carried out at the Department of International Health, Immunology, and Microbiology, University of Copenhagen, to which I hereby extend my gratitude. I also acknowledge Radiometer for financial support.

The focus of this study is on the Quorum Sensing regulatory system of *Pseudomonas aeruginosa* called the Las system. In this thesis, two distinct methods to obtain information about the system are considered. First, Surface Enhanced Raman Spectroscopy (SERS) is applied to the signal molecule known as *N*-dodecanoyl-L-homoserine lactone. Secondly, a conventional fluorescent monitor system is used to follow the response to signal molecules. Both methods are evaluated and in the latter case a kinetic model is applied in order to extract knowledge about the interaction between signal molecule and regulator.

A short introduction to the system and the motivation behind the study is given in the first chapter. The results of my research are presented in chapter 2 and 3, the SERS experiments in the former and the experiments with the monitor system in the latter. The kinetic model is presented as part of the third chapter concomitant to the monitor system. Conclusions are drawn at the end of each chapter. In the Appendix, the two research papers as first-author are attached, one accepted for publication and the other not yet submitted, Appendix A and B. Furthermore, a third co-author paper to which I have made a contribution is attached but will not be discussed as part of the phD work, Appendix C. However, the experimental protocol for this contribution can be seen in Appendix G

Kongens Lyngby, November 2012

Anetta Claussen

Abstract

Quorum sensing (QS) is an intercellular communication system by which some bacterial cells are capable of indirectly monitoring their own population density through exchange of signal molecules. The expression of virulence factors is kept low until the population density (signal molecule concentration) reaches a threshold value, after which the host system is surprised by a stealth attack. The focus of this study is on the Quorum Sensing regulatory system of *Pseudomonas aeruginosa* called the Las system.

In this thesis, two distinct methods to obtain information about the system are considered. First, Surface Enhanced Raman Spectroscopy (SERS) is applied to the signal molecule known as *N*-dodecanoyl-L-homoserine lactone. To the best of our knowledge we here for the first time demonstrate SERS to detect a QS signal molecule below 1 nM concentration in both ultrapure water and under physiological conditions. Based on our results, SERS shows promise as a highly suitable tool for *in situ* measurements of low Acyl-Homoserine Lactone (AHL) concentrations in biofilms containing QS bacteria. Secondly, a conventional fluorescent monitor system is used to follow the response to signal molecules. A kinetic model is applied in order to extract knowledge about the interaction between signal molecule and regulator. In the model, the regulator monomer is decaying rapidly due to proteases while all dimerized regulators are protected against proteases. Moreover, the LasR regulator can fold into its stable dimer conformation in the absence of its cognate signal. In the presence of signal the dimer is activated through cooperative binding of the two signal molecules.

Dansk resumé

Quorum sensing (QS) er et intercellulært kommunikationssystem, hvorved nogle bakterieceller er i stand til indirekte at overvåge celletætheden gennem udveksling af signalmolekyler. Udtryk af virulensfaktorer holdes lavt, indtil celletætheden (signalmolekyle koncentrationen) når tærskelværdien, hvorefter værtssystemet udsættes for et overraskelsesangreb.
Det er af stor betydning at forstå de mekanismer, der anvendes til at kontrollere udtryk af sygdomsfremkaldende gener, således at der kan udtænkes strategier til at kontrollere og/eller behandle bakterielle infektioner.
I dette arbejde har vi undersøgt QS systemet Las, som forefindes i *Pseudomonas aeruginosa*. Studiet tager to forskellige metoder til at indhente oplysninger om systemet i betragtning.
Først er Surface Enhanced Raman spektroskopi (SERS) anvendt på signalmolekylet kendt som *N*-dodecanoyl-L-homoserinelacton. Det er lykkes os at detektere signalmolekyle koncentrationer under 1 nM i både ultrarent vand og under fysiologiske betingelser. Baseret på vores resultater, viser SERS sig særdeles lovende som et redskab til *in situ* målinger af lave Acyl-homoserinlacton koncentrationer i biofilm, der indeholder QS bakterier.
Den konventionelle måde at undersøge Las systemet er igennem monitor stammer. Monitor stammen er i vores tilfælde en E. coli stamme med et plasmid, der koder for Las systemet. Vi undersøger systemet ved at tilsætte forskellige koncentrationer af signalmolekyle for dernæst at se det tilhørende respons som fluoresens, hvilket måles med et fluorometer.
En matematisk model anvendes med henblik på at uddrage viden om samspillet mellem signalmolekyle og LasR. I modellen henfalder LasR monomeren hurtigt, mens de dimeriserede LasR proteiner er beskyttet og henfalder langsomt. LasR proteinet kan endvidere folde til en stabil dimer konformation i fravær af dets beslægtede signal. I nærvær af signalmolekylet aktiveres dimeren gennem kooperativ binding af de to signalmolekyler.

Papers Included in the Thesis

[A] Anetta Claussen, Salim Abdali, Rolf W. Berg Michael Givskov, and Thomas Sams. Detection of the QS autoinducer C12-HSL below 1 nM using SERS. Quantum Nanobiology and Biophysical Chemisty special issue of *Current Physical Chemistry*,volume 2, issue 4, 2012.

[B] Anetta Claussen, Tim Holm Jakobsen, Thomas Bjarnsholt, Michael Givskov, Martin Welch, Jesper Ferkinghoff-Borg and Thomas Sams. Kinetic Model for Signal Binding to the Quorum Sensing Regulator LasR. To be submitted.

As part of my phD work I have made a contribution to a third paper, this however is not included in thesis, but can be seen in Appendix C.

Acknowledgements

I would like to express my gratitude to all the people who has helped me during my Ph.D. studies.
First of all, I would like to thank Thomas Sams for believing in me and giving me the opportunity to do this Ph.D. Thank you for always being there to give me good advice and helpful discussions. I would also like to thank him for all the trust he has put in me in letting me influence the study to such an extent. It has been a true pleasure to work under his supervision.
Furthermore, I would like to Michael Givskov who has welcomed me into his group at Panum as one of the group. I would like to thank him for the many discussions at Wednesdays meetings and for being such a positive and festive person.
I would also like to thank Rolf W. Berg who was kind enough to lend me his Raman instrument and to teach me a lot about Raman. And also Salim Abdali for lending me his superb colloids and for teaching me how to use them for SERS.
Furthermore, I would like to thank the Panum group for welcoming me into their group. You're such a great and festive group. It has been a delight to spend every day with you all. Especially a thanks to Anne for teaching a physicist like me the ways in the laboratory. Thanks to Thomas Bjarnsholt for his good ideas and advice. And thanks to Helle, for all the talks and funny times.
I would also like to thank the Friday- cake group, although I have not been there a lot I have greatly appreciated the occasional cake and talk once and a while.
I would especially like to thank my husband, mother, farther-in-law, Sonja and all the rest of my family for believing in me and being a great help while writing the thesis together. Thank you Jimi for all the time you have spend on house chores and watching out for Mathias making sure that he had everything so I

did not have to worry. Thank you mum for all the food you cooked for us so we did not have to prepare food the last month. And thank you Jan and Sonja for taking Mathias off our hands, especially the last weekend. Last but not least I would like to thank Mathias, who came into the world during my studies and have greatly improved my world.

List of Abbreviations

QS	Quorum sensing
P. aeruginosa	Pseudomonas aeruginosa
AHL	Acyl homoserine lactone
OdDHL	*N*-3-oxododecanoyl-L-homoserine lactone
BHL	*N*-butanoyl-L-homoserine lactone
bioassay	biological assay
GFP	green fluorescent protein
SERS	Surface Enhanced Raman Spectroscopy
C12-HSL	*N*-dodecanoyl-L-homoserine lactone
3-oxo-C12-HSL	*N*-3-oxo-dodecanoyl-L-homoserine lactone
SEM	Scanning Electron Microscope
UV-VIS	Ultraviolet-visible
FWHM	full width half max
HLPC	High-performance liquid chromatography
MQ-water	Milli-Q water
TBS	Tris-buffered saline
DMSO	dimethyl sulfoxide
ABtGcasa	supplemented minimal medium, see Paper A
OD	optical density
E. coli	Escherichia coli
RNA	Ribonucleic acid
LB medium	Luria Bertani medium

Contents

Chapter 1

Introduction

1.1 Quorum Sensing

Quorum sensing (QS) is a cell-cell signaling system which exist in many species of bacteria, gram negative as well as gram positive. The bacteria produce signaling molecules and once the concentration of these reach a certain threshold (at high cell densities), expression of a large suite of genes begins, in some cases followed by regulation of virulence factors. It would be of great importance to understand the mechanisms used to control the expression of virulence genes, e.g. the process of signaling, thus strategies could be devised for the control or treatment of bacterial infections.

Quorum sensing has been well studied in the gram negative bacteria *Pseudomonas aeruginosa* (*P. aeruginosa*). It lives in soil and freshwater environments but it is also an opportunistic pathogen, infecting immunocompromised individuals such as people with cystic fibrosis [50]. Quorum sensing in P. aeruginosa controls adhesion, biofilm formation, and the expression of virulence factor, which allow persistence in the lung of patients with chronic respiratory infection [65].

P. aeruginosa has two Acyl homoserine lactone (AHL) dependent QS systems - the Las and the Rhl systems. In the Las system, the LasI AHL synthase directs the synthesis of the signal molecule, *N*-3-oxododecanoyl-L-homoserine lactone (OdDHL), that binds to LasR at high cell density. The LasR-OdDHL complex

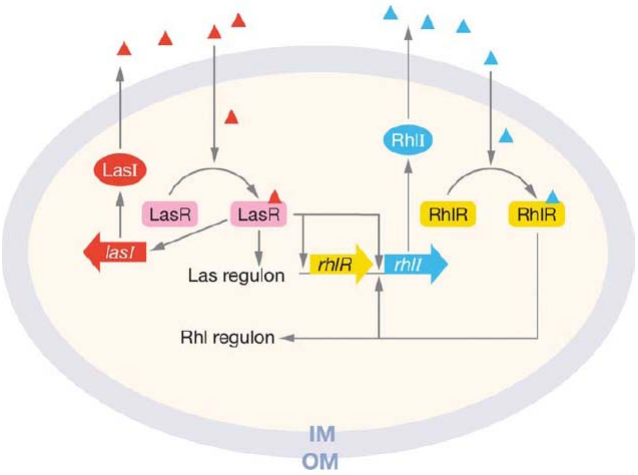

Figure 1.1: A simplified sketch of the AHL mediated QS regulatory network in *Pseudomonas aeruginosa*. The two AHL-mediated QS networks are seen, Las and Rhl. Red triangles are OdDHLs and blue triangles are BHLs. *Source: [65]*

.

regulates the expression of many target genes among others genes encoding virulence factors: protease (*lasA*), alkaline phosphatase (*aprA*), endotoxin A (*toxA*), and elastase (*lasB*) [23]. It also activates the expression of *lasI*, that again activates the LasI synthesis, creating a positive feedback loop. The expression of *rhlI* and *rhlR* is also activated by the LasR-OdDHL complex. In the Rhl system, the RhlI synthase directs the synthesis of *N*-Butyryl-L-homoserine lactone (BHL). RhlR binds to BHL at high cell density and activates certain target genes. Furthermore, the RhlR-BHL complex creates a positive feedback loop as LasR-OdDHL. See Figure 1.1 for a sketch of the regulatory network. A third part of the quorum sensing system in P. aeruginosa has been recognized as the Pseudomonas quinolone system (PQS). This system serves as a link between the Las and Rhl systems [23], we will not concentrate on this system here.
It was found that some genes, regulated by the QS system, responded specifically to OdDHL alone, other genes responded specifically to BHL alone and yet some genes responded to OdDHL but increased activation by addition of BHL [59, 27]. These genes are not regulated at once, but are differentially regulated with increased cell density. In the presence of excess added signal some genes are triggered early in the exponential phase and some genes are induced during the stationary phase, but most of the genes are induced during the transition from the exponential phase to the stationary phase [59]. Thus, timing of gene expression is not related to signal molecule concentration alone. It has been suggested that the limiting factor might be the level of the regulator LasR [59].

It was found that the Rhl system is controlled by the Las system at the transcriptional and posttranslational level and thus the AHL mediated QS system in *P. aeruginosa* is often referred to as hierarchial system with *las* in the top.

1.2 The LasR Protein and OdDHL

There is a broad range of signaling molecules that bacteria use but in gram negative bacteria the commonly used are AHLs. Several hundred structural variants of the basic AHL molecule have been discovered, synthesized, and characterized [20]. AHLs are composed of a conserved homoserine lactone and a fatty acid side chain which can vary in length (4-18 carbon atoms), level of saturation, and side-chain (oxo- or hydroxyl-) substitutions [20].
The distribution of the AHLs inside the bacterial cell is thought to depend on two different mechanisms with the short-chain AHLs freely diffusing in/out of the cells and the long-chain AHLs using an active-efflux mechanism to transport themselves in/out of the cells [20, 49]. Outside the cell it has been proposed that the long-chain AHLs, should not easily be able to move between cells in a diffusion-mediated manner owing to their poorer solubility relative to the short-chain AHLs [20].

It is generally believed that LuxR homologues, including LasR cannot fold into its active form in the absence of an appropriate signal molecule. This assumption is mainly based on the inability to purify active regulator protein grown in the absence of signal which is seen in the regulators QscR [37], LasR [60], LuxR [63] and TraR [67, 68]. However when grown in the presence of signal it was possible to purify active regulator from all these regulators. Furthermore, LasR and TraR are seen to retain signal even after purification steps and dialysis against signal-free buffer suggesting that the binding is irreversible. This view has been challenged by the same group which made the majority of above mentioned studies (QscR, LasR, LuxR). They presented evidence that LasR can fold into an active conformation in the absence of OdDHL and evidence indicating that LasR and OdDHL dissociate and reassociate in the cell [54].
If binding is irreversible this would mean that the cells would not be able to respond quickly to a decrease in signal concentration, at least not faster than than the proteolytic decay or dilution by cell division. In this case inhibitors would not be able to competitively inhibit activity of active LasR proteins.
In Size-exclusion chromatography and dynamic light scattering purified LasR was found to be a dimer in solution [60]. Furthermore, the crystal structure of the LasR ligand-binding domain bound to its cognate signal was found to be a symmetrical dimer bound to two signals [18].

1.3 Motivation

By monitoring the signal molecules one can get insight into the processes used to control the expression of virulence genes. Detection of signal molecules are usually done by biological assay (bioassay). Detection through bioassay is done by a monitor strain with a reporter gene and lacking all AHL synthesis. Countless monitor strains have been constructed with various reporter genes, such as *lacZ*[54], *lux*[44] and several different *gfp* variants [13]. In this setup it is possible to determine any cell-density dependent production since the cell can be monitored through growth. However, it is very important to construct a monitor with limited background and which response quickly and quantitatively to the addition of autoinducer.
However, even though bioassay is indeed an in vivo system it is an artificial system suffering under all the alterations done to the cell in order to be able to monitor the system. The plasmid concentration is shifted up (if plasmids are used), gene manipulations e.g. to increase signal, artificial response systems are constructed etc. It would give a more true image of the QS system if we had a system where nothing needed to be altered or disturbed in order to monitor the system.
This was the motivation that led us into investigating whether Raman spectroscopy and in particular Surface Enhanced Raman Spectroscopy (SERS) could provide such a system. SERS is a technique already used in the detection, differentiation and identification of bacteria [22, 56, 30, 25]. However, it has not yet been used to identify and quantitatively access a particular molecule in the bacteria. Our hope was that among all the substances in the bacteria and their corresponding spectra it would be possible to isolate the contribution arising from the signal molecules in QS. We succeded in measurering the signal molecule down to concentrations below nM which is never seen before. Unfortunately, it was not possible to make the technique truly quantitative in the concentration interval needed. Thus, we turned to the conventional way of monitoring QS systems, by bioassays.
The bioassay method using a fluorescent monitor, *gfp*(ASV) was succesfully applied and a conventional kinetic model was proposed to explain the behavior of the system. Through comparison of data and model (and experiments from the literature) it was possible to explain the interaction of LasR and its cognate signal. The signal, OdDHL, previously thought to be essential, is shown not to be needed for the proper folding of LasR

Chapter 2

Detection of Signal Molecules using SERS

The suggestion of using Raman and in particular SERS to monitor signal molecule concentrations was formed from the idea of having an in vivo system where nothing in the cell was altered or disturbed. Normally, the monitor systems used have a lot of alterations done to the native cell. The plasmid concentration is shifted up, gene manipulations e.g. to increase signal, artificial response systems are constructed etc.
The aim was first and foremost to be able to monitor signal molecule alone down to concentrations as low as nano Molar which has never been done before. The next step would be to see if the measurements can be made quantitative in the interval needed, which is from μM down to nM. If made quantitative the whole procedure should be tested in the bacteria. We succeeded with the first goal but unfortunately it was not possible to make the process quantitative in the region required.

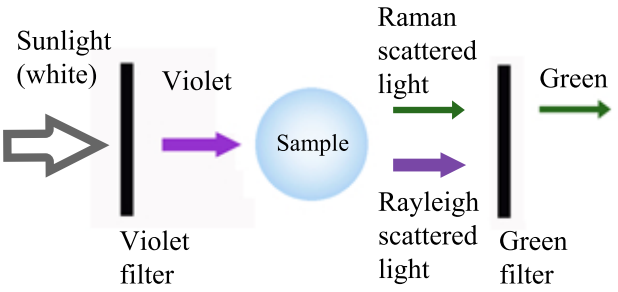

Figure 2.1: The fundamentals of Raman's experiment. The violet light of the sunlight is isolated with a violet filter and passed through the liquid sample. Most of the light emerging from the liquid sample is the same color as the incident violet beam - the Rayleigh scattered light. However, Raman showed that some of the scattered light was a different color, which he isolated by using a green filter placed between the observer and the sample

2.1 From Raman to SERS

In 1928, C.V. Raman discovered that when a beam of colored light enters a liquid, it scatters and some of it emerges as a different color, see Figure2.1[1]. What happens is that the incident photons interact with the molecules/atoms in such a way that energy is either gained or lost so that the scattered photons are shifted in frequency, see Figure 2.2. This is called inelastic scattering. It is a very weak effect and only one in a million photons create this effect [2]. The invention of the laser in the 1960s created a more intense source of light to amplify the effect and observation of the scattered light.

The Raman spectroscopy technique provides a fingerprint that can be used for qualitative analysis, even in a mixture of materials. The intensity of the spectral lines is related to the amount of the substance. Raman spectroscopy can be applied not only to liquids but also to gases and solids. And unlike many other analytical methods, it can be applied easily to the analysis of aqueous solutions. It is a technique, giving information on what and how much is present in an abundance of samples.

It is used in the areas of biotechnology, semiconductors, colors, art, archeology and forensics. Raman spectroscopy is used in the carbon industry to check the quality of products. In the pharmaceutical industry the technique is for example used for in-situ quality control of manufacturing and formulation.

In 1974 Fleischman *et al.* published an unexpected large Raman scattering of pyridine adsorbed on electrochemically roughened silver [41] - the first surface

[1]The effect had already been predicted theoretically by Adolf Smekal in 1923

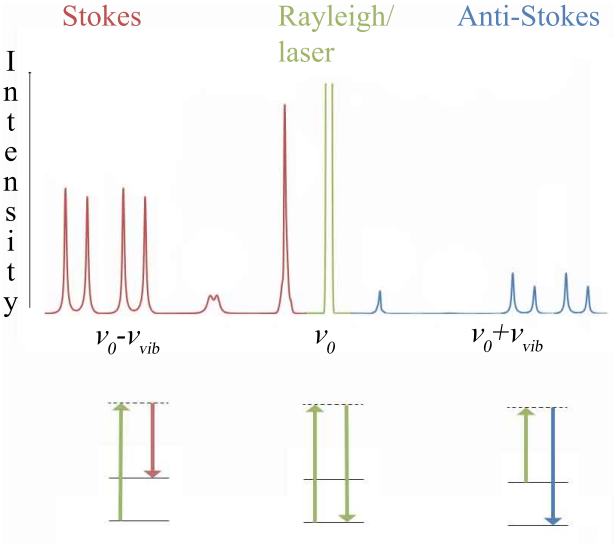

Figure 2.2: If monochromatic light is scattered by molecules or crystal lattices spectral analysis shows an intense spectral line matching the wavelength of the light source. Additionally, more weaker lines are observed at wavelengths which are shifted compared to the wavelength of the light source. These lines are called Raman lines.

enhanced Raman spectroscopy (SERS) spectrum. However, the major enhancement seen in SERS was not recognized until 1977. Jeanmaire and Van Duyne [31] proposed an electromagnetic effect, while Albrecht and Creighton [11] proposed a chemical (charge-transfer) effect. Their theories are still accepted as explaining the SERS effect. The inherent weakness[2] of the Raman signal represents a severe limitation to the investigation of materials in low concentrations (e.g., self-assembled mono layers, ultra thin polymer films, nanomolar analyte solutions). This limitation was removed with the discovery of SERS, however other limitations occurred.

2.2 SERS

Because the intensity of the Raman signal is proportional to the square of electric dipole moment $P = \alpha E$, two possible reasons to account for enhancement can be considered: the enhancement of polarizability α and the enhancement of electrical field E. The first enhancement of polarizability α may occur because of a charge-transfer effect or chemical bond formation between the metal surface and molecules under observation, which is called chemical enhancement. The second one takes into account the interaction of the laser beam with irregularities on metal surfaces, such as metal micro-particles, or roughness profile. It is believed that laser light excites conduction electrons at the metal surface leading

[2]Except for special cases of resonating molecules (Resonance Raman, RR)

to a surface plasma resonance and a strong enhancement of electric field E, known as electromagnetic enhancement.
SERS requires metal with feature sizes much smaller than the wavelength of light.

2.2.1 The Electromagnetic Enhancement

Most of the features of the electromagnetic enhancement can be understood by examining the electrostatics of a polarizable metal sphere in a uniform external electric field. The electromagnetic enhancement is the dominating contribution to the SERS signal and can be as high as $10^{10} - 10^{11}$ [24]. SERS can be observed when the sample being studied adsorbs to the surface of a metal. The surface of a metal is covered with electrons, which can be considered as free electrons that can move across the surface. When a laser beam hits the surface of the metal, it interacts with these electrons and causes them to oscillate as a collective group. These oscillations are called surface plasmons. These plasmons have a resonance frequency at which they absorb or scatter light most efficiently and this frequency depends on the nature of the surface and on the metal. Gold, silver and copper nanoparticles have resonance frequencies in the visible region. The electromagnetic enhancement can be described by considering a model of an applied electromagnetic field on a single metallic sphere. This is of course a very coarse description for once because the metal's surface roughness, which seems to be so important experimentally is not included. This can be seen as an approximation of a single colloidal particle, even though we know that it is the aggregation which gives the high enhancements in SERS. When the laser light is resonant with the surface plasmon the metal sphere radiates its own dipolar field E_{SP}. A small metal sphere with radius r, much smaller than the wavelength of the incident light, is subjected to an applied electric field, E_0 from the laser and the field due to the surface plasmon the distance d from the surface, E_{SP} is described as:

$$E_{SP} = \frac{\varepsilon(\omega) - \varepsilon_0}{\varepsilon(\omega) - 2\varepsilon_0} \left(\frac{r}{r+d} \right)^3 E_0 \tag{2.1}$$

$\varepsilon(\omega)$ is the dielectric constant of the metal[3] and ε_0 is the dielectric constant for the medium surrounding the sphere. In a normal medium $\varepsilon_0 > 0$, for vacuum it is 1 and water ≈ 80. Thus, the maximum g is found when ε is close to $-2\varepsilon_0$ and the imaginary part of ε is as small as possible. Negative dielectric constants are found in metals and the condition to have the imaginary part of ε is as small as possible corresponds to the excitation of a surface plasmon in the metallic nanoparticle [9].
At any point on the surface the field may be described by two components, the

[3] take the form $\varepsilon_1 + i\varepsilon_2$

average field perpendicular to the surface and the average field parallel to the surface. Since the greatest electrical field is seen for $\theta = 0°$ or $180°$ the greatest enhancement is found for a molecule adsorbed to the surface and polarized perpendicular to it. E_{tot} explains what the net electric field around a dielectric particle is and we want to consider a Raman active molecule near a metal nanoparticle and how much the emitted field is enhanced. The incident field at the nanostructured metal is, as before E_0 and the plasmonically enhanced field is $E_{SP} = gE_0$ where $g = g(\omega_0)$ is the average enhancement over the metal surface and is dependent on the frequency of E_0. The emitted Raman field will then be $E_R \propto \alpha_R E_s \propto \alpha_R g E_0$ where α_R is the Raman tensor which originates from the polarizability of the molecule. The emitted Raman field is also enhanced by the nanoparticle by $g' = g'(\omega') = g'(\omega_{in} \pm \omega_{vib})$, now dependent on the Raman emission frequency. Thus the total SERS emitted field is $E_{SERS} \propto \alpha_R g g' E_0$. The intensity of the SERS signal is then $I_{SERS} \propto |\alpha_R|^2 |gg'|^2 I_0$ where I_0 is the incident intensity. For low energy vibrations where $\omega' \approx \omega$ the enhancements will be similar ($g' \approx g$) and $I_{SERS} \propto |\alpha_R|^2 |g|^4 I_0$. Often SERS is reported to scale like $|E_L|^4$ where E_L is the normalized local incident electric field such that $|E_L|^4 = |\frac{E_S}{E_0}|^4 = |g|^4$. The fourth power dependence on the electric field can result in large SERS enhancements. [8]
It is important to note that the major contribution to the SERS scattering is from the metal particle and not from the molecule itself, the molecules scattering is merely reflected in the SERS spectrum of the light scattered by the metal. When the molecule is adsorbed to the metal particle's surface it will include contributions from the metal and may, as a result, be greatly altered both in its magnitude, symmetry and resonant properties from the Raman polarizability of the isolated molecule.
As mentioned in the start of this section the greatest enhancement occurs from interactions between particles. The point at which two particles touch will generate enormous electrical fields thus points of contact will give particular effective SERS. These active parts are called "hot spots".

2.2.2 Chemical Effect

The chemical enhancement accounts for 10-100-fold amplification of the bare Raman signal.
This contribution relies on modification of the Raman polarizability tensor of the molecules adsorbed onto the metal surface. A new analyte-metal species is formed through a bond which enables transfer of charge (electrons or holes) from the metal's surface into the analyte resulting in an increased molecular polarizability. Enhancement is thought to proceed through new electronic states, which cause an increase of the Raman cross-section.
Biomolecules have been found to have a pH dependent adsorption [28] and the

chemical effect can thus change with pH.

2.2.3 Problems in SERS: Selection Rules, Reproducibility and Quantitative Measurements

The selection rules that normally prevail in Raman spectroscopy does not apply in SERS. New peaks are formed and some peaks that are strong in normal Raman become very weak or disappear altogether. It also follows that the mutual exclusion rule (no band can be active in both Raman scattering and infrared absorption) no longer applies. New bands usually occur because of the different symmetry of the molecule/metal complex. The appearance of new bands and the disappearance of existing bands makes it much more difficult to interpret a SERS spectrum and compare it to the conventional Ramen spectrum. This can also be seen in our experiments were the conventional Raman spectrum of solid C12-HSL is very different from the solvent C12-HSL. This is also in part due to the different material state (solid vs. liquid).
Another difficulty with SERS is that the intensity changes which occur at different concentrations can be nonlinear. This is seen for pyridine [2]. For small concentrations of pyridine when it is well below mono layer coverage the spectrum is weak, but when mono layer coverage is approached the spectrum grows strong. The reason is that the pyridine ring is parallel to the surface below mono layer coverage which results in low enhancement. When approaching mono layer coverage the plane of the ring is forced into a position perpendicular to the surface to allow the molecules to pack, hence the strong enhancement. In the literature experiments concerning concentrations in SERS (using colloids) are often restricted to a certain concentration interval of around 2-3 decades and described as semi-quantitative [57, 53, 42, 43]. But this seems to depend on the analyte in question and experiments with broader range of quantitative behavior are seen [17].
A major problem in quantitative analysis in SERS is in reproducing the SERS amplification processes which largely rely on the metal structures. A slight variation in cluster sizes and shapes in a colloidal solution of silver produce changes in the enhancement factors by several orders of magnitude [53]. Thus preparation of SERS colloids demands special attention. The quality of the silver colloids, size, shape and the state of aggregation, the reproducibility, correct storage, the ratio of the silver colloid, the quantity of the analyte solution, the additional water for dilution, the order of mixing and pH are all important [53]. Furthermore, care have to be taken during data acquisition. Small changes in the setup as e.g. simple sample positioning can cause variation in signal levels [17]. In Figure 2.3 two spectra have been taken of the same sample, the sample being repositioned and optimized again for the second spectrum. Reproducibility is seen, even though the sample positioning is not fixed in our setup and

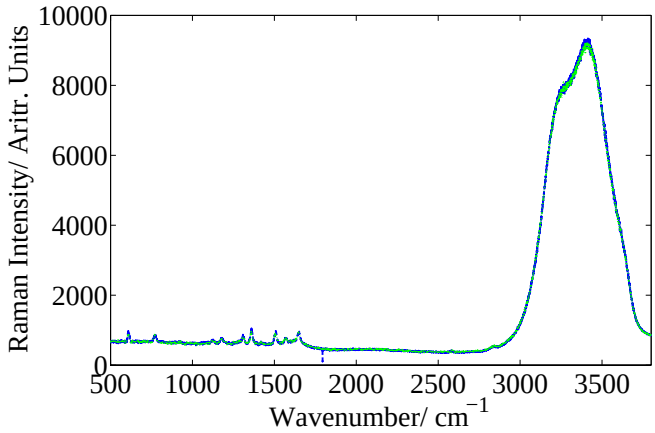

Figure 2.3: Testing the reproducibility of sample positioning and focusing. Two spectra taken of an identical sample. The sample is repositioned and optimized again for the second spectrum. The concentration of C12-HSL is 1 μM and the sample colloid ratio is 50:50. Mode1, macro (HPLC vial).

we rely on the precision of the eye. Still this only test sample positioning and focusing, and not the change that can occur between samples due to different aggregation for one. Different samples were tested in the same manner seen in Figure 2.4. Also signal degradation either through photochemical damage to the sample or to the colloids have to watched. Degradation can be prevented by keeping the laser power per unit area is kept under the damaging threshold. A strong doublet of bands appear at sample degradation at approximately 1360 cm^{-1} and 1560 cm^{-1} (formation of graphitic or amorphous carbon on surface) [17]. Variations in laser power and the alignment/focussing can be corrected by adding an internal standard, non- SERS active compound [17].
The colloids have to be mono disperse, size specific, time stable and above all the state of aggregation has to be controlled. The colloid is stable because of the surface charge. Usually an aggregating agent is used to reduce this charge and cause controlled aggregation (less stable colloids). Aggregation agents such as sodium chloride (NaCl) and poly-L-lysine react with the surface (NaCl- forms a silver chloride layer on the surface) or coat the surface, respectively. The aggregation will continue, but suspensions are stable up to several hours. The enhancement from each molecule is likely different but when averaging over many molecules and many hot spots it it is in some cases possible to be semi-quantitative. Still a case like e.g. pyridine could happen. Only molecules on the surface will be active.
This is not possible for small numbers of molecules, here the Raman signal will burst every time a hot spot passes through the beam. Furthermore, the sensi-

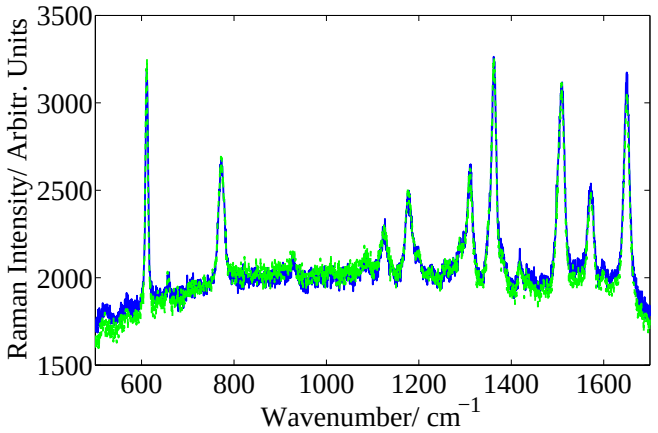

Figure 2.4: Testing the reproducibility of different samples. Both samples had a concentration at 1 nM with a sample colloid ratio at 60:40 and 10 μl NaCl to a total volume of 200 μl. Mode 1, macro (HPLC vial).

tivity of SERS is huge compared to normal Raman, and a contaminant could turn out to be the dominant feature in the spectra if it sticks strongly to the surface.
As mentioned there is a requirement that the laser wavelength should be chosen to match the enhancing medium. Our silver colloids have a peak absorbance at 405 nm and the excitation wavelength is 532 nm, which is some distance from the apparent optimum value. However, successful enhancement is seen, which is possible because the UV-VIS spectra of the colloid is broadened to the red end of the spectra during aggregation [17].

2.3 Method

2.3.1 The Raman Spectrometer

The experiments were performed with a dispersive spectrometer, a Dilor-XY Raman spectrometer. An overview of the Dilor-XY Raman spectrometer is shown in Figure 2.5. The sample is either placed at the position "Sample 1" or at "Sample 2". At "Sample 1" the scattered light is sampled at 90° to the incoming beam. At "Sample 2" the incoming light is focused onto the sample through a microscope objective and the scattered light is sampled at 180° to the incoming beam. In the region marked with the blue box, the scattered light

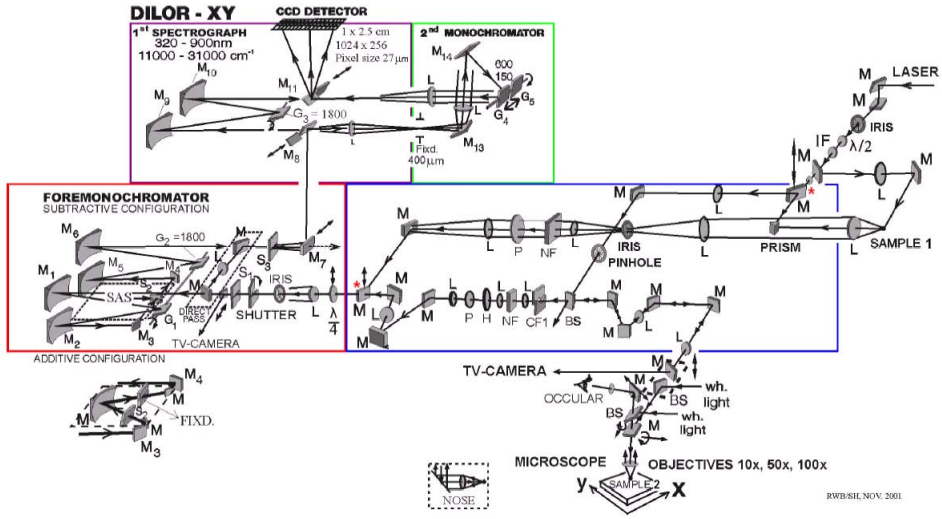

Figure 2.5: Overview of the Dilor-XY Raman spectrometer at the Chemistry Department of DTU. M stands for mirror, L for lens, NF for notch filter, G for grating and S for slit. *Source: Rolf W. Berg, Department of Chemistry, Energy and Materials, Technical University of Denmark, DK-2800 Lyngby.*

is sampled and then focused. A notch filter is placed in the beam path to filter the Rayleigh scattered light. The V-configuration of the mirrors is to increase the path length of the beam.
The region marked with the red box is a fore monochromator, which is a double monochromator that can be switched between additive and subtractive configurations. The fore monochromator can be used to filter the Rayleigh scattered light instead of the notch filter if one wants to look at Raman scattered light close to the laser line. The mirrors are not perfectly reflecting, so the intensity of the light will be reduced every time it is reflected from a mirror. The use of the fore monochromator involves using more mirrors compared to the situation when using the notch filter, hence the intensity of the spectrum when using the fore monochromator will be lower than when using the notch filter.
The fore monochromator can be avoided by using the direct pass configuration in which the light is sent directly to the mirror M8 in the purple region. The position of M8 determines whether the light is sent to the region marked with the green box before it is finally sent to the CCD detector, or whether it only propagates in the purple region. Utilizing the region marked with the green box, also called the "2nd monochromator", makes it possible to measure a quick spectrum covering a much wider wavelength region than when using the "1st spectrograph." The resolution of the spectrum taken with the "2nd

monochromator" is not as fine as that taken with the "1st spectrograph." With the help of a step motor the grating in the "1st spectrograph" can be rotated, making it possible to change the center wavelength of the region being scanned. It is thus possible to cover the same wavelength region as that of the "2nd monochromator" in several steps. There are however some problems associated with scanning in several steps. The step motor, which moves the grating, causes some shift in the x- and y-axes. When the spectra are then added, some weak peaks may result, which are just artifacts.
The beam focus on the CCD camera was optimized for red light because the "1st spectrograph" is not optimal for red light. The CCD camera was cooled with liquid nitrogen. The Raman spectrometer was controlled using the software Labspec. The x-axis was calibrated by measuring a spectrum of cyclohexane and adjusting the laser wavelength in Labspec.

2.3.2 Colloids and UV-VIS

The greater part of the overall enhancement of SERS is due to an electromagnetic enhancement mechanism that is a direct consequence of the presence of metal roughness features at the metal surface. These features can be developed in a number of ways: oxidation-reduction cycles on electrode surfaces, vapor deposition of metal particles onto substrate, metal spheroid assemblies produced via lithography, metal colloids, and metal deposition over a deposition mask of polystyrene nanospheres. In appendix E I have attached a protocol describing the production of Ag colloids and Au colloids, which I was introduced to at the University af Strathclyde in Glasgow under the guidance of Professor Duncan Graham. Unfortunately these colloids were not further used for the experiments. The colloid used was made by Salim Abdali, Department of Chemistry, University of Copenhagen in Denmark. The Scanning Electron Microscope (SEM) pictures of the colloids can be seen in Figure 2.6.

From the SEM pictures the shape and size of the colloids can be seen. The particles are roughly 25 nm, spherical and mono disperse in the region 25±5 nm.
Another way to check colloids is with Ultraviolet-visible spectroscopy (UV-VIS). The UV-VIS spectrophotometer measures the intensity of light passing through a sample (I), and compares it to the intensity of light before it passes through the sample (I_0). This is called the transmittance ($T = I/I_0$). The more light the sample absorbs the smaller the transmittance. The UV-VIS spectrophotometer display absorbance on the vertical axis ($A = \log I_0/I$). If no absorption has occurred, $T = 1$ and $A = 0$. The wavelength of maximum absorbance is a characteristic value, designated as λ_{max}. Different compounds may have very different absorption maxima and absorbances. Intensely absorbing compounds must be examined in dilute solution, so that significant light is received by the

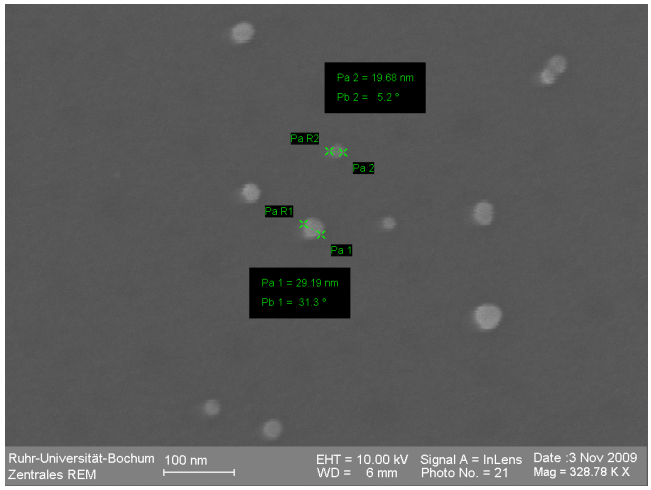

Figure 2.6: Scanning Electron Microscope, SEM of the Ag colloids used in the experiments. *Source: Salim Abdali, Biophysical Chemistry Group, Department of Chemistry, H.C. Ørsted Institute, University of Copenhagen, DK-2100 Copenhagen, Denmark*

detector. The method is most often used to determine concentrations by the help of Lambert-Beer's law: A=log(I_0/I) = ϵ c z, were c is concentration, z is the path length and ϵ is the molar extinction coefficient and is a measurement of how strongly a chemical species absorbs light at a given wavelength, thus being case specific.
A light beam passing through a colloidal dispersion of metal nanoparticles gets attenuated by the combined contribution of absorption and scattering, as given by [58]

$$I(z) = I_0 e^{-n_0 C_{ext} z},$$

were I_0 is the intensity of the incident beam, I(z) is the intensity of the beam after traveling path length, z within the sample, n_0 is the number density of particles and $C_{ext} = C_{abs} + C_{sca}$ is the extinction cross section of a single particle and is the sum total of the absorption and scattering cross sections respectively. This explains what happens in the colloid sample and thus the UV-VIS spectrum is a measure of attenuation or extinction and is in this way related to the absorption cross section. This is why it is called the extinction spectrum by some.
For spherical silver particles with a diameter smaller than 10 nm dipolar absorption is dominant and one can use the dipole approximation from Mie scattering theory to find a simple relationship between the FWHM and the radii of the particle [32, 15]. This approximation gives a band of Lorentzian shape. For larger radii particles, the absorption band begins to shift to longer wavelengths due to additional magnetic-dipole terms, thus the full expression of Mie's theory applies [46]. One can thus use the absorption maximum of the measured UV-VIS spectrum to see the average particle size. Furthermore, the smaller

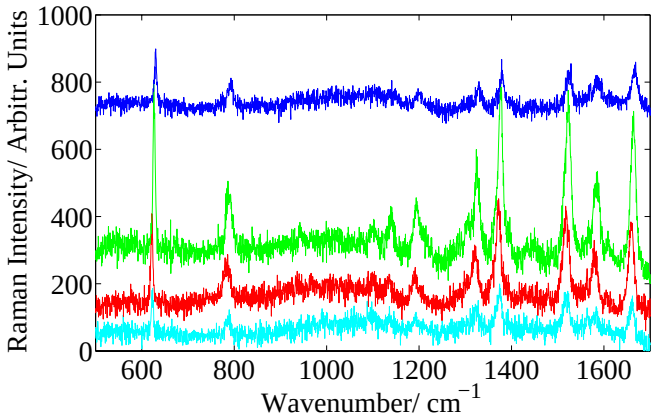

Figure 2.7: C12/ABT solution: 10^{-6} M with varying amount of colloids [Sample:colloid]. From the bottom up: 6:4, 5:5, 4:6, 3:7. Displayed with an offset. Mode1, micro, alu plates, 250mW,x20 lens.

the band width the more mono disperse the colloid solution. With a collection of sizes, several bands would melt together creating one broad band, thus the FWHM says something about the particle dispersion. In the case of nanorods and nanoparticle aggregates, the plasmon absorption can split into two bands corresponding to the oscillation of the free electrons along and perpendicular to the long axis of the rods [40, 58]. If only one peak is seen one can assume that the particles have a roughly spherical shape. Particles in colloidal dispersions often show a size and shape distribution, leading to a broadening of the resonance.

Addition of salt is usually used because of the aggregation effect. For the purpose of optimizing our measurements we tested different amounts of colloid and salt used. In Figure 2.7 different ratios of colloid can be seen and in Figure 2.8 the variation of salt is seen. The analytes ability to bind to the surface of the colloid determines whether the analyte gives a large SERS signal. In some cases the compound of interest binds strongly to the Ag surface and it is only necessary to give them the opportunity. The most important factor determining the binding is the medium's surface charge (Ag has a negative surface potential).
As mentioned, colloids need to aggregate to obtain optimum enhancement. If the compound does not aggregate the colloids an aggregating agent can be added. In our case 0.1 M sodium chloride (NaCl) was added: 1 μl ($\approx$ 0.5 mM), 2 μl ($\approx$ 1.0 mM), 3μl ($\approx$ 1.5 mM), 4μl ($\approx$ 2.0 mM) and 5 μl ($\approx$ 2.4 mM) to a volume of 200 μl. The highest enhancement can be seen for 3 μl. However, we choose not to use any aggregating agent since the enhancement was sufficient without. Furthermore, an aggregating agent may, in some cases, interact directly with the enhancing surface which can lead to precipitation of the colloid rather than

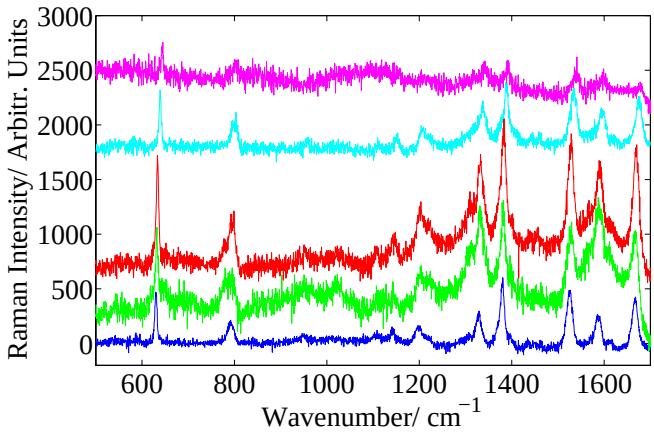

Figure 2.8: C12/ABT solution: 10^{-6}M with colloids [C12/ABT : colloids]=4:6. Vary NaCl from 1μL to 5 μL, bottom-up. Displayed with an offset. Mode1, micro, alu plates, 250mW, x20 lens.

formation of metastable aggregates (can cause reduction in enhancement over minutes)[17]. NaCl alters the nature of the colloid surfaces. Another consequence of adding any material to the enhancing surface is that their signals will also be enhanced, this is however not the case in our experiment.

2.3.3 Sample Holder: From Aluminum Plates to HPLC Glass Vials

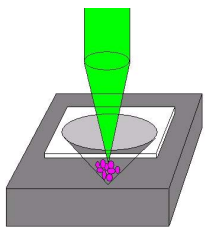

Figure 2.9: The special constructed aluminum plates.

In the initial experiments we used the "Sample 2" mode, were the incoming light is focused onto the sample through a microscope objective. This gave rise to the production of plates were we could contain the sample. Plates with 8 wells were constructed and a thin glass plate functioned as a cover. A sketch of such a plate with one well is seen in Figure 2.9.
The aluminum plates were cleaned by first immersing them in 4 M of HCl to remove aluminum oxide and oil from the manufacturing process. The acid removes the outermost layer of aluminum and thereby the layer of oil and aluminum oxide. The plates were then rinsed with water and immersed

in NaOH to remove $AlCl_3$. The following equations describe the reactions:

$$2Al + 6H^+ \rightarrow 2Al^{3+} + 3H_2$$
$$2Al + 2OH^- + 6H_2O \rightarrow 2AlOH_4^- + 3H_2$$

The initial experiments were made without the glass cover but because of the resulting contamination of the lens (evaporation) a glass cover was used. Later, the aluminum plates were replaced with clear HLPC glass vials partly because of the evaporation problem.

2.3.3.1 Contamination

We have had a lot of problems with contamination. The problem was that the spectrum of the analyte, C12-HSL could be seen even though it was not added in the sample. Colloids, MQ-water, salt were exchanged for new batches to exclude them from suspicion. The aluminum wells were cleaned every time first with HCl and then NaOH and left overnight to evaporate. In the end the lens was found to be the source of contamination. All lenses were cleaned. The sample was shown to evaporate and attach itself to the surface of the lens. A glass cover was then used. To make sure that the this was the source of contamination the lenses were cleaned and a spectrum was taken before and after a cover-less spectrum of the C12-HSL, see Figure 2.10. It was confirmed that the glass cover is needed for the lens to remain clean and hence to prevent contamination.

Spectra of the colloids taken with the clean lenses, x10, x20 and x50, can be seen in Figure 2.11. It can be seen that lens x10 has a lot more feature (mostly from water), this is due to its larger focus area. The peak at 2336 cm^{-1} is due to N_2 in the air, while the peak at 1558 cm^{-1} is due to O_2

Because of evaporation of the sample in the aluminum wells it was decided to switch to closed glass vials. The sample evaporation sometimes made a mist on the glass cover scattering the light before hitting the surface, and since the amount of sample only was 10 μL the evaporation might result in a change in concentration. The amount of sample was therefore changed to 200 μL.

2.3.4 Dilution

C12-HSL is barely soluble in aqueous buffers mainly due to the hydrophobic nature of the acyl chains [20]. For maximum solubility in aqueous buffers the solid C12-HSL should first be dissolved in an organic solvent and then diluted with the aqueous buffer of choice. Tris-buffered saline (TBS) buffer[10] was tried but it was not possible to dilute it to a concentration of 10 mM. The solvent

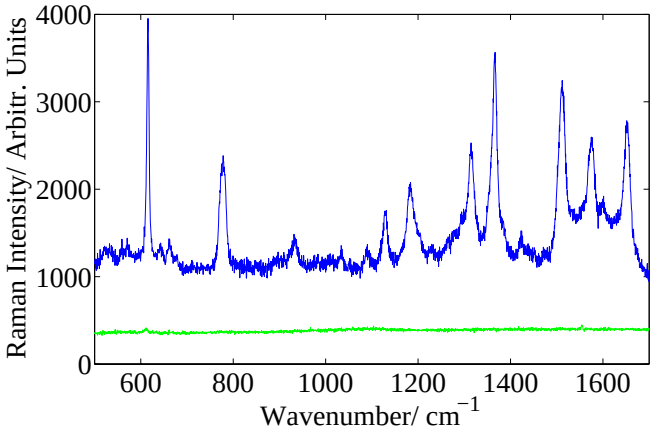

Figure 2.10: The SERS spectrum of the colloid solution with the 50x lens before (green) and after (blue) exposure of a C12-HSL sample without glass cover. Before there was no sign of the spectrum of C12-HSL, see green spectrum. Then a colloid solution with added C12-HSL was measured in the Raman spectrometer without glass cover. Hereafter a clean colloid solution was measured and a spectrum of C12-HSL was seen, see blue spectrum. Mode 1, micro, alu plate, 250mW

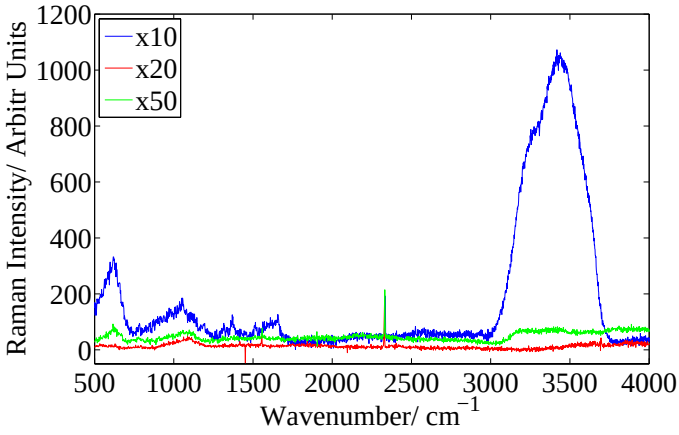

Figure 2.11: Spectra of the colloids taken with the clean lenses, x10, x20 and x50. It can be seen that lens x10 has a lot more feature because of its larger focus area. The peak at 2336 cm^{-1} is due to N_2 in the air, while the peak at 1558 cm^{-1} is due to O_2. Mode 1, micro, alu plate, 250mW

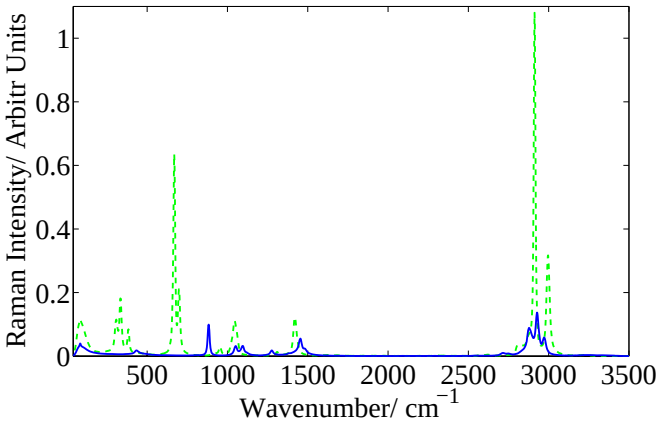

Figure 2.12: Conventional raman spectra of DMSO (green) and ethanol 96% (blue).

chosen had to be without significant structure in the fingerprint region of the Raman spectrum (500-1800 cm^{-1}). We considered dimethyl sulfoxide (DMSO) used by Pearman *et al.*[48] and ethanol. In Figure 2.12 the spectrum of DMSO and ethanol can be seen.

DMSO has a stronger spectrum than ethanol, up to 8 times stronger. However, they both have approximately the same amount of interfering peaks in the fingerprint region. Ethanol has the advantage of being the preferred solvent of C12-HSL in the laboratory at Department of International Health, Immunology, and Microbiology, Panum Institute, Denmark. Because the ethanol spectrum is relatively weaker we have chosen to use ethanol to dilute C12-HSL.

The sample diluted in ethanol has a concentration of 10 mM and a normal Raman spectrum was taken of this sample. Unfortunately, the only thing visible was the ethanol. A Raman spectrum was then made on the diluted (with water) sample, see Figure 2.13. As seen in the figure the only thing visible is a couple of bands belonging to ethanol. Thus it is not possible to obtain a conventional Raman spectra of the diluted C12-HSL. Therefore, a Raman spectra of the solid state was made, see Figure 2.14. The solid spectra were made with two different Raman spectrometers, the dilor XY and a Bruker FRS 100 FT-Raman spectrometer[4] with a wavelength of 1064 nm. It can be seen that this new spectrometer is much weaker and has less fluorescence. Conventional Raman scattering intensity is as mentioned in appendix D proportional to λ^{-4} where λ is the laser wavelength. Thus an infra-red laser like 1064 nm results in a decrease in scattering intensity by a factor of 16, when compared with a

[4]Kindly provided by Professor Ole Faurskov Nielsen at Copenhagen University, Department of Chemistry

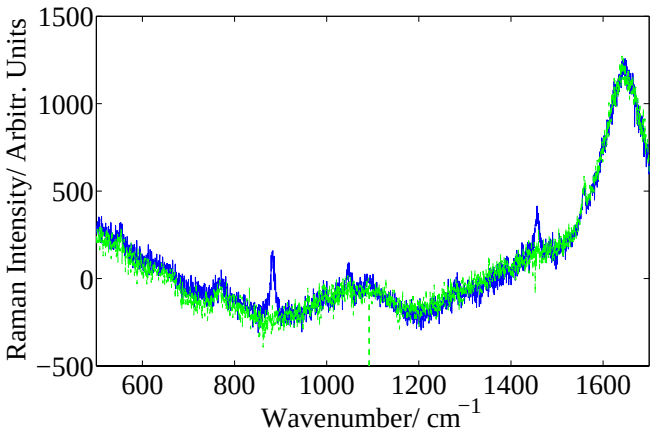

Figure 2.13: Conventional Raman spectra of 1 mM (blue) and 0. 1 mM (green) concentrations. The amount of ethanol amounts to 10% in the case of 1 mM concentration and 1% in the case of 0.1mM. Mode1, micro, alu plate, x10 lens, 500mW and a total of 10 μL in each well.

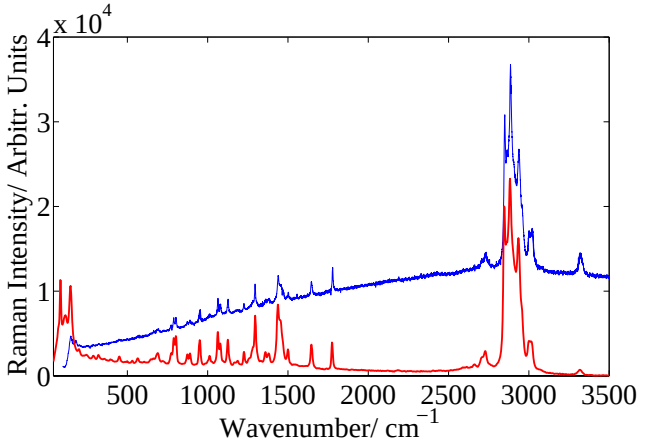

Figure 2.14: C12-HSL solid state. Blue spectrum is obtained with the dilor XY while the red spectrum is obtained with the Bruker FT-Raman. The latter is upscaled by 2 10^5

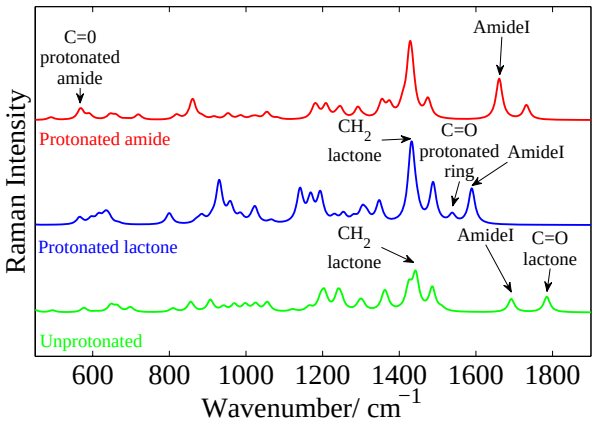

Figure 2.15: The theoretical Raman spectra of the unprotonated, the protonated amide carbonyl and the protonated lactone carbonyl C2-HSL. The wave numbers are scaled by the factor of 0.9602 and a Lorentz lineshape with FWHM at 10 cm^{-1} is assumed.

visible laser like 532 nm. Thus, to be able to see the diluted C12-HSL we have to use SERS due to its poor solubility.

2.3.5 Quantum Lactone Ring Model

Quantum chemical calculations were performed with the GAUSSIAN 09 program [1] of a simplified acyl-HSL with only two carbon atoms in the acyl chain, called C2-HSL. Three versions of C2-HSL were compared to find the energy minimum: protonation on the amide carbonyl, protonation on the lactone carbonyl and the unprotonated C2-HSL. The LC-wPBE density functional [61] combined with the 6-31Gdp [52, 51] basis set were used and the energy minimum was found for the unprotonated version. For exact numbers see Paper A. The B3PW91 density functional [16] and the 6-31Gdp basis set was used to obtain the Raman spectra of the three versions, which can be seen in Figure 2.15. The theoretical wave numbers are scaled by the factor of 0.9602 [45] and a Lorentz lineshape with FWHM = 10 cm^{-1} is assumed.
As mentioned, in SERS the selection rules from Raman does not apply and new peaks can be formed and others disappear, thus we cannot assume to directly compare the theoretically calculated Raman spectra with the experimentally obtained SERS spectra. However, the calculated spectra has been used as a help to assign the experimental SERS spectra.

2.4 Discussion and Results

The main results of this study can be seen in the accepted paper for Current Physical Chemistry, see Paper A.
The measured SERS spectra for C12-HSL dissolved in water are presented in Figure 2.16, with the highest concentration depicted in the top, decreasing in concentration towards the bottom, the concentrations being 20 μM, 2 μM, 200 nM, 20 nM, 2 nM, 0.2 nM and 0 M. The lowest spectrum is the control spectrum, that is, the spectrum of the same sample without C12-HSL. For the corresponding spectra of C12-HSL dissolved in ABtGcasa see Paper A.
The proposed assignment of the spectrum can be seen in the table in Paper A

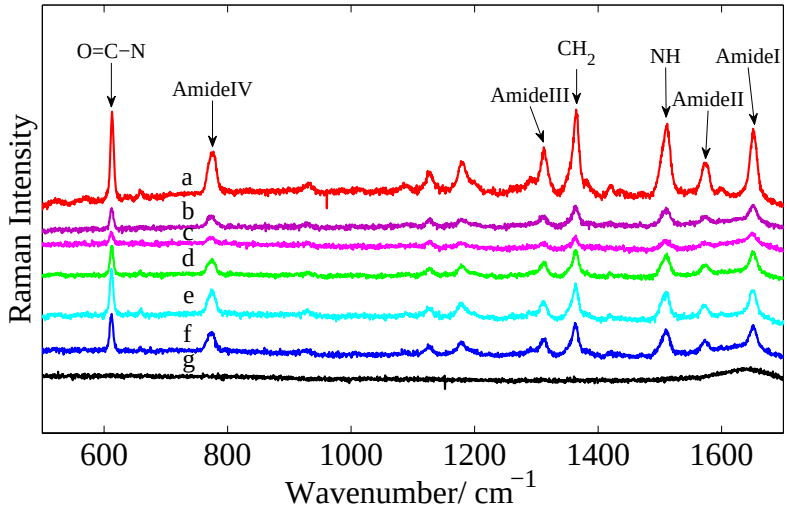

Figure 2.16: SERS of C12-HSL suspended in ultrapure water for the following concentrations (top down): 20 μM (a), 2 μM (b), 200 nM (c), 20 nM (d), 2 nM (e) and 0.2 nM (f). The lowest spectrum (g) is without any C12-HSL, thus only ultrapure water and Ag colloids are present. Mode 1, macro, 250mW

and shows all peaks observed both for the C12-HSL in water and in ABtGcasa and it is indicated at which concentrations the peaks were seen. The strongest peaks are indicated in Figure 2.16. The C12-HSL spectra are dominated by contributions from the amide portion of the molecule, that is the majority of the strong spectral bands originates from the chain of C12-HSL. This was also seen in the work of Pearman *et al.* [48]. The vibrations attributed to the lactone ring are weak, except for the very strong vibration at 1363 cm^{-1} which is the CH_2 wagging vibration of the lactone ring according to the quantum chemical calculation conducted in this study and also according to Jakubczyk *et al.* [29].

Furthermore, the medium band seen at 1178 cm^{-1} is attributed to the C-O stretch of the lactone ring.
The very strong amide I band at 1650 cm^{-1} could also contain contributions from C=O in lactone. The amide I, II, III and IV bands at 1650 cm^{-1}, 1573 cm^{-1}, 1312 cm^{-1} and 773 cm^{-1}, respectively are all clearly identifiable for C12-HSL in the water solution while the amide II and III are less pronounced for the C12-HSL spectra in ABtGcasa for all concentrations except the highest, 20 μM where they are very clear. The band for the O=C-N bending vibration at 612 cm^{-1} is consistently the strongest band observed in the SERS spectra of C12-HSL both for the water solution and the ABtGcasa-solution.
The control spectrum for the water solution is featureless, see Figure 2.16(g).

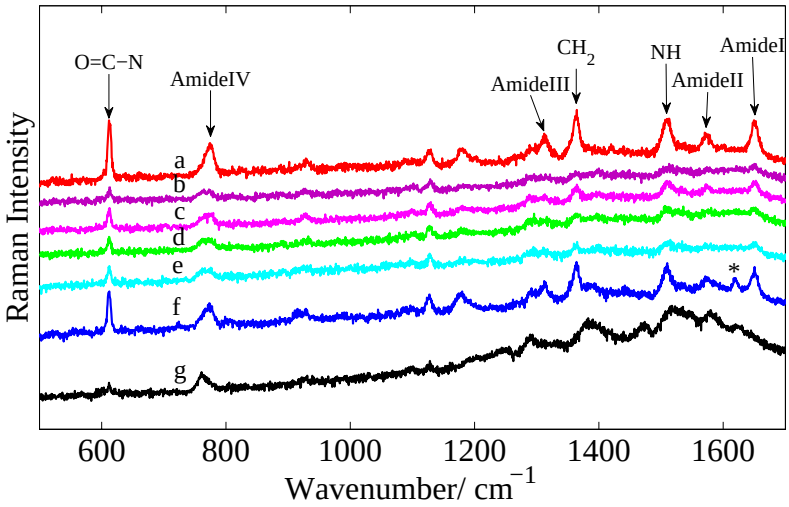

Figure 2.17: SERS of C12-HSL suspended in ABtGcasa for the following concentrations (top down): 20 μM (a), 2 μM (b), 200 nM (c), 20 nM (d), 2 nM (e) and 0.2 nM (f). The lowest spectrum (g) is without any C12-HSL, thus only ultrapure water and Ag colloids are present. Mode 1, macro, 250mW

Clearly a reduction of the water background is seen, which is due to the adsorption by the silver nanoparticles. We chose to obtain spectra of C12-HSL in ABtGcasa solution, because this is a typical environment in which to grow bacteria. In this way we tested whether the solution interfered with the spectrum. A number of peaks were seen in the ABtGcasa but these peaks do not seem to dominate in the combined spectra. However, many of the ABtGcasa-baseline peaks are positioned in similar areas as the C12-HSL peaks; this may result in the peaks in the C12-HSL spectra dissolved in ABtGcasa having an extra contribution from the ABtGcasa media. When comparing with the water dissolved C12-HSL spectra it can indeed be seen that the amide IV band at 773

cm^{-1} is broader since this band coincides with a band in the ABtGcasa spectra at an identical position. Because of the enhanced fluorescence caused by ABtGcasa to the right part of the spectra, the peaks in this part are less enhanced. Furthermore, the majority of peaks in the ABtGcasa spectra lie in this right hand-side of the spectra causing the peaks of the C12-HSL to be broader and less identifiable. When inspecting the lowest concentration an additional peak can be seen at the wavelength 1620 cm^{-1}, see Figure 2.17 marked with *. This is proposed to be due to the ABtGcasa contribution which has a peak at 1622 cm^{-1}. Why it is not present for the higher concentrations could be due to the ratio of ABtGcasa to C12-HSL being much higher for low C12-HSL concentration. There is simply a much higher risk that ABtcasa bands are enhanced. In this figure the peak at 1620 cm^{-1} proposed to be from the ABtGcasa solution is clearly seen.
As has been mentioned the strongest band in the C12-HSL spectra is the O=C-N band at 612 cm^{-1} both for the water and the ABtGcasa solution. However, the strongest band amongst the amide bands differs between the two solutions. For the water solution the strongest amide band is the amide I band while the strongest band for the ABtGcasa solution is the amide IV band, closely followed by the amide III band. The weakest band in both solutions is the amide II band. This suggest that the O=C-N band experiences a greater SERS enhancement and thus would also suggest an orientation of the molecule where the O=C-N is both closer to and nearly normal to the metal surface, thus experiencing maximum enhancement. That the second strongest band differs between the two solutions could mean that the orientation of the molecule adsorbed to the nanoparticle has changed.
The pH of the C12-HSL in ABtGcasa is assumed to be approximately 7, but it is not fixed and thus could be higher. At higher pH C12-HSL could undergo hydrolysis, resulting in opening of the lactate ring. In the study of Pearman *et al.* hydrolysis was investigated and the following new additional peaks observed: 1270 cm^{-1} attributed to carboxylic CO stretch band and 1432 cm^{-1} to a combination band, the latter due to carboxylic CO stretch and OH deformation [48]. None of these bands are found in the spectra in our study, thus we assume that no hydrolysis is occurring. Since hydrolysis halftime is found to be 27 hours for a pH of 7.2 and the longer acyl chain of C12-HSL makes it less susceptible to hydrolysis, we would not expect to see any signs of hydrolysis in our experimental conditions.
In Figure 2.18 the spectra of the signal molecule *N*-3-oxo-dodecanoyl-L-homoserine lactone (3-oxo-C12-HSL) can be seen. This molecule only differs from C12-HSL by addition of an oxo group at the C-3 position. This should make the molecule slightly more hydrophilic, thus more soluble in water [21]. Beside the difference in sidechain the spectra resembles that of C12-HSL.

When inspecting the spectra of the C12-HSL in water in Figure 2.16 the intensity of the spectra can be seen not to drop with decreasing concentration.

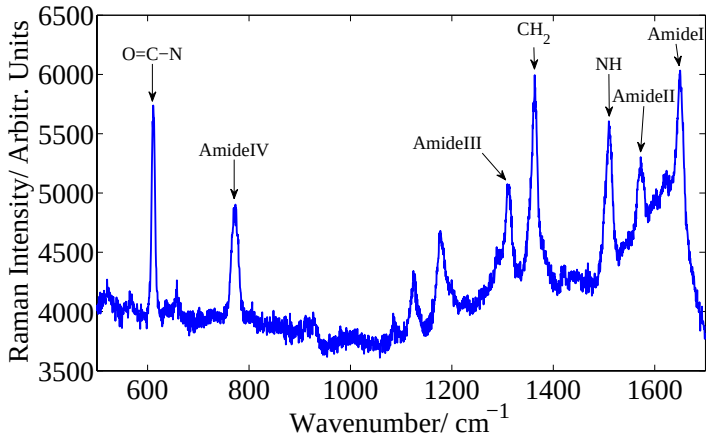

Figure 2.18: The SERS spectrum of C12-3O-HSL with sample colloid ratio of 5:5 and a concentration of 1mM and 100 μl NaCl (0.1M) into a sample size of 200μl ($\approx$ 33 mM). NEW -not shown in the article.

The highest intensity is found in the spectrum for the highest concentration, 20 μM . From 20 μM the intensity of all the peaks decreases with concentration until the concentration of 200 nM. At 20 nM the intensity level rises above the intensity levels of 200 nM and 2 μM. The intensity rising for 2 nM and hereafter decreasing for 0.2 nM. This non-linearity can be seen in Figure 2.19. The peak height at 612 cm^{-1}, corresponding to the O=C-N bending vibration and the peak heights of the amide I-IV bands, are followed and plotted against the different concentrations. All monitored peaks follow the same trend. In the case of C12-HSL suspended in water the intensity of the spectra seems to stop decreasing at around the concentration 200 nM. The decrease in intensity with falling concentration until 200 nM is what one would expect because the silver surface area has less molecules adsorbed. However the fall can also be seen to be non-linear, which is seen in literature and thus why a small concentration range is often chosen [53, 57]. After 200 nM the intensity increases until 2 nM. The increase in enhancement for the low concentrations could be explained by the existence of hot spots in the cluster structures, caused by thermally and non thermally activated diffusion of molecules into and out of hot areas, or trapping and release of molecules in high-field gradients [36]. It could also be due to the different adsorption geometries that can exist at different concentrations, as seen in [53, 12]. A major problem in SERS is not only the difficulty in reproducing amplification processes and variations in colloid sizes and shapes, but also the orientations of the adsorbed molecules on the colloid surfaces and whether they change orientation due to pH or other factors which may be changing. The same strange behavior is seen in C12-HSL in ABtGcasa, see Paper A.

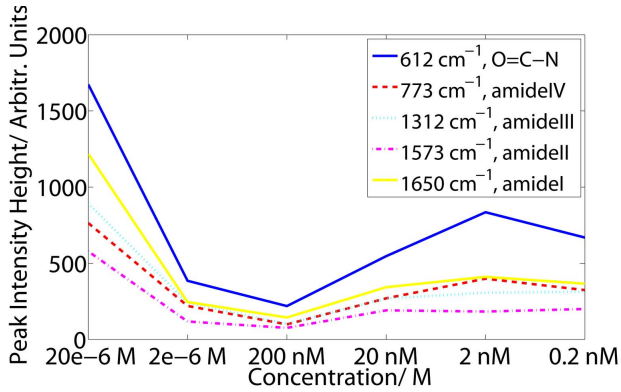

Figure 2.19: The peak intensity height at 612 cm^{-1}, corresponding to the O=C-N bending vibration, is followed through the different concentrations and plotted against the concentration. Likewise are the amide bands. Here we have the plot for C12-HSL in water solution.

To be able to use SERS to observe the change in concentration of signal molecules in bacterial cell cultures the technique has to be quantitative. This behavior is not achieved in this experiment, at least not over the many decades wanted. In conventional Raman all bands would scale linearly to our concentration, which is unfortunately not the case for SERS. Furthermore, since Ag ions and Ag nanoparticles have shown to be toxic to bacteria [66] future work should use coated Ag nanoparticles. The coatings could be polymers or antibodies and be designed to capture as well as protect the bacteria. The coating procedure has been successfully used in order to measure SERS spectra of unique or rare cancer cells [62].

2.5 Conclusions

We have demonstrated that it is possible to detect the signal molecule C12-HSL down to a concentration as low as two tenths of a nM. This is obtained in water and for the first time in ABtGcasa medium. The addition of ABtGcasa medium was shown to not interfere with the vibrations of C12-HSL. The first step towards using the SERS method for *in situ* measurements of low AHL concentrations in biofilms is thus met. However, to be able to deduce the AHL concentration from the SERS spectrum it is necessary to have quantitative measurements. This warrants further investigation.

Chapter 3

Regulator and Signal Molecule Interaction

It has long been assumed that many regulator molecules, including LasR, are a special case of proteins that need the signal molecules in order to properly fold into their active conformation. However, this assumption has been challenged by Sappington *et al.* that provides evidence not only that the regulator LasR can fold into an active conformation in vivo in the absence of OdDHL but also evidence indicating that LasR and OdDHL dissociate and reassociate quickly in the cell [54]. This prompted us to investigate the process of regulator and signal binding of the LasR protein and OdDHL in a study were we combine experimental data with a conventional kinetic model. In particular we investigate whether the dimerization of the regulator takes place before or after the ligand binding.

In this study several observations support that the dimerization of the regulator molecule must occur prior to the signal molecule binding. First, we show that there must be fully cooperative binding of the two signal molecules in order for the data to fit the model. If the signal molecule binds before dimerization the resulting kinetics does not fit the data. Second, when growing from quasistationary inoculum the system has an instant huge response to OdDHL indicating the presence of stable LasR (long-lived) even in the absence of OdDHL. Third, we observe identical timescales to the response to different concentrations of OdDHL which means that the regulators present must have the same life-time (degradation rate). Dimers are frequently better protected against proteolytic

decay compared to monomers. It thus follows that the regulators present must be dimers (in the case of binding before dimerization, we would have a RS and $(RS)_2$ present).
Furthermore, the findings of Sappington *et al.* suggest that the regulator dimer has a large degradation rate in the absence of signal and the *lasR* transcription turned off. This does not correspond to the low proteolytic decay normally seen in dimers. However, the apparent decay is explained by the kinetic model as the dissociation of dimer to monomer and the following degradation of the monomer, keeping the dimer proteolytically protected.

3.1 Method

3.1.1 The Experiment

We are investigating the Las system of Quorum Sensing (QS) in P. aeruginosa, previously described in the introduction 1.2. Briefly described, the LasR regulator binds to its cognate signal and activates certain genes, e.g. *lasI* and *lasB*. In order to study this system the *E. coli* strain MH155 with the plasmid pMHLAS is used. The reporter system consists of a *lasB-gfp*(ASV) fusion, which is a translational fusion of the *lasB* promoter to a gene encoding an unstable variant of GFP, GFP(ASV)[13]. LasR from P. aeruginosa controls expression of the reporter under control of the *lac* promoter, see Figure 3.1.
The *lasR* express the regulator protein, LasR which then is activated by its cognate signal OdDHL, activating the fused *gfp*. In short, the monitor strain responds to OdDHL (input) though the synthesis of GFP(ASV) (output), while lacking the ability to produce OdDHL itself.

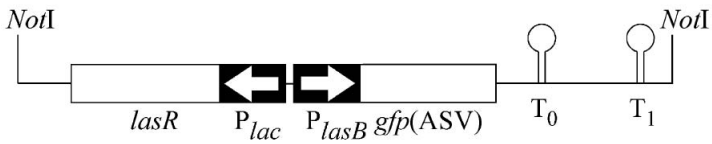

Figure 3.1: The plasmid pMHLAS with *lasB-gfp*(ASV) translational fusion and *lasR* expressed from the *lac* promoter. *Source: [26].*

$\lambda_c = 0.34\ h^{-1}$	$\lambda_c = 0.54\ h^{-1}$	$\lambda_c = 1.7\ h^{-1}$
25 ml A-10	25 ml A-10	25 ml A-10
225 ml BT	225 ml BT	225 ml BT
625 μl thiamin	625 μl thiamin	625 μl thiamin
12.5mL glycerol 10%	12.5mL glucose 10%	12.5mL glucose 10%
6.25 ml 20% L-leucine	6.25 ml 20% L-leucine	6.25 ml 20% casamino acid

Table 3.1: The different media used to obtain a certain growth rate.

3.1.1.1 Optical density and fluorescence spectroscopy

The synthesis of GFP(ASV) is monitored with fluorescence spectroscopy and the optical density is used for the normalization.
Manual OD was measured on Shimadzu UV-1800. The optical density (OD) is the same as the absorbance in spectroscopy and the same rules apply as described for the UV-VIS measurements in Chapter 2.3.2. The difference is that UV-VIS uses a sweep of wavelengths were OD is fixed at a particular wavelength, in this case 450 nm. At high concentrations it is necessary to dilute the sample, because of multiple scattering (non-linear) [64]. The concentration at which this occurs is sample specific. In stead of diluting the sample it is possible to shorten the path length, it will have the same effect. In our case when measuring the OD of bacteria dilution is used. However, in the microtiter plate reader (wallac 1420 VICTOR2) it is not possible to dilute and the OD should not be trusted outside the linear regime (above 0.2).
Fluorescence from gfp(ASV) was measured manually by using a Shimadzu RF-5301PC fluorimeter. Furthermore results was obtained from the wallac 1420 VICTOR2/3(Perkin Elmer) which measures the optical density and the fluorescence from a 96 welled microtiter plate, details found in Appendix F. Fluorescence spectroscopy involves using a beam of light, that excites the electrons in molecules of certain compounds as gfp(ASV) and causes them to emit light.
The protocol for the experiments can be found in Appendix F.

3.1.1.2 Control of Growth

The doubling times of *E. coli* in experimental cultures ranges from 20 min to several hours [35]. Many parameters of the cells such as macromolecular composition and cell size are dependent on growth conditions. In *E. coli* this dependency can be expressed as a growth rate dependency in stead of growth media. Growth experiments with many different media have shown that media that supports the same growth rate produce cells with the same macromolecular

composition [5].

3.1.2 The Kinetic Model

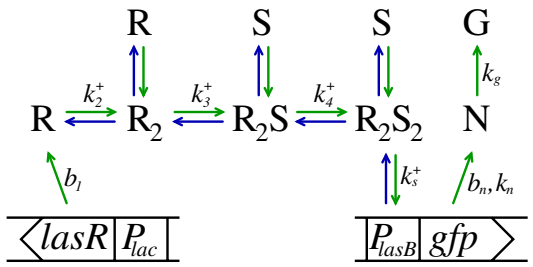

Figure 3.2: The diagram shows the interaction between LasR (R) and OdDHL (S). On-rates are written as k^+ and visualized by a green arrow. Corresponding off-rates are visualized by a blue arrow. LasR is constitutively produced at rate b_1 and either decays rapidly at rate λ_1 or forms a dimer, which decays slowly at rate λ_2. If OdDHL is present two signal molecules bind cooperatively to the dimer, which is protected against proteolytic decay. The *lasB-gfp*(ASV) reporter is used to monitor the R_2S_2 concentration which leads to the production of non-fluorescent GFP(ASV) (N) which matures into fluorescent GFP(ASV) (G) at rate k_g.

The conventional proposed model, which is seen to fit the experimental data very well is seen in Figure 3.2. The corresponding kinetic equations are seen and described in the following. The transcription (and translation) of regulator molecules R with concentration r_1 is given by equation 3.1 and is proportional to the concentration of *lasR* sites (R_t) and the transcription rate (b_1). This results in a steady production of LasR regulator which rapidly decays at rate λ_1.[1].
In the model we find support for that the LasR dimerizes (equation 3.2) into a stable state before binding OdDHL. The activation of the regulator occurs through the binding of the two signal molecules (equation 3.3 and 3.4). Cell division is included through the addition of the growth rate λ_c and proteolytic decay is included through the rates $\lambda_1, \lambda_2, \lambda_3 \text{and} \lambda_4$.

$$\frac{dr_1}{dt} = b_1 R_t + 2k_2^- r_2 - 2k_2^+ r_1^2 - (\lambda_1 + \lambda_c) r_1 \tag{3.1}$$

[1]However, the growth rate dependencies are neglected. The transcription rate and the plasmid copy number has been seen to be dependent on growth rate, see section 3.1.4. These dependencies work in opposite directions (in the interval 0.5 to 1.9 h^{-1}) which would limit the effect to some extend.

$$\frac{dr_2}{dt} = k_2^+ r_1^2 + k_3^- r_3 - 2k_3^+ r_2 s - (k_2^- + \lambda_2 + \lambda_c) r_2 \tag{3.2}$$

$$\frac{dr_3}{dt} = 2k_3^+ r_2 s + 2k_4^- r_4 - k_4^+ r_3 s - (k_3^- + \lambda_3 + \lambda_c) r_3 \tag{3.3}$$

$$\frac{dr_4}{dt} = k_4^+ r_3 s - (2k_4^- + \lambda_4 + \lambda_c) r_4 \tag{3.4}$$

The stable green fluorescent protein (GFP) from the jellyfish *Aequorea victoria* was made in several unstable versions by Andersen *et al.* [13]. We used the type called GFP(ASV) with a half life of the order 110 min[13].
An ideal reporter protein should reflect its promoters activity. However, this is not exactly the case for *lasB-gfp(ASV)*. The GFP must undergo modifications before becoming fluorescent. This is called the maturation process. This creates a rate-limiting step. The appearance of fluorescent lags some 25-48 min[2] behind the actual synthesis of protein. Furthermore, the GFP is quite resistant to proteolysis, with a half-life of 110 min, which means that once made the protein will persist in the cell even after the promoter is shut down. The growth rate should also be added since the faster the cells divide the faster the GFP is is diluted. [38]
A bacterium's fluorescent GFP (g) matured from the non fluorescent GFP (n) can be expressed mathematically including all previous considerations which has been done by Leveau and Lindow [38]. The non-fluorescent GFP concentration is depleted by maturation ($k_g n$), proteolytic degradation ($\lambda_n n$) and the cell division ($\lambda_c n$) and replenished by promoter activity (P), see equation 3.6. The non-fluorescent GFP becomes activated by the maturation step only depleted by degradation λ_g and cell division.

$$\frac{dS_a}{dt} = k_S^+ r_4 (S_t - S_a) - (k_S^- + \lambda_c) S_a \tag{3.5}$$

$$\frac{dn}{dt} = P - k_g n - \lambda_n n - \lambda_c n \tag{3.6}$$

$$\frac{dg}{dt} = k_g n - \lambda_g g - \lambda_c g \tag{3.7}$$

$$P = b_n S_t + (k_n - b_n) S_a \tag{3.8}$$

The promoter activity P is the sum of a small background production proportional to the number of free *lasB* promoter sites $S_f = S_t - S_a$ and an induced production proportional to the number of occupied sites S_a (S_t is the total concentration of sites).

[2] for a growth rate of $1.7h^{-1}$ and 0.5, respectively. Degradation rate λ_g=$0.7h^{-1}$

The sensor for the activated dimer level is the *lasB-gfp(ASV)* translational fusion. The rate of binding R_2S_2 to the *lasB* promoter site is proportional to the concentration of free sites $S_f = S_t - S_a$ and the concentration of activated dimers, see equation 3.5. The dissociation rate is proportional to the number of occupied sites S_a.

3.1.2.1 Model Behavior

This is a very short description of the model with focus on selected model properties, the details can be found in the paper B
Since the response follows second order cooperative kinetics, $\frac{s^2}{K_d^2+s^2}$, it is fair to assume that the regulator forms a dimer prior to binding to its cognate signal. Let us for the moment assume that the regulator molecule is a transient monomer. We then get a linear system for the total dimer concentration $r_d = [R_2] + [R_2S] + [R_2S_2] = r_2 + r_3 + r_4$:

$$\frac{dr_d}{dt} = \frac{b_1 R_t}{2} - (\lambda_d + \lambda_c) r_d, \tag{3.9}$$

$\lambda_d = (r_2\lambda_2 + r_3\lambda_3 + r_4\lambda_4)r_d$ and with the static solution:

$$r_d = \frac{b_1 R_t}{2(\lambda_c + \lambda_d)} \tag{3.10}$$

The total dimer concentration is seen to be independent of the signal molecule concentration, s. Thus, the dimer concentration can grow even though there is no signal molecules present. Of course, in the case of no signal molecules the total dimer would be equal to r_2 (R_2). In the next we will see that the signal molecule concentration determines the distribution between the dimers.
We assume that all dimers are well protected against proteases ($\lambda_c \gg \lambda_2, \lambda_3, \lambda_4$) and that the off rates for the ligand (signal molecule) binding is much larger than the growth rate ($\lambda_c \ll k_3^-, k_4^-$). The static solution becomes:

$$r_4 = [R_2S_2] = \frac{s^2}{s^2 + 2K_4 s + K_3 K_4} r_d \overset{K_3 \gg K_4}{\approx} \frac{s^2}{s^2 + K_d^2} r_d, \tag{3.11}$$

where $K_3 = \frac{k_3^- + \lambda_c}{k_3^+} \approx \frac{k_3^-}{k_3^+}$ and $K_4 = \frac{k_4^- + \lambda_c}{k_4^+} \approx \frac{k_4^-}{k_4^+}$. The last step in 3.11 is valid when there is cooperative binding ($K_3 \gg K_4$), that is binding of the second signal molecules follows the first instantly. We have $K_d^2 = K_3 K_4$ which is the effective dissociation constant. It will be shown later that we indeed have cooperative binding with Hill coefficient 2 as the data collapse give a good description of the data, seen in Figure 3.10.

In the case of cooperative binding λ_d changes to $\lambda_\mathrm{d} = (\mathrm{r}_2\lambda_2 + \mathrm{r}_4\lambda_4)/\mathrm{r}_\mathrm{d}$ and equation 3.9 becomes:

$$\frac{dr_d}{dt} = \frac{b_1 R_t}{2} - \left(\frac{K_d^2}{s^2 + K_d^2}(\lambda_2 + \lambda_c) + \frac{s^2}{s^2 + K_d^2}(\lambda_4 + \lambda_c) \right) r_d \tag{3.12}$$

The time scale in equation 3.12 is highly dependent on OdDHL (s) concentrations. When adding small concentrations of OdDHL the term proportional to $\lambda_2 + \lambda_\mathrm{c}$ is dominating while the timescale follows $\lambda_4 + \lambda_\mathrm{c}$ for large OdDHL concentrations. This will be used later to show that λ_2 and λ_4 must be equal.
The measured response of the system is the concentration of mature GFP, g and it is found by solving the equations 3.5, 3.6 and 3.7, see Paper B.

$$\begin{aligned} \frac{G(t) - G_0(t)}{OD} \overset{\lambda_c \gg \lambda_d}{=} & \underbrace{\frac{S_t b_1 R_t}{2K_S}(k_n - b_n)k_g}_{\mathrm{A}} \frac{1}{\Lambda_n}\frac{1}{\Lambda_g}\frac{1}{\lambda_c}\frac{s^2}{s^2 + K_d^2} f(t) \\ f(t) = & 1 - \frac{\Lambda_n}{\Lambda_n - \Lambda_g} e^{-\Lambda_g t} + \frac{\Lambda_g}{\Lambda_n - \Lambda_g} e^{-\Lambda_n t}, \\ \Lambda_n = & k_g + \lambda_n + \lambda_c, \quad \Lambda_g = \lambda_g + \lambda_c, \quad K_S = \frac{k_S^- + \lambda_c}{k_S^+} \end{aligned} \tag{3.13}$$

There are 4 parameters: A, λ_g, λ_n + k_g and K_d. The K_d is the effective dissociation constant and can be fitted separately, which will be seen in the data collapse in section 3.2.3. The resulting parameters can be seen in the Paper B. Since λ_c is seen to suppress the induced response through $\lambda_c^{-1}\Lambda_n^{-1}\Lambda_g^{-1}$ in equation 3.13 an increase in induced response should be seen for smaller growth rates. The parameter A depends non trivially on growth rate and is chosen for each of the growth rates separately. It contains the copy number effect and scales up for slower growth rates.
In order to explain the large response from the quasitationary inocula and the "overshoot" in the exponential inocula, that has not been in exponential mode long enough, we include a "memory" term. The activated dimer is written as a sum of the static growth term 3.11 and a "memory" term.

$$r_4 = \frac{b_1 R_t}{2(\lambda_d + \lambda_c)} \left(1 + m e^{-(\lambda_c + \lambda_d)t}\right) \frac{s^2}{K_d^2 + s^2}, \tag{3.14}$$

where m is the excess dimer fraction from past growth conditions. With this active dimer expression The OD-normalized response only differs by the f(t) becoming $\mathrm{f}_m(\mathrm{t})$

$$\begin{aligned} f_m(t) = & \frac{\Lambda_n \Lambda_g}{(\Lambda_n - \lambda_c)(\Lambda_n - \Lambda_g)(\Lambda_g - \lambda_c)} \\ & \left((\Lambda_n - \Lambda_g)e^{-\lambda_c t} + (\Lambda_g - \lambda_c)e^{-\Lambda_n t} + (\Lambda_n - \lambda_c)e^{-\Lambda_g t}\right) \end{aligned} \tag{3.15}$$

3.1.3 Is the Degradation Rate of Regulator Dimer Fast, Gone in 20 Minutes?

It is generally believed that LuxR homologues, including LasR cannot fold into its active form in the absence of an appropriate signal molecule. This assumption is mainly based on the inability to purify active regulator protein grown in the absence of signal which is seen in the regulators QscR [37], LasR [60], LuxR [63] and TraR [67, 68]. However when grown in the presence of signal it was possible to purify active regulator from all these regulators. Furthermore, LasR and TraR are seen to retain signal even after purification steps and dialysis against signal-free buffer suggesting that the binding is irreversible.

Recently contradicting evidence has been presented by Sappington *et al.*, thus challenging their previous work on the LasR regulator presented in [60]. They have presented evidence that LasR can fold into an active conformation in the absence of OdDHL and evidence indicating that LasR and OdDHL dissociate and reassociate in the cell [54].

LasR was produced in the absence of OdDHL by an arabinose inducible LasR, henceforth the cells were centrifuged and suspended in an arabinose free medium (LasR production turned off) where after OdDHL was added 0, 10, 20 and 30 minutes after resuspension. The LasR activity was monitored by the *lasI-lacZ* reporter by β-galactosidase activity.

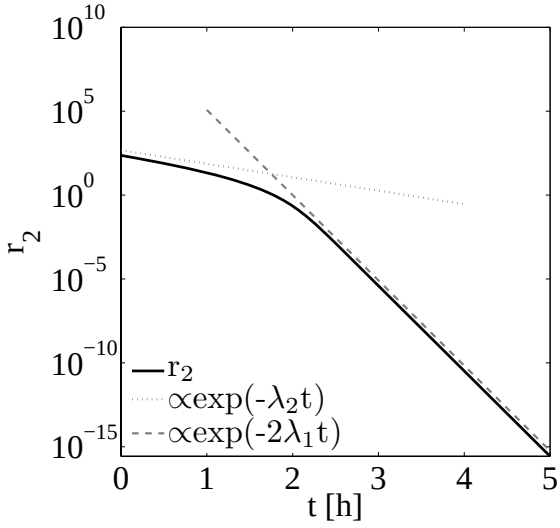

Figure 3.3: The concentration of dimer R_2 (r_2) in the absence of OdDHL and the production of LasR turned off. For the following values: λ_c=1.69, λ_1=20, λ_2=0.01, k_2^+=30 and k_2^-=10. Initial values, $r_1(0)$=9.54 and $r_2(0)$=233

When investigating Sappingtons data we found it strange that the response to OdDHL was lower when adding OdDHL later, as if the active dimer disappears rapidly, around 20 minutes. However, the dimer is found to be protected against proteases and if this is true it should not die out. We set out to try explain this with our model. We found that the apparent decay rate visible in the data

of Sappington *et al.* can be explained by that the dimer (R_2) is dissociating to monomer (R) which in turn are decaying fast.
The response to the OdDHL is instant suggesting the presence of active LasR before OdDHL was added though it seems to die out in 20 minutes. To find out why this happens we looked at our model in the limit of no OdDHL. We have a system only with the equations 3.1 and 3.2 were the regulator production is turned off ($b_t R_t$=0). When solving the quasistationary case (see Paper B) we get the relation $r_1^2 = K_2 r_2$, with $K_2 = \frac{k_2^- + \lambda_2 + \lambda_c}{k_2^+}$. From this it can be seen that for high values of regulator concentrations (r_1, r_2) the system is shifted towards dimer protein (r_2) while for small values of regulator concentrations the system is shifted towards monomer (r_1). For the values at which this occurs see details in Paper B.
The concentration of regulator dimer concentration (r_2) is seen in Figure 3.3 for the system (3.1 and 3.2, $b_1 R_t$=0) solved with ode45 in Matlab. The starting value is a high concentration of regulator and thus we see that the majority of regulator is on dimer form (plot of r_1 not shown). It is evident that two distinct decays are present. The first part of the curve can be fitted to a decay with rate $\propto \lambda_2$, thus the dimer is degrading with this slow rate for high concentrations of regulator. Likewise the monomer disappears at the slow rate ($\propto \lambda_2/2$) for high regulator concentrations. However, for very small concentrations of regulator the degradation rate becomes rapid. As seen in Figure 3.3 there is a "shoulder" after which a much more rapid decay is seen. For the dimer the decay rate is $\propto 2\lambda_1$ for small concentrations of regulator while the decay rate is twice as big for the monomer, $\propto \lambda_1$.
In the case of the data of Sappington *et al.* the decrease in response can be explained by looking at Figure 3.3. The system in question must be between the two degradation rates, on the shoulder of the curve in Figure 3.3. This is the only place where the apparent degradation accelerates with time, as is seen in [54]. Thus, the appearance is that the dimer degrades but it is actually the dissociation followed by degradation of the monomer which is seen.
In addition, this shows us that in a system with high plasmid copy number the entire system would be shifted towards dimer form (r_2) and thus the decay $\propto \lambda_2$, because of the high regulator concentration. However, a system with low plasmid copy number might be shifted towards the monomer form. We use a strain with a higher plasmid copy number and find the system in the dimer form while Sappington *et al.* use the plasmid pBR322 which has a low plasmid copy number and this might be why their system operate closer to the monomer region.

3.1.4 Growth Rate Dependency: Copynumber and Transcription Rate

The plasmid copy number has to our knowledge not been reported for the pMLAS in *E. coli*. However, the plasmid pMLAS is made on the basis of the pUCP22NotI plasmid which again originates from PUC18 with the parental plasmid pBR322. The high copy number of pUC18 compared to pBR322 is the result of a (G→A) point mutation in RNA II and deletion of the *rom*[3] gene [39]. Introduction of a corresponding point mutation into pBR322 results in elevated copy number only in the absence of Rom [39]. Moreover, the copy number of the plasmid with the point mutation alone or the *rom* knockout plasmid or the plasmid with both features was seen to increase for high temperatures and decrease for low [39]. However, this was not seen for pBR322. The copy number for the pUC18 plasmid at 37°C is reported to be around 50 and the copy number for pBR322 was reported to be around 20 by Lin Chao *et al.* [39]. Unfortunately the growth rate is not given, but since the growth medium is nutrition rich (LB broth) it must be at a relative high rate which means that this is a low estimation for copy number [14]. Elsewhere, the copy number has been predicted to be above 100 in *E. coli* (pUCP18)[55].
In Atlung *et al.* they investigate copy number as a function of growth rate for the pBR322 plasmid and the pBR322 plasmid without the *rom* gene [14]. They found that the copy number per mass increased proportionally to generation time (from 22 - 100 min) both for the pBR322 strain and the rom^- plasmid. However, the plasmid with rom^- increased approximately twice as steeply. For both plasmids the increase stops at 80-100 min doubling times and is flat untill a generation time of 200 min. Thus for slow growth rates the copy number per mass is approximately constant. For the plasmid lacking the *rom* gene the copy number per mass increased approximately 7-10 fold when going from 22 to 100 min doubling time (growth rate from 1.9h^{-1} to 0.42h^{-1}). At high growth rates no difference was seen in copy numbers for the plasmid with or without the *rom* gene.

When in exponential growth, the RNA polymerases and ribosomes are growth rate dependent and it thus follows that the gene expression is growth rate dependent also [35]. In constitutive promoters, as P_{lac}, transcription rate was found to increase at slow growth and saturate at fast growth [35]. From a growth rate of 0.5 h^{-1} to 2 h^{-1} the transcription rate per gene increases approximately 3 fold proportional to the growth rate. This effect is the opposite of the copy number versus the growth rate for approximately the same growth rate interval. The rate of a constitutive expressed protein is given by the following by Klumpp

[3]Previously called rop gene.

et al. [35]:

$$b_1 = \frac{\alpha_m \alpha_p}{\beta_m} \tag{3.16}$$

Where α_{m} is the transcription rate per copy of the gene, β_{m} is the mRNA degradation rate, and α_{p} is the translation rate per mRNA. The translation rate was determined for the LacZ transcript and was found to be independent of growth rate in the range between 0.6 to 3 doublings per hour[35]. The finding is found typical by Klumpp *et al.* and the translation rate is thus assumed growth rate independent. Likewise, the degradation of mRNA is found independent of growth rate [35].
In our case the total dimer is described as equation 3.12, where the first term is production of regulator molecules, b_1 being the rate and R_t being the concentration of *lasR* sites. Indeed, it is exactly these two parameters that contain the transcription rate and the copy number, which means that they are a function of growth rate. The transcription rate is included in the parameter b_1, see equation 3.16 were α_{p} and β_{m} are measured and found constant by Klumpp *et al.*[34]. The decay rate of the protein is included in the other terms in equation 3.12. The copy number is directly related to the number of *lasR* sites, R_t. Thus, for lower growth rates copy number should increase and the transcription rate should decrease (in the interval: $0.42\mathrm{h}^{-1}$ to $1.89\mathrm{h}^{-1}$) resulting in a big R_t value and a low b_1. However, we have not included the growth rate dependencies in our model and this will therefore produce an effect scaling the output up for low growth rates. The transcription rate will remove some of the effect arising from the copy number.
The same effect is seen for the description of the production of GFP. Again the copy number is directly related to the *lasB-gfp(ASV)* sites, S_t [4], see equation 3.8. Likewise, the transcription rate of the non- constitutive promoter, P_{lasB} will be included in k_n-b_n. The effect is the same as for the LasR production and is not included in this model. Due to the growth rate dependencies of the copy number and the transcription rate we shall not attempt to use the absolute scale in our interpretations.

3.2 Results and Discussion

Our results have been obtained from fluorescence spectroscopy. With the fluorimeter and the gfp(ASV) reporter gene it is possible to follow the induction of the gene-product. The production rate, the slow turnover, and the maturation all cause a significant delay.

[4] $\mathrm{S}_t = \mathrm{R}_t$, they only have different names to distinguish them.

3.2.1 Victor Measurements

The results obtained from the wallac 1420 Victor2/3 (Perkin Elmer) is described in this section. We have used three microplate readers, one wallac 1420 Victor2 and two wallac 1420 Victor3, henceforth known as Victor1, Victor2 and Victor3, respectively. How the instruments differ is not relevant in our study, but there can be instrumental variations. When comparing experiments it will always be from the same instrument unless otherwise explained.
In every experiment several concentrations of signal molecule are measured by making dilution rows: $C_0, 2^{-1}C_0, 2^{-2}C_0, 2^{-3}C_0, ...2^{-n}C_0$, where C_0 is the max concentration and n is number of dilution rows. Furthermore, the gfp background is measured, this is denoted g_0, and also an OD reference measurement. There are 6-12 repetitions of the gfp background, of the OD reference and of each of the concentrations.
To get a comparative measure for the gfp level of each concentration the background gfp, g_0 is subtracted. The gfp is normalized with OD to get a value of gfp per cell mass, but since we have no possibility to dilute the sample during the measurement we run into the multiple scattering problem described earlier. However, in lack of better we normalize with the OD. The gfp background value is used to find the growth rate by fitting to an exponential when in exponential growth phase.

In Figure 3.4 the results from four almost identical experiments are seen. The only differences lie in the concentration and the instrument. The concentrations range between 500 nM and 16 μM, the first two being identical (a and b). Each experiment has 12 concentration with 7 repetitions. For all four experiments saturation is achieved at the same concentration of 62.5 nM. Furthermore, the concentration at which we are half way to the maximal induced state is at 16nM for all 4 experiments. This value corresponds to the the dissociation constant, K_d. The exponential growth rates are 0.64, 0.68, 0.66 and 0.65 h^{-1}. From this figure it can be seen that the the results are comparable and it is possible to make reproducible results.
In Figure 3.5 two different OdDHLs are compared. The experiment is made in the same microtiter plate with the exact same bacterial culture batch, the only difference is the OdDHL used. Furthermore, 2 measurements are made where the OdDHL is substituted with the supernatant of Pseudomonas aeruginosa PAO1 in order to have a measure for the highest activity possible. It is seen as 7 in Figure 3.5, b and c. The level of the normalized gfp production does not differ but the saturation level and dissociation constant K_d does.
As mentioned the LasR regulator binds the OdDHL and activates the gfp production in the strain MH155. It is thus critical how well the OdDHL binds to the regulator LasR. The exact form of the OdDHL, the length of the acyl chain, and the 3-oxo-moiety, have been shown to be very important for binding to the

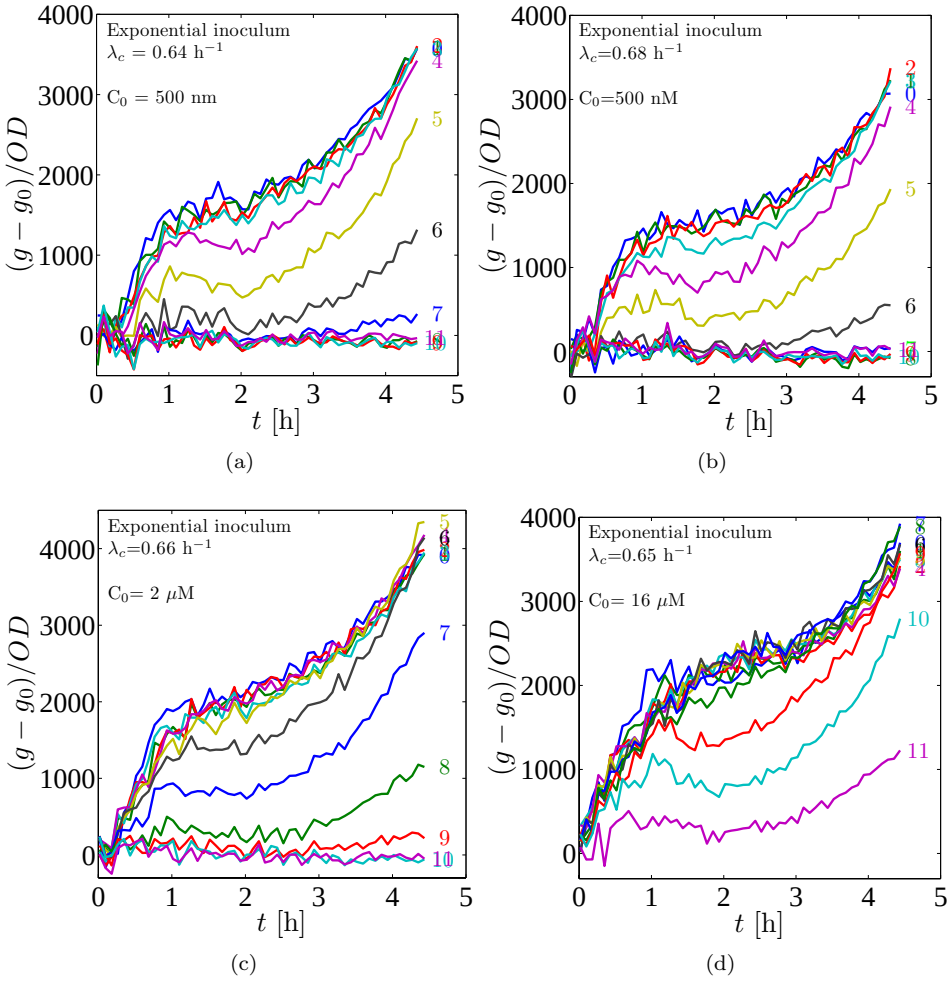

Figure 3.4: Background subtracted (G_0) GFP and normalized with OD. Exponential inoculum. In Figure (a) and (b) the same concentration of 500 nM is the max concentration, C_0. In (c) the concentration max is 2μM and in (d) it is 16 μM. For all four experiments the same concentration of 62.5 nM is the saturation limit. The exponential growth rate is 0.64, 0.68, 0.66 and 0.65 h^{-1}. Instrument used (a) Victor2, (b) Victor3, (c) Victor2 and (d) Victor3.

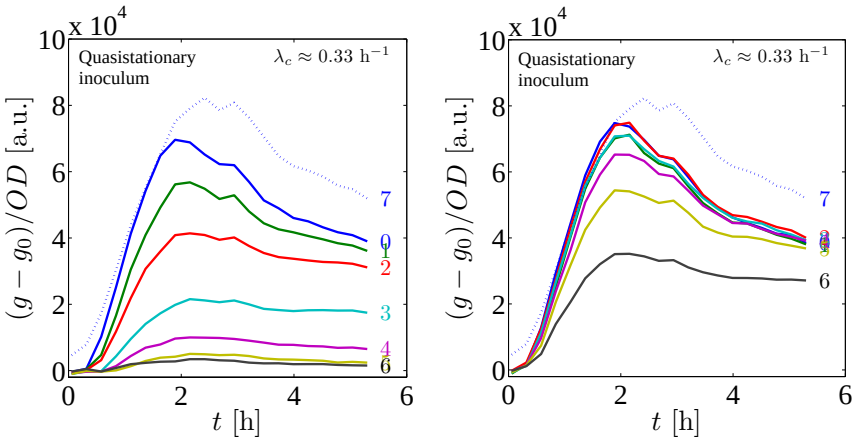

Figure 3.5: Background subtracted (G_0) GFP and normalized with OD. Quasistationary inoculum. Two different batches of OdDHL, my old one has a lower efficiency (a), and the new one (b) has a high efficiency, it is saturated for a concentration of 6.3nM. The concentration in both figures are: 100 nM (0), 50 nM (1), 25 nM (2), 12.5 nM (3), 6.3 nM (4), 3.1 nM (5) and 1.6 nM (6). (7) is with added supernatant from PA01. Instrument used Victor1

LasR regulator [47]. It could be imagined that a small ratio of the less active OdDHL in some way has changed to a form less active. Or that the less active OdDHL is less pure.

Another interesting observation in Figure 3.5 is the larger response to the introduction of OdDHL than we have seen in previous studies, see Figure 3.4. This is due to the fact that the culture is from quasistationary inocula and not from exponential inoculum, and the same behavior is seen in many experiments, not shown here. This large reponse only fades after generations of exponential growth. This observation suggest either that growth dependency of the copy number makes the signal go up or that the regulator protein dimer under the low growth rates is accumulated and does not disappear readily because it is long-lived. This prompted us to examine whether the maximal concentration of active LasR is a measure of the growth rate, which it would actually be in both cases.

We would like to compare different growth rates so we first thought of reducing the temperature from 37°C to 30°C to obtain a change of the growth rate. In Figure 3.6 these two temperatures are compared. A small change in growth rate can indeed be seen, from 0.69 h^{-1} to 0.57 h^{-1}. Furthermore, the saturation happens at slightly different concentrations, 12.5 nM for 30°C and 3.1 - 6.3 nM

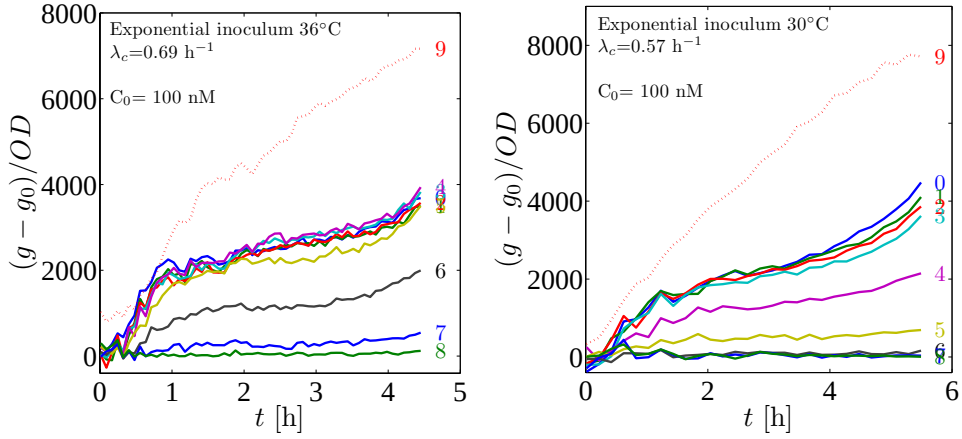

(a) (b)

Figure 3.6: Background subtracted (G_0) GFP and normalized with OD. Exponential inoculum. (a) is 36°C and (b) is 30°. OD measurements are fitted to a growth rate of 0.69 h^{-1} and 0.57 h^{-1}, respectively. The concentration in both figures are: 100 nM (0), 50 nM (1), 25 nM (2), 12.5 nM (3), 6.3 nM (4), 3.1 nM (5), 1.6 nM (6), 0.8 nM (7) and 0.4 nM (8). Instrument used Victor2 for both experiments.

for 37°C. The dissociation constant is around 6.3 nM for 30°C and 1.6 nM for 37°C. Also the plot of the lower temperature seems to be more flat, increasing more slowly to the same value (1500 vs 2000).
In the works of Lin-Chao *et al.* it was found that the copy number of the pUC18 plasmid varies greatly with temperature. From a copy number of around 50 at 37°C to a copy number around 20 at 30°C and increasing to around 180 at a temperature at 42°C. This temperature dependence is thought to stem from an alteration of RNA II formation due to the point mutation [39]. At 42°C the increase in copy number is followed by a decrease in growth rate approximately one hour after the temperature up-shift. This does not fit with the higher growth rate that we see for the higher temperature and we must dismiss this result as being an uncertainty of the fit of the growth rate.
There are slight variations between the two different temperatures but nothing significant.

3.2.2 Manual Measurements

When preparing a series of *in vitro* experiments to investigate the binding of LasR to OdDHL (reported as activation of *lasB-gfp* expression) we made an interesting observation. Cultures brought to exponential growth directly from overnight inocula had a much larger response to the introduction of OdDHL than inocula that had been growing exponentially for a long time. Only after many generations does this "memory" fade. This observation could suggest that the regulator protein enters a long-lived, dimerized form which enables it to "remember" the growth status of the overnight culture. However, an elevated plasmid copy number in starting could produce a similar effect.

We measured the response to introduction of signal molecules at two different growth rates. ($\lambda_c = 0.54 h^{-1}$ and 1.7 h^{-1}). The effect is present at both growth rates. In Figure 3.7 the two growth rates can be seen, both for exponential inoculum, (a) and (b), and for quasistationary inoculum, (c) and (d).

According to our model we should see an increase in response for lower growth rates because of the suppression from the growth rate (through $\lambda_c^{-1}\Lambda_n^{-1}\Lambda_g^{-1}$) but also from the scaling factor A, see equation 3.13. This is exactly what we see in Figure 3.7 when comparing (a) and (b) we see around an 8 fold increase. The cultures are brought up to exponential growth from exponential inocula and thus there should be no or a limited effect from the slow growth of the overnight culture. However, when fitting the model we do see an effect in both experiments (however very small in the slow growth) see Figure 3.10c for the fit. This is because the cultures have not been kept in exponential growth mode sufficiently long to bring down the "memory" (which is a result of elevated copy number or an accumulation of long-lived dimer from the previous quasistationary state). The effective dissociation constant is 11 nM and 7 nM for the slow and fast growth, respectively.

The experiments starting from quasistationary cultures have an enhanced response compared to the experiments starting from exponential inocula but with approximately the same growth rate. The response increases around 4 fold for the lower growth rate and 8 fold for the higher growth rate. This is either caused by the build-up of long-lived dimer regulator proteins or the enhanced copy number of slow growth. In Figure 3.8 we see the slowest growth at $\lambda_c = 0.34$ h^{-1} obtained in our study. The experiment is from exponential inoculum and is comparable to the experiment with growth rate $\lambda_c = 0.54$ h^{-1} in the induced response. At first one would expect the response to be further increased because of the low growth rate, but this is not the case. The growth rate at $\lambda_c = 0.34$ h^{-1} is outside the interval where the copy number is inversely proportional to the growth rate (for the plasmid pBR322 rom^-). As seen in the study of Atlung *et al.* the copy number becomes constant for growth rates smaller than 0.5 h^{-1} therefore the increase due to copy number is gone for the growth rate of 0.34 h^{-1}. However, the transcription rate is thought to continue to decrease

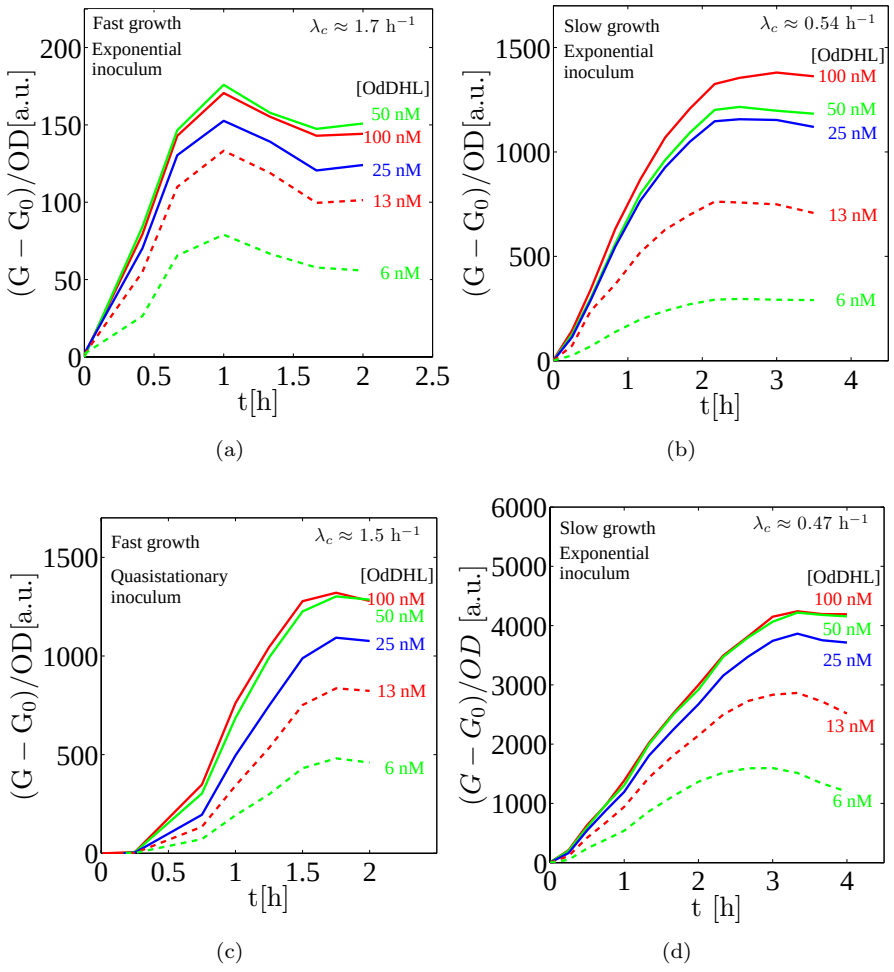

Figure 3.7: Background subtracted (G_0) GFP and normalized with OD. Figure (a) and (b) are the response of exponentially growing cultures from exponentially growing inocula at two different growth rates. The fast growth (a) is obtained using casamino acids as amino acid source. The slow growth (b) is obtained with L-leucine as sole amino acid source. Figure (c) and (d) are the response of exponentially growing cultures from quasistationary inocula (OD_{450nm} of 3.4 and 2.9 respectively). Due to the build-up of regulator molecules the experiments starting from quasistationary cultures have an enhanced response. This show that the regulator dimerization occurs before its binding to the signal molecules. The growth rates are 1.7h^{-1} (a), 0.5h^{-1} (b), 1.5h^{-1} (c) and 0.5h^{-1} (d). The concentrations are: 100 nM (0), 50 nM (1), 25 nM (2), 12.5 nM (3) and 6.3 nM (4).

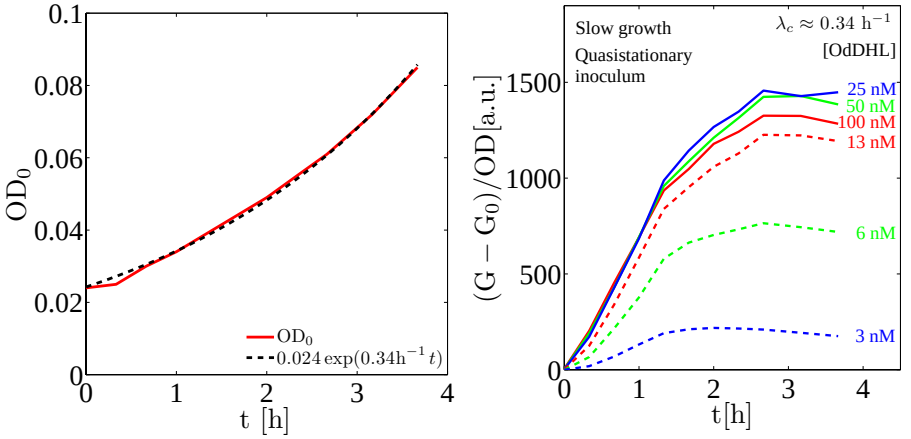

Figure 3.8: Background subtracted (G_0) GFP and normalized with OD. Figure (a) and (b) are the EXP in the media (glycerol and leucine). The growth rate is 0.34 h^{-1}. The concentrations are: 100 nM (0), 50 nM (1), 25 nM (2), 12.5 nM (3) and 6.3 nM (4).

with deceasing growth rate down to 0.3 h^{-1}[5] so this would make the induced response smaller compared to at $\lambda_c = 0.54$ h^{-1}. We do not see any decrease in induced response and it could be speculated that the small "overshoot" or in this case "memory" is caused by accumulation of long-lived dimer from the previous quasistationary state.

3.2.3 Dimerization Formed before Ligand Binding

Several observations support that the dimerization of the regulator molecule must occur prior to the signal molecule binding. First, we show that there must be cooperative binding of the two signal molecules in order for the data to fit the model. Second, the system has an instant huge response to OdDHL indicating the presence of stable LasR (long-lived) even in the absence of OdDHL. Third, we observe identical timescales to the response to different concentrations of OdDHL which means that the regulators present must have the same life-time (degradation rate).

[5]Unpublished, email correspondence with Dr. Stefan Klumpp, Max-Planck-Institut für Kolloid- und Grenzflächenforschung, Wissenschaftspark Golm, 14424 Potsdam, Germany (klumpp@mpikg.mpg.de)

In section 3.1.2.1 we make the assumption that we have cooperative binding of OdDHL and thus we make the second approximation in 3.17.

$$\begin{array}{lllll} a) & R \rightarrow RS \rightarrow (RS)_2 & \left(\frac{s}{s+K}\right)^2 & Ligand\ \ binding\ \ before \\ b) & R \rightarrow R_2 \rightarrow R_2S_2 & \frac{s^2}{s^2+K^2} & Cooperative \\ c) & R \rightarrow R_2S \rightarrow R_2S_2 & \frac{s^2}{s^2+2Ks+K^2} & Non-cooperative \end{array} \tag{3.17}$$

Second order cooperative binding is seen to to give a very good description of the dependence on s by the data, as seen in Figure 3.10. However, it could be that the case without cooperative binding fits just as well or that the case of ligand binding before dimerization is a good fit, seen in 3.17 c and a respectively. To see whether we have made an appropriate approximation we first look at the case without cooperative binding. A fit with a s-dependence as in 3.17 c can be seen in Figure 3.9 b. The figure displays a data collapse, that is the modeled response is divided by the s-dependence, in this case $\frac{s^2}{s^2+2Ks+K^2}$. This should make all the curves for different concentrations gather into one if the fit is appropriate. Compared to the cooperative binding this is a poor fit, thus we must conclude that according to the kinetic model cooperative binding is a better approximation than non-cooperative binding. The first approximation in 3.17 a, is where ligand binding occurs before dimerization and this is the case that is generally thought to occur. In 3.17 a) is indistinguishable to c). However, a) is expected to have response times dependent on on s. The fit to $\frac{s}{s+K}$ can be seen in Figure 3.10 a, and it is seen to be very poor, which shows that the signal molecule does not bind to a regulator monomer according to our data.

The "overshoot" seen in the quasistationary inocula experiments and the exponential inocula experiments where the culture has not been kept in exponential growth mode sufficiently long can either be explained by the elevated level of plasmid copy number due to low growth rate or residues of the long-lived dimerized regulator from the overnight inoculum or a combination of the two. Both of these explanations would give the same form of contribution to the kinetic model, see equation 3.14. Furthermore, both would lead to elevated levels of the regulator and both explanations arise from lower growth rates.
In the case where the explanation is residues of regulator from the overnight inoculum the regulator would have to be in a stable form, thus dimerized. Then when adding signal molecules the dimers would become rapidly activated, explaining the elevated response. In the case of the quasistationary inocula you could say that the system "remembers" its previous state due to the dimer protein level.
The activated dimer level is written as a sum of a static growth term and a

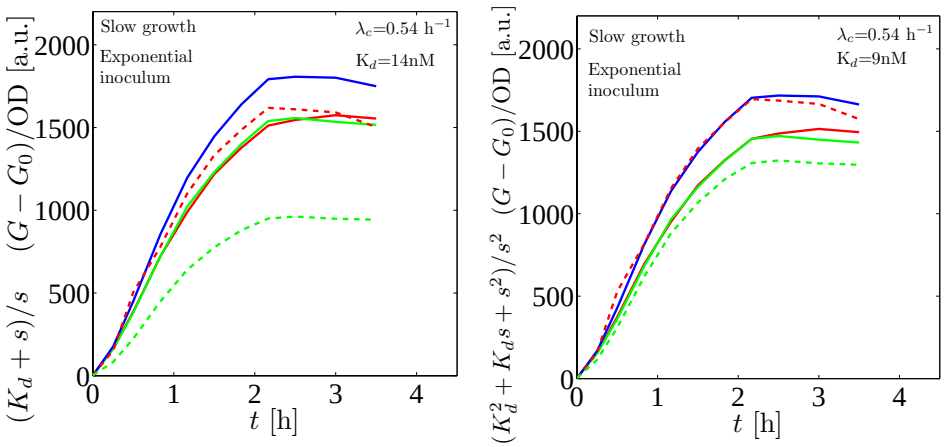

Figure 3.9: Data collapse of the induced response of MH155 to predetermined concentrations of OdDHL (100nM, 50nM, 25nM, 12nM and 6nM). The data collapse is obained by dividing with a) $\frac{s}{s+K}$ and b) $\frac{s^2}{s^2+2Ks+K^2}$ as indicated on the ordinate. This shows that the behavior of the data cannot be explained by any of these forms. Both figures are from exponentially growing inocula at the growth rate $\lambda_c = 0.54$ h^{-1}.

"memory" term, see equation 3.14. This explains the elevated response for overnight cultures as well as the "overshoot" observed in cultures that have not been kept in exponential growth mode sufficiently long to bring down the concentration. In Figure 3.10 the fit is seen with and without the memory contribution for the three growth rates available and from exponential inocula. It is clear that the fit is improved by adding this memory term, which is very evident in the fast growth were there seems to be a large "overshoot", probably due to the fact that it has not been in exponential mode long enough to bring down the concentration of dimers or the copy number.
The lowest growth rate is outside the interval of the inversely proportional relationship between copy number and growth rate, as mentioned before, which means that the memory term fitted here cannot arise from copy number. It could be speculated that this reflects that the long-lived residues of dimer do indeed explain at least some of the memory term and that the regulator present must be dimer in order to be stable enough to survive from overnight cultures.

Since we have assumed cooperative binding the degradation rates of the dimer are dependent on λ_2 and λ_4. Furthermore, we have assumed that all dimers are stable, also without its cognate signal. To rule out that r$_2$ could be short lived

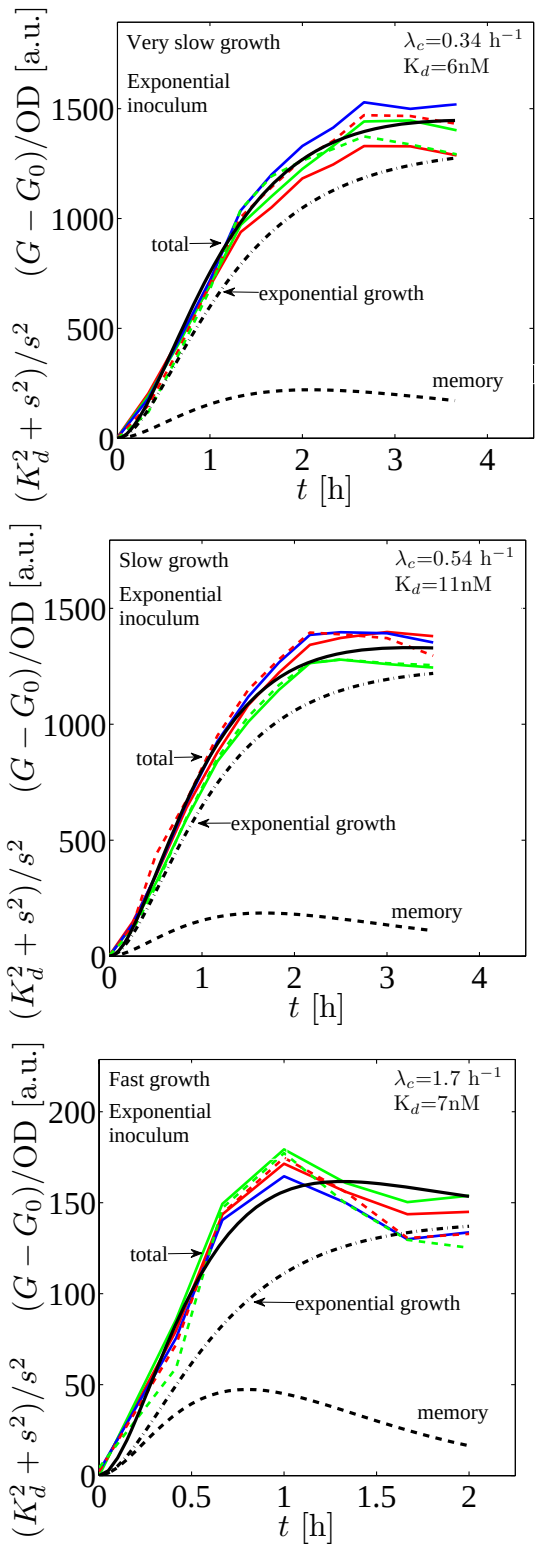

Figure 3.10: Data collapse of the induced response of MH155 to predetermined concentrations of OdDHL (100nM, 50nM, 25nM, 12nM and 6nM). The data collapse is obained by dividing with $\frac{s^2}{s^2+K^2}$ and is seen to fit the data very well for all growth rates. This shows that our data supports cooperative binding. The growth rates are a) $\lambda_c = 0.34$ h^{-1}, b) $\lambda_c = 0.54$ h^{-1} and c) $\lambda_c = 1.7$ h^{-1}. All three figures are from exponentially growing inocula.

we can imagine what would happen if we had $\lambda_2 \gg \lambda_4$. If we had different decay rates for λ_2 and λ_4 we would see that the active dimer would be dependent on the signal molecule concentration, following λ_2 for smaller s and λ_4 for higher concentration. Thus if λ_2 is short lived we would see fast response times for small signal concentrations and slow response times for large concentrations of signal. This time rate dependence can be seen in:

$$\lambda_d = \frac{K_d^2}{K_d^2 + s^2}\lambda_2 + \frac{s^2}{K_d^2 + s^2}\lambda_4 \tag{3.18}$$

However we do not see any dependence on signal molecule concentration. The response is instantaneous at all concentrations, thus both dimer forms must be well protected against proteases and equal, which is seen in equation 3.12.

3.3 Conclusion

A conventional kinetic model has been established which is greatly supported by our data. Furthermore, apparent contradictions between our data and other available data is resolved by this model.
The data together with the model explains several aspect of the interaction between regulator and signal molecule. In the model, the regulator monomer is decaying rapidly due to proteases while all dimerized regulators are protected against proteases. Moreover, the LasR regulator can fold into its stable dimer conformation in the absence of its cognate signal. In the presence of signal the dimer is activated through cooperative binding of the two signal molecules.

Appendix A

Paper I

Accepted for publication in Quantum Nanobiology and Biophysical Chemisty special issue of *Current Physical Chemistry*, volume 3, issue 2.
In this article we applied Surface Enhanced Raman Spectroscopy to the signal molecule *N*-dodecanoyl-L-homoserine lactone. We were able to detect signal molecule concentrations to below 1 nM concentrations.
This is a first author article and I was involved in all aspects of the work.

Detection of the quorum sensing signal molecule *N*-Dodecanoyl-DL-homoserine lactone below 1 nanomolar concentrations using surface enhanced Raman spectroscopy

Anetta Claussen[1,4,*], Salim Abdali[2], Rolf W. Berg[3], Michael Givskov[4,5], and Thomas Sams[1]

[1]*Biomedical Engineering, Department of Electrical Engineering, Ørsteds Plads 349, Technical University of Denmark, DK-2800, Denmark*

[2]*Biophysical Chemistry Group, Department of Chemistry, H.C. Ørsted Institute, University of Copenhagen, DK-2100 Copenhagen, Denmark*

[3]*Department of Chemistry, Energy and Materials, Technical University of Denmark, DK-2800 Lyngby*

[4]*Department of International Health, Immunology, and Microbiology, Panum Institute, Blegdamsvej 3B, DK-2200, Denmark*

[5]*Singapore Centre on Environmental Life Sciences Engineering, Nanyang Technological University, Singapore 637551*

[*]*Address correspondence to this email: acl@elektro.dtu.dk*

Keywords: Acyl-Homoserine Lactone, *N*-Dodecanoyl-DL-homoserine lactone, signal molecules, autoinducer, Surface-enhanced Raman spectroscopy, Quorum sensing.

Abstract

To the best of our knowledge we here for the first time demonstrate surface enhanced Raman spectroscopy (SERS) to detect a quorum sensing (QS) signal molecule below 1 nM concentration in both ultrapure water and under physiological conditions. Based on our results, SERS shows promise as a highly suitable tool for *in situ* measurements of low Acyl-Homoserine Lactone (AHL) concentrations in biofilms containing QS bacteria. Signal molecules communicate information about their environment and coordinate certain physiological activities in QS systems that exist in many bacteria. SERS enables detection of different AHLs at low concentrations due to structural differences observed in the corresponding SERS spectra. Ag colloidal nanoparticles, produced by the hydroxylamine reducing method, were used for the SERS measurements. SERS spectra of C12-HSL suspended in ultrapure water and in supplemented minimal medium were collected for 5 concentrations ranging from 2 μM to 0.2 nM, and a comparison between the spectra from these two media is also presented. We have been able to detect biologically relevant concentrations of AHL molecules ranging from 1 nM to 1 μM using SERS.

1 Introduction

Quorum sensing (QS) is an intercellular communication system by which some bacterial cells are capable of indirectly monitoring their own population density through exchange of signal molecules [1]. The expression of virulence factors is kept low until the population density (signal molecule concentration) reaches a threshold value, after which the host system is surprised by a stealth attack [1]. There are several different classes of signal molecules, which include Acyl-Homoserine Lactones (AHLs), autoinducing oligopeptides (AIPs), cyclic dipeptides, such as 2,5-diketopiperazines (DKPs), cholera autoinducer-1 (CAI-1), furanosyl diesters (also called autoinducer-2, AI-2), γ-butyrolactones (GBLs), Pseudomonas quinolone signals (PQSs), and diffusible signaling factors (DSFs) [2]. Furthermore, several hundred structural variants of the basic AHL molecule have been discovered, synthesized, and characterized [2]. In our study here we have looked at the signal molecule known as *N*-Dodecanoyl-DL-homoserine lactone or C12-HSL, where HSL corresponds to homoserine lactone, that originates from the class of AHLs. AHLs are composed of a conserved homoserine lactone and a fatty acid side chain which can vary in length (4-18 carbon atoms), level of saturation, and side-chain (oxo- or hydroxyl-) substitutions [2]. The distribution of the AHLs inside the bacterial cell is thought to depend on two different mechanisms with the short-chain AHLs freely diffusing in/out of the cells and the long-chain AHLs using an active-efflux mechanism to transport themselves in/out of the cells [2]. Outside the cell it has been proposed that the long-chain AHLs, like C12-HSL, should not easily be

able to move between cells in a diffusion-mediated manner owing to their poorer solubility relative to the short-chain AHLs [2].

The vibrational spectroscopic techniques of infrared (IR) absorption and Raman scattering spectroscopy are both noninvasive methods that yield molecular fingerprint information and have been shown to be fast and reliable methods to detect and identify/classify bacterial cells [3, 4, 5]. A comparison of the application of the two spectroscopies can be found in Harz *et al.* and Kirshner *et al.* [4, 5]. Kirshner *et al.* found that there is a consistency between the two methods, both spectroscopic techniques are able to be used to discriminate accurately at the strain level, and in addition both techniques showed themselves to be superior to conventional phenotypic methods. Raman spectroscopy has furthermore been used to study the metabolic states of bacteria [6], and the cultivation time dependence of bacterial cellular surface biopolymers [7]. In the work by Bak *et al.* the infrared spectra of the AHL *N*-butanoyl-L-homoserine lactone (C4-HSL) in the crystalline form and dissolved in CCl_4 have been measured and the IR and the Raman spectra have been calculated using Gaussian03 with the B3LYP hybrid exchange correlation functional (Kohn Sham, density functional theory) and the cc-pVTZ basis set for the solid state cluster model (a trimer mode)l [8].

In general, symmetric vibrations give the largest scattering cross section in Raman spectroscopy, while the asymmetric vibrations are the most intense in IR spectroscopy. This arises from what is known as the selection rules: bands which are strongly absorbing in the IR are weak in Raman and vice versa. For centrally symmetric molecules, there is even a mutual exclusion principle. The two techniques are often complementary, and used together, give a better view of the vibrational structure of a molecule. In the infrared, modes/bands which involve large changes in the electric dipole moment vector while in the Raman, modes/bands which involve large changes in the electric dipole - electric dipole polarizability tensor are intense.

A major limitation of Raman spectroscopy is the weakness of the Raman effect which results in very low signals, often below the limit of detection for dilute biological samples. Furthermore it suffers from a strong fluorescence background when lasers are used in the visible region which means that fluorescence from impurities or from the sample itself can mask the Raman spectrum. One can also use lasers at 632.8, 785, 833 and 1064 nm to alleviate problems due to fluorescence, but since the Raman signal is proportional to λ^{-4} the intensity is reduced. IR is much more sensitive than Raman, but its use in biological systems is very limited due to the strong absorbance of water in the fingerprint region, 500 cm^{-1} to 1800 cm^{-1}. Since we want to measure the spectra of AHLs in aqueous solutions, Raman spectroscopy is more suited for our studies. But since we also want to study very small concentrations, in the range between 10 μM and 1 nM, an enhancement of the conventional Raman scattering signal is needed. Such enhancements are known to be achieved by e.g. Surface Enhanced Raman Spectroscopy (SERS) [9, 10, 11], Resonance Raman (RR) [12], and Surface Enhanced Resonance Raman Spectroscopy (SERRS) [13]. Resonance Raman occurs when the frequency of the laser beam is close to the frequency of an electronic transition of a chromophore within the system under study. The enhancement is selective for the parts of the molecule involving the chromophore which adsorbs. Often fluorescence is a problem. In SERS the enhancement is a result of the plasmon resonance of the nanoparticle and even single molecules can be detected [14]. In SERS the native fluorescence associated with biological material seen in conventional Raman is suppressed. SERRS uses both the chromophore of RR and the plasmon resonance of SERS to achieve high enhancements, also here single molecules have been detected [13]. Like Raman, SERS has been applied with even greater success to bacteria samples in order to detect, identify and classify bacteria [15, 16, 17, 18].

Pearman *et al.* have investigated seven different types of signal molecules (differing by acyl chain lengths and varying from 4 to 12 carbons) using SERS with silver colloids, but not in the relevant concentration range, and not under physiological conditions [19]. It was found that all spectra were similar, however, the species with acyl chain length of 4 and 6, i.e. C4-HSL and C6-HSL, differed significantly from the others. For the signal molecule C12-HSL the authors were able to detect concentrations between 10 μM and 100 μM, which however is too concentrated to be biologically relevant for our QS system. Our requirement is to be able to detect AHLs at concentrations at least in the nanomolar range.

The C12-HSL molecule has 12 torsion angles that have

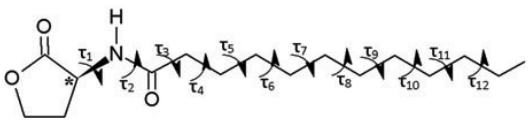

Figure 1: *N*-Dodecanoyl-DL-homoserine lactone, C12-HSL, and its 12 torsion angles.

different values in the different conformations that can change in order to place itself in different possible stable conformations, see Figure 1. The Newman projections for

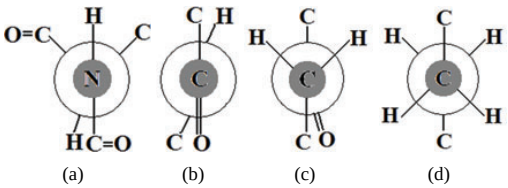

(a) (b) (c) (d)

Figure 2: The Newman projections for the first four torsion angles: τ_1, τ_2, τ_3 and τ_4.

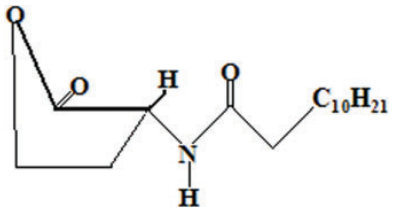

(a)

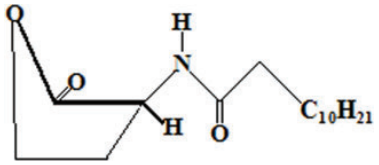

(b)

Figure 3: The ring puckerings, the endo (a) and exo (b) forms.

the first four torsion angles can be seen in Figure 2. Furthermore, since the molecule has a ketone group there is the possibility of keto and enol tautomerization in addition to the ring puckerings (endo and exo forms). Finally because of the asymmetric carbon (labeled with * in Figure 1) the molecule can be present in L or D states (configurations). Thus there are many structural possibilities. For some of the related AHLs some preferred states have been found. In the work of Bak *et al.* (using quantum calculations) the presence of two stable conformations, with respect to rotation around the NC bond linking the butyryl and the lactone moieties, of C4-HSL was revealed, corresponding to endo- and exo-conformations [8], see Figure 3. When including a contribution from a solvent medium by means of the polarized continuum model the preferred state was endo. In another work, Kim *et al.* investigated C6-HSL comparing quantum calculations with IR-spectroscopies, and found the preferred state also to be endo over exo [20]. In a study by Soulére *et al.* the focus was on the acyl chain. They investigated C14-HSL using molecular dynamics and found that the binding mode involved a curved conformation, for more information one is referred to [21].

It has been found that signal molecules can be changed by changes in the environment such as pH, or other species being present such as nitrates, oxidating agents, and degrading enzymes [22]. Alkaline pH catalyses the AHL hydrolysis, which leads to the lactone ring opening [23]. AHLs with longer acyl chain, such as C12-HSL used in this study, tend to be more resistant to hydrolysis than their shorter chain counterparts [23]. The AHL C6-HSL was shown to convert to several oxo forms when incubated in the presence of nitrates [22]. In the same way, oxidation of AHLs with photo generated HO was shown to lead to the formation of the corresponding oxo analogues [2]. The reaction of AHLs with oxidants, including hypohalites (salt of a hypohalous acid such as hypoiodite, hypobromite, hypochlorite, or hypofluorite) and hydroxyl radicals, can result in attenuation of AHLs by oxidation and subsequent inhibition of QS [2]. AHLs without additional functional groups on the acyl chain, such as C12-HSL, have been shown to be nonreactive to added hypohalites, while all AHLs were reactive with the hydroxyl radical.

Here we show that it is possible to acquire SERS spectra of C12-HSL from μM down to concentrations as low as 0.2 nM. This concentration range is well within the biological concentrations found in bacteria, the threshold typically being in the nanomolar range [2]. These spectra were acquired not only in aqueous solution, but also in a solution mimicking physiological conditions. The spectra are seen not to be quantitative, they do not appear to follow Beers law for their concentrations. This requires further investigation.

2 Materials and method

2.1 Materials

The *N*-Dodecanoyl-DL-homoserine lactone (C12-HSL) used in this study was purchased from Sigma-Aldrich. The molecular structure, the Newman projections for the first four torsion angles and the ring puckerings for the lactone ring (endo and exo form) can be seen in Figures 1, 2, and 3. A conventional Raman spectrum measured with a wavelength of 532 nm is seen in Figure 4. Supplementary minimal medium, ABtGcasa, was used as the physiological environment. ABtGcasa is made from ABt(B medium [24] plus 2.5 mg/l thiamine and 10% A10 [24]) supplemented with 0.5% glucose and 0.5% Casa amino acids. Water used in the experiments was ultrapure water from the Milli-Q Ultrapure Water System. Referring to ethanol

it is always ethanol 96%.

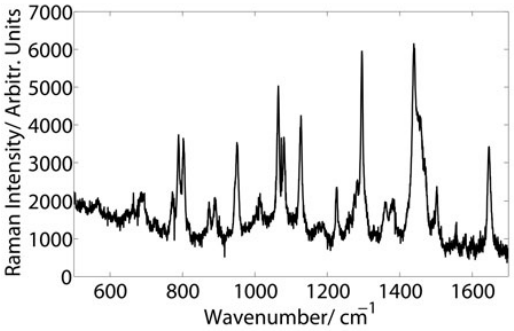

Figure 4: Conventional Raman spectra of *N*-Dodecanoyl-DL-homoserine lactone (C12-HSL) in the solid phase using a 532 nm wavelength laser, same as used for the SERS measurement.

2.2 Instrumentation

Surface-enhanced Raman spectra were recorded with the use of a frequency doubled Nd:YVO_4 laser at an excitation wavelength of 532 nm. Output power for all measurements was 250 mW. The experiments were performed with a dispersive Dilor-XY Raman spectrometer. Raman spectra were obtained using a liquid nitrogen cooled CCD using the Labspec software. The Raman spectrum of cyclohexane (C_6H_{12}), which is an alkane widely used to calibrate spectrometers since it exhibits very strong Raman lines at 801 cm^{-1} and 2852 cm^{-1}, was used for validation and calibration purposes. The band at 801 cm^1 was used for calibration. All spectra were collected with an exposure time of 6.7 sec and averaged over 2 accumulations. No baseline or background corrections were applied to the spectra shown. Gas chromatography target vials were used to contain the samples in the SERS measurements. The target vials were made from glass to ensure minimum interference in the spectra and had a diameter of 9 mm.
Ultraviolet visible (UV-VIS) extinction data was collected using a Shimadzu UV-1800 spectrophotometer. A quartz cuvette with a path length of 10 mm was used.

2.3 Ag preparation

The silver colloids used here for the SERS measurements were produced by reduction of $AgNO_3$ by hydroxylamine ions, following the method of Leopold *et al.* [25]. Under a steady stirring and at room temperature, 90 ml of 3.3 mM NaOH was mixed with 0.5 ml of 0.3 M hydroxylamine hydrochloride (HA HCl) and 10 mL of 0.01 M $AgNO_3$. The reduction took place immediately and the colloids were examined by UV-VIS and checked by Scanning Electron Microscope, SEM. The extinction spectrum of the resulting Ag hydrosol can be seen in Figure 5. The spectral top is found to be $\lambda_{max} = 405.25$ nm and the full width at half maximum (FWHM) is measured to be 68 nm.

For nanorods and nanoparticle aggregates, the plasmon

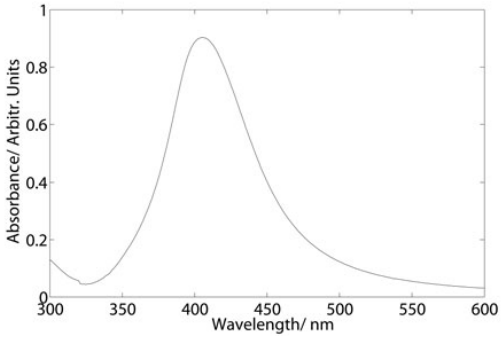

Figure 5: UV-VIS extinction spectrum of Ag colloids produced via hydroxylamine reduction method. A 9 times dilution is used.

absorption splits into two bands corresponding to the oscillation of the free electrons along and perpendicular to the long axis of the rods [26, 27, 28]. Since we only have one peak we therefore assume that the particles have a roughly spherical shape.
The absorption maximum of the measured UV-VIS spectrum of the colloidal solution provides information on the average particle size, whereas its FWHM can be used to estimate particle dispersion [25, 29]. For silver particles with a diameter smaller than 10 nm dipolar absorption is dominant [29, 30] and one can use the dipole approximation from Mie scattering theory to find a simple relationship between the FWHM and the radii of the particle. This approximation gives a band of Lorentzian shape. For larger radii particles, the absorption band begins to shift to longer wavelengths due to additional magnetic-dipole terms, thus the full expression of Mie's theory applies.
The extinction spectra obtained for the silver particles are quite broad with a tail on the higher wavelength side of the peak, see Figure 5. The tail could be due to the dipolar scattering and quadrupole absorption, and it indicates that the size of the particles must be large [31]. Since the absorption maximum is 405.25 nm the mean diameter of the silver colloid particles can be assumed to be approximately 23 nm according to [25] which uses the same

production method as this work. Also from [32] the mean diameter can be assumed to be between 20 and 24 nm. This is validated by SEM.

2.4 Sample preparation

N-Dodecanoyl-DL-homoserine lactone (C12-HSL) is only slightly soluble in water mainly due to the hydrophobic nature of the acyl chains. Thus, we decided to dissolve the solid C12-HSL in an organic solvent and thereafter dilute it with ultrapure water. The solvent chosen had to be without significant structure in the fingerprint region of the Raman spectrum (500-1800 cm^{-1}). We considered dimethyl sulfoxide (DMSO) used by Pearman *et al.*[19] and ethanol. Ethanol was chosen because of its weaker spectrum as compared to the DMSO spectrum. A stock solution of 10 mM was prepared by dissolving 1 mg of C12-HSL in 353 μl of 96% ethanol. A part of this stock solution was added to an eppendorf tube containing ultrapure water or ABtGcasa medium and manually shaken. The final C12-HSL concentrations ranged from 2×10^{-10} M to 2×10^{-6} M both in ultrapure water and in ABtGcasa media.

2.5 Setup and spectra

In order to achieve the best condition, which yields highest peak intensity, optimization of the volume ratio of the sample at 2 μM concentration to the colloids was carried out, using the same approach as in [33]. The volume ratios tested were 40 % sample to 60 % colloids, 50 % sample to 50 % colloids, 60 % sample to 40 % colloids, 70 % sample to 30 % colloids, and 80 % sample to 20 % colloids for the C12-HSL in water. For C12-HSL in ABtGcasa the volume ratios tested were 30 % sample to 70 % colloids, 40 % sample to 60 % colloids, 50 % sample to 50 % colloids, 60 % sample to 40 % colloids. For C12-HSL in water the spectra with the highest intensity was seen for the 60 % sample to 40 % colloids, and for the C12-HSL in ABtGcasa the 40 % sample to 60 % colloids gave the highest intensity.
The final AHL concentrations were 2×10^{-10} M, 2×10^{-9} M, 2×10^{-8} M, 2×10^{-7} M and 2×10^{-6} M for samples in water and ABtGcasa medium. Our smallest concentrations is 0.2 nM which is the equivalent of 0.2×10^{-9} mol/l or 1.2×10^{14} molecules per liter. The recording parameters were kept the same in all these measurements including the sample volume of 200 μL.
The sample diluted in ABtGcasa medium was controlled at a pH of 6.3 due to the A-10 buffer in the ABtGcasa solution. The pH in the sample diluted in water is assumed to be approximately 7, which is the pH of the colloid solution [25]. It is known that under alkaline conditions AHLs are susceptible to hydrolysis [2]. AHLs having longer acyl-chain (C12-C14) are significantly less susceptible to hydrolysis of the lactone, the half-life for C12-HSL being between 1 (pH=9.55) and 64 hours [23], 27 hours for a pH of 7.2. All sample solutions were measured within hours after preparation to limit any possible hydrolysis of the parent AHL.

3 Quantum lactone ring model

Quantum chemical calculations were performed with the GAUSSIAN 09 program [34] of a simplified acyl-HSL with only two carbon atoms in the acyl chain, called C2-HSL. Three versions of C2-HSL were compared to find the energy minimum: protonation on the amide carbonyl, protonation on the lactone carbonyl and the unprotonated C2-HSL, see Figure 6. The LC-wPBE density functional [35] combined with the 6-31Gdp [36, 37] basis set were used and the energy minimum was found for the unprotonated version, see Table 1. Hence, the B3PW91 density functional [38] and the 6-31Gdp basis set was used to obtain the Raman spectra of the unprotonated C2-HSL,

	Energies
structure	ΔE [kcal/mol]
UP	0
PL	17.811859
PA	51.24348

Table 1: Energy of the C2-HSL in the three states: protonation on the amide carbonyl (PA), protonation on the lactone carbonyl (PL) and the unprotonated C2-HSL (UP)

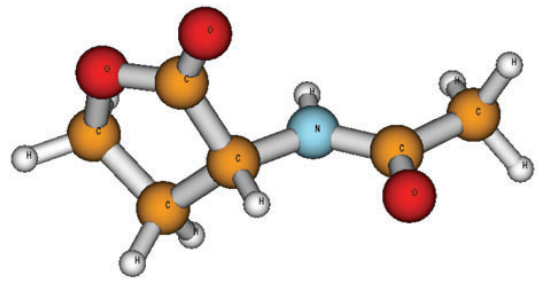

Figure 6: The optimized form of the unprotonated C2-HSL.

which can be seen in Figure 7. The theoretical wave num-

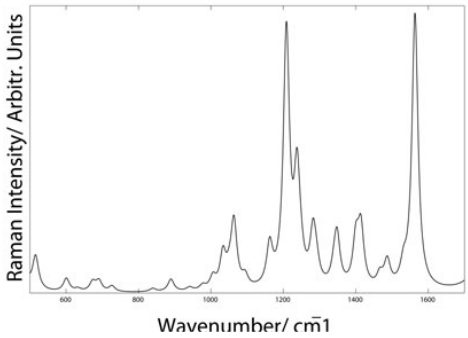

Figure 7: The theoretical Raman spectra of the unprotonated C2-HSL. The wave numbers are scaled by the factor of 0.9602 and a Lorentz lineshape with HWHM at 10 cm^{-1} is assumed.

bers are scaled by the factor of 0.9602 [45] and a Lorentz lineshape with HWHM = 10 cm^{-1} is assumed.

4 Discussion and results

The measured SERS spectra for C12-HSL with the range of concentrations given in the Materials and Methods section are presented in Figure 8 and 9. In these Figures the highest concentration is depicted in the top, decreasing in concentration towards the bottom, the concentrations being 20 μM, 2 μM, 200 nM, 20 nM, 2 nM, 0.2 nM and 0 M. The lowest spectrum is the control spectrum, that is, the spectrum of the same sample without C12-HSL. Figure 8 shows the spectra of C12-HSL dissolved in water and Figure 9 shows the spectra of C12-HSL dissolved in ABtGcasa.

The proposed assignment of the spectrum can be seen in Table 2 and shows all peaks observed both for the C12-HSL in water and in ABtGcasa and it is indicated at which concentrations the peaks were seen. Furthermore, Table 2 shows the positions at which we found ethanol and ABtGcasa in order to see whether these could interfere with the C12-HSL spectra. The C12-HSL spectra are dominated by contributions from the amide portion of the molecule, that is the majority of the strong spectral bands originates from the chain of C12-HSL. This was also seen in the work of Pearman *et al.* [19]. The vibrations attributed to the lactone ring are weak, except for the very strong vibration at 1363 cm^{-1} which is the CH_2 wagging vibration of the lactone ring according to the quantum chemical calculation conducted in this study and also accord-

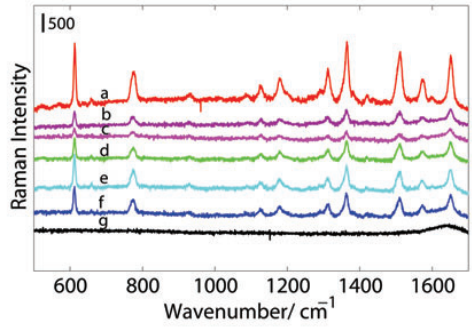

Figure 8: SERS of C12-HSL suspended in ultrapure water for the following concentrations (top down): 20 μM (a), 2 μM (b), 200 nM (c), 20 nM (d), 2 nM (e) and 0.2 nM (f). The lowest spectrum (g) is without any C12-HSL, thus only ultrapure water and Ag colloids are present.

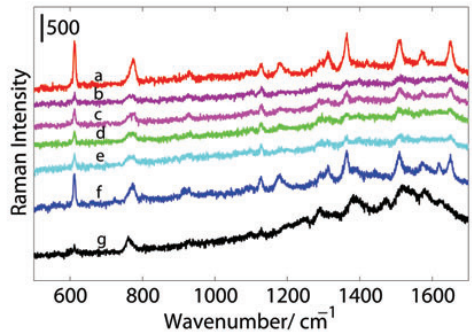

Figure 9: SERS of C12-HSL suspended in ABtGcasa medium for the following concentrations (top down): 20 μM (a), 2 μM (b), 200 nM (c), 20 nM (d), 2 nM (e) and 0.2 nM (f). The lowest spectrum (g) is without any C12-HSL, thus only ABtGcasa medium and Ag colloids are present.

ing to Jakubczyk *et al.* [47]. Furthermore, the medium band seen at 1178 cm^{-1} is attributed to the C-O stretch of the lactone ring. The very strong amide I band at 1650 cm^{-1} could also contain contributions from C=O in lactone. The amide I, II, III and IV bands at 1650 cm^{-1}, 1573 cm^{-1}, 1312 cm^{-1} and 773 cm^{-1}, respectively are all clearly identifiable for C12-HSL in the water solution while the amide II and III are less pronounced for the C12-HSL spectra in ABtGcasa for all concentrations except the highest, 20 μM where they are very clear. The band for the O=C-N bending vibration at 612 cm^{-1} is consistently the strongest band observed in the SERS spectra of C12-HSL both for the water solution and the ABtGcasa-solution.

Assignment C12-HSL

$\tilde{\nu}_{Ethanol}$ [cm^{-1}]	$\tilde{\nu}_{ABtGcasa}$ [cm^{-1}]	$\tilde{\nu}_{solid}$ [cm^{-1}]	$\tilde{\nu}_{calc}$ [cm^{-1}]	$\tilde{\nu}_{SERS}$ [cm^{-1}]	Observed in	Assignment	Ref.
		523	496	523$_{vw}$	1,2,4,5,6,a,f	O=C-C(lactone) scissoring, N-H def	calc
		566	578	573$_{vw}$	1,5,6,f	C-C=O scissoring/C-C, chain	calc/[19, 47]
	612			612$_{vs}$	1,2,3,4,5,6, a,b,c,d,e,f	O=C-N bending	[19, 47]
			647	639$_{vw}$	1,2,a,e,f	C-C-C symmetric stretch	calc
		664	662	660$_{w}$	1,2,3,4,5,6,a,e,f	asymmetric stretch ring	calc
		747-687					
	760	802-772		773$_{s}$	1,2,3,4,5,6,a,b,c,d,e,f	amide IV,	[19, 47]
						C=O deformation, N-H bend	
		888-874	856			ring stretch symmetric	calc
880$_{vs}$	928			929$_{w}$	1,2,3,4,5,6,a,b,c,d,e,f	C-O-C assymetric stretching (cyclic)	[19]
		950	967			CH_2 wagging	calc
		1014	992			CH def	calc
1052$_{m}$		1065	1021	1010$_{vw}$	1,6	C-C-C stretch, lactone	[19, 47]
1094$_{m}$	1098	1080	1050	1093$_{w}$	1,2,4,5,6,a,b,c,d,e,f,g	CH_2 rocking, lactone	[19, 47]
	1128	1127	1117	1128$_{m}$	1,2,3,4,5,6,a,b,c,d,e,f	C-H def./C-C-C	calc
	1197	1178	1161	1178$_{m}$	1,2,3,4,5,6,a,b,c,d,e,f	C-O stretch(lactone)	calc,[47]
	1246	1191	1188	1201$_{vw}$	1,2,5,a,c	CH_2 rocking	[46], calc
1277$_{w}$	1293			1291$_{vw}$	1,5,6,a,c,d,e,f	CH_2 wagging+bending, lactone	[47]
	1313	1296	1294	1312$_{s}$	1,2,3,4,5,6,a,b,c,d,e,f	amide III, C-N def.	[19]
	1333	1359	1356	1363$_{vs}$	1,2,3,4,5,6,a,b,c,d,e,f	CH_2 wagging, lactone	[47], calc
	1383			1382$_{vw}$	1,4,5,b,c,d,e,f	CH_2 wagging, lactone	[47],calc
				1419$_{vw}$	1,2,4,5,6,a	C-N stretch	[47]
1455$_{s}$		1380	1411	1439$_{w}$	1	CH_2 scissoring, lactone	[19, 47]
	1474	1439	1427	1469$_{vw}$	1,2,5,6,f	CH_2/CH_3 deformation, chain	[19]/calc
	1529			1511$_{vs}$	1,2,3,4,5,6,a,b,c,d,e,f	NH bending	[19, 47]
	1580	1503	1501	1573$_{s}$	1,2,3,4,5,6,a,b,c,d,e,f	amide II, NH def.	[19], calc
						(trans co-planar)	
				1601$_{w}$	1,2,4,5,6,a	NH deformation	[19]
	1622			1620$_{s}$	f	ABtGcasa	
		1646	1690	1650$_{vs}$	1,2,3,4,5,6,a,b,c,d,e,f	amide I, C=O ketone stretch	[19, 47], calc
		1779	1784			C=O lactone stretch	[47], calc

Table 2: Intensity codes: v=very, w=weak, m=medium, s=strong.
20 μM = 1,a, 2 μM = 2,b, 200 nM = 3,c, 20 nM = 4,d, 2 nM = 5,e, 0.2 nM = 6,f
solid, refers to the Raman spectrum of the solid crystal C12-HSL, calc refers to the calculated Raman spectrum of the C2-HSL using GAUSSIAN 09 with B3PW91/6-31Gpd, and SERS refers to the SERS spectra of the C12-HSL both in water and ABtGcasa.

The control spectrum for the water solution is featureless, see Figure 8(g). Clearly a reduction of the water background is seen, which is due to the adsorption by the silver nanoparticles. We chose to obtain spectra of C12-HSL in ABtGcasa solution, because this is a typical environment in which to grow bacteria. In this way we tested whether the solution interfered with the spectrum. A number of peaks were seen in the ABtGcasa but these peaks do not seem to dominate in the combined spectra, see Figure 9(g). However, many of the ABtGcasa-baseline peaks are positioned in similar areas as the C12-HSL peaks; this may result in the peaks in the C12-HSL spectra dissolved in ABtGcasa having an extra contribution from the ABtGcasa media. When comparing with the water dissolved C12-HSL spectra it can indeed be seen that the amide IV band at 773 cm^{-1} is broader since this band coincides with a band in the ABtGcasa spectra at an identical position. Because of the enhanced fluorescence caused by ABtGcasa to the right part of the spectra, see Figure 9, the peaks in this part are less enhanced. Furthermore, the majority of peaks in the ABtGcasa spectra lie in this right hand-side of the spectra causing the peaks of the C12-HSL to be broader and less identifiable. When inspecting the lowest concentration (Figure 9(g)) an additional peak can be seen at the wavelength 1620 cm^{-1}. This is proposed to be due to the ABtGcasa contribution which has a peak at 1622 cm^{-1}. Why it is not present for the higher concentrations could be due to the ratio of ABtGcasa to C12-HSL being much higher for low C12-HSL concentration. There is simply a much higher risk that ABtcasa bands are enhanced. The comparison of the C12-HSL in the two solutions at the lowest concentration can be seen in Figure 10. In this figure the peak at 1620 cm^{-1} proposed to be from the ABtGcasa solution is clearly seen.

As has been mentioned the strongest band in the C12-HSL spectra is the O=C-N band at 612 cm^{-1} both for the water and the ABtGcasa solution. However, the strongest band amongst the amide bands differs between the two solutions. For the water solution the strongest amide band is the amide I band while the strongest band for the ABtGcasa solution is the amide IV band, closely followed by the amide III band. The weakest band in both solutions is the amide II band. This suggest that the O=C-N band experiences a greater SERS enhancement and thus would also suggest an orientation of the molecule where the O=C-N is both closer to and nearly normal to the metal surface, thus experiencing maximum enhancement. That the second strongest band differs between the two solutions could mean that the orientation of the molecule adsorbed to the nanoparticle has changed.

As mentioned in the section, Setup and spectra the pH

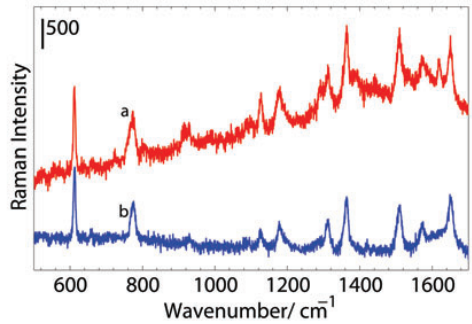

Figure 10: SERS of C12-HSL suspended in ABtGcasa medium (a: red) and for C12-HSL suspended in ultrapure water (b: blue) at 0.2 nM. The spectra of the lowest concentrations from Figure 4 (b:blue) and Figure 5 (a:red).

of the C12-HSL in ABtGcasa is assumed to be approximately 7, but it is not fixed and thus could be higher. At higher pH C12-HSL could undergo hydrolysis, resulting in opening of the lactate ring. In the study of Pearman *et al.* hydrolysis was investigated and the following new additional peaks observed: 1270 cm^{-1} attributed to carboxylic CO stretch band and 1432 cm^{-1} to a combination band, the latter due to carboxylic CO stretch and OH deformation [19]. None of these bands are found in the spectra in our study, thus we assume that no hydrolysis is occurring. Since hydrolysis halftime is found to be 27 hours for a pH of 7.2 and the longer acyl chain of C12-HSL makes it less susceptible to hydrolysis, we would not expect to see any signs of hydrolysis in our experimental conditions.

When inspecting the spectra of the C12-HSL in water in Figure 8 the intensity of the spectra can be seen not to drop with decreasing concentration. The highest intensity is found in the spectrum for the highest concentration, 20 μM . From 20 μM the intensity of all the peaks decreases with concentration until the concentration of 200 nM. At 20 nM the intensity level rises above the intensity levels of 200 nM and 2 μM. The intensity rising for 2 nM and hereafter decreasing for 0.2 nM. This non-linearity can be seen in Figure 11. The peak height at 612 cm^{-1}, corresponding to the O=C-N bending vibration and the peak heights of the amide I-IV bands, are followed and plotted against the different concentrations. All monitored peaks follow the same trend. In the case of C12-HSL suspended in water the intensity of the spectra seems to stop decreasing at around the concentration 200 nM. The decrease in intensity with falling concentration until 200 nM is what one would expect because the silver surface

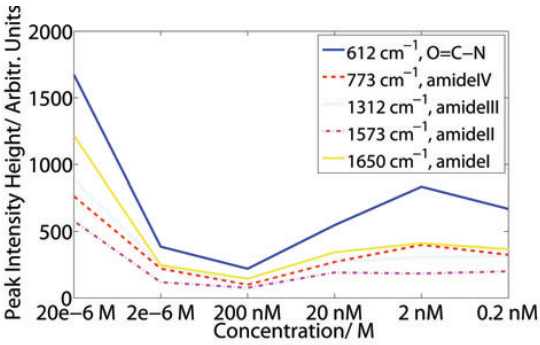

Figure 11: The peak intensity height at 612 cm^{-1}, corresponding to the O=C-N bending vibration, is followed through the different concentrations and plotted against the concentration. Likewise are the amide bands. Here we have the plot for C12-HSL in water solution.

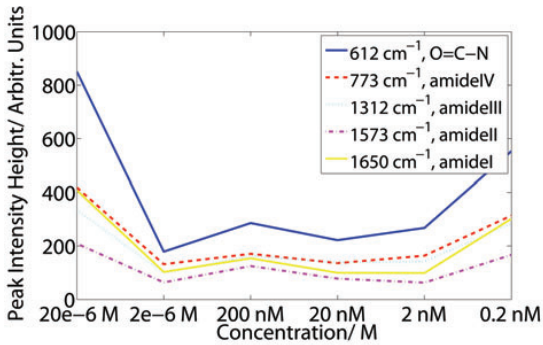

Figure 12: The peak intensity height at 612 cm^{-1}, corresponding to the O=C-N bending vibration, is followed through the different concentrations and plotted against the concentration. Likewise are the amide bands. Here we have the plot for C12-HSL in ABtGcasa solution.

area has less molecules adsorbed. However the fall can also be seen to be non-linear, which is seen in literature and thus why a small concentration range is often chosen [40, 42]. After 200nM the intensity increases until 2 nM. The increase in enhancement for the low concentrations could be explained by the existence of hot spots in the cluster structures, caused by thermally and non thermally activated diffusion of molecules into and out of hot areas, or trapping and release of molecules in high-field gradients [39]. It could also be due to the different adsorption geometries that can exist at different concentrations, as seen in [40, 41]. A major problem in SERS is not only the difficulty in reproducing amplification processes and variations in colloid sizes and shapes, but also the orientations of the adsorbed molecules on the colloid surfaces and whether they change orientation due to pH or other factors which may be changing. The same strange behavior is seen in C12-HSL in ABtGcasa, as can be seen in Figure 12.

To be able to use SERS to observe the change in concentration of signal molecules in bacterial cell cultures the technique has to be quantitative. This behavior is not achieved in this experiment, at least not over the many decades wanted. In conventional Raman all bands would scale linearly to our concentration, which is unfortunately not the case for SERS. Furthermore, since Ag ions and Ag nanoparticles have shown to be toxic to bacteria [43] future work should use coated Ag nanoparticles. The coatings could be polymers or antibodies and be designed to capture as well as protect the bacteria. The coating procedure has been successfully used in order to measure SERS spectra of unique or rare cancer cells [44].

5 Conclusions

We have demonstrated that it is possible to detect the signal molecule C12-HSL down to a concentration as low as two tenths of a nM. This is obtained in water and for the first time in ABtGcasa medium. The addition of ABtGcasa medium was shown to not interfere with the vibrations of C12-HSL. The first step towards using the SERS method for *in situ* measurements of low AHL concentrations in biofilms is thus met. However, to be able to deduce the AHL concentration from the SERS spectrum it is necessary to have quantitative measurements. This warrants further investigation.

6 Acknowledgments

We thank Radiometer for the funding of the PhD-project. We are grateful to Charlotte Ijeoma Falk and Diana Chinyere Anyaogu for the support in the search for knowledge prior to the experiments.

References

[1] Rice, S.A; McDougald, D.; Givskov, M.; Kjelleberg, S. Detection and Inhibition of Bacterial Cell-Cell Communication. *Methods Mol Biol.*, **2008**, *431*, 55-68.

[2] Decho, A.W.; Frey, R.L.; Ferry, J.L. Chemical Challenges to Bacterial AHL Signalling in the

Environment. *Chem. Rev.* **2011**, *111*, 86-99.

[3] Almarashi, J.F.M.; Kapel, N.; Wilkinson, T.S.; Telle, H.H. Raman Spectroscopy of Bacterial Species and Strains Cultivated under Reproducible Conditions. *Spectroscopy: An International Journal*, **2012**, *27*, 361-365.

[4] Harz, M.; Rösch, P.; Popp, J. Vibrational Spectroscopy-A Powerful Tool for the Rapid Identification of Microbial Cells at the Single-Cell Level. *Cytometry A.*, **2009**, *75*, 104-13.

[5] Kirschner, C.; Maquelin, K.; Pina, P.; Thi, N.A.N.; Choo-Smith, L.P.; Sockalingum, G.D.; Sandt, C.; Ami, D.; Orsini, F.; Doglia, S.M.; Allouch, P.; Mainfait, M.; Puppels, G.J.; Naumann, D. Classification and identification of enterococci: A comparative phenotypic, genotypic, and vibrational spectroscopic study. *J. Clin. Microbio.*, **2001**, *39*, 1763-1770.

[6] Escoriza, M.F.; Vanbriesen, J.M.; Stewart, S.; Maier, J. Studying bacterial metabolic states using Raman spectroscopy. *Appl. Spectrosc.*, **2006**, *60*, 971-976.

[7] McEwen, G.D.; Wu, Y. Zhou, A. Probing Nanostructures of Bacterial Extracellular Polymeric Substances (EPS) versus Culture Time by Raman Microspectroscopy and Atomic Force Microscopy. *Biopolymers*, **2010**, *93*, 171-177.

[8] Bak, J.; Spanget-Larsen, J. Molecular and vibrational structure of the extracellular bacterial signal compound N-butyryl-homoserine lactone (C4-HSL). *Vibrational Spectrosc.*, **2009**, *49*, 237-241.

[9] Fleishmann, M.; Hendra, P.J.; McAuillan, A.J. Raman spectra of pyridine adsorbed at a silver electrode. *Chem. Phys. Lett.*, **1974**, *26*, 163-166.

[10] Jeanmaire, D.L.; van Duyne, R.P. Surface raman spectroelectrochemistry: Part I. Heterocyclic, aromatic, and aliphatic amines adsorbed on the anodized silver electrode. *J Electroanal Chem.*, *84*, 1-20.

[11] Albrecht, M.G.; Creighton, J.A. Anomalously intense Raman spectra of pyridine at a silver electrode. *J Am Chem Soc.*, **1977**, *99*, 5215-5217.

[12] Efremov, E.V.; Ariese, F.; Gooijer, C. Achievements in resonance Raman spectroscopy: Review of a technique with a distinct analytical chemistry potential. *Analytica Chimica Acta*, **2008**, *606*, 119-134.

[13] Nie, S.; Emory, S.R. Probing Single Molecules and Single Nanoparticles by Surface-Enhanced Raman Scattering. *Science*, **1997**, *275*, 1102-1106.

[14] Kneipp, K.; Wang, Y.; Kneipp, H.; Perelman, L.T.; Itzkan, I.; Dasari, R.R.; Feld, M.S. Single Molecule Detection Using Surface-Enhanced Raman Scattering (SERS). *Phys. Rev. Lett.*, **1997**, *78*, 1667-1670.

[15] Efrima, S.; Zeiri, L. Understanding SERS of bacteria. *J. Raman Spectrosc.*, **2008**, *40*, 277-288.

[16] Sengupta, A.; Mujacic, M.; Davis, E.J. Detection of bacteria by surface-enhanced Raman spectroscopy. *Anal Bioanal Chem.*, **2006**, *386*, 1379-1386

[17] Jarvis, R.M.; Brooker, A.; Goodacre, R. Surface-enhanced Raman scattering for the rapid discrimination of bacteria. *Faraday Discuss.*, **2006**, *132*, 281-292.

[18] Guicheteau, J.; Christesen, S.; Emge, D.; Tripathi, A. Bacterial mixture identification using Raman and surface-enhanced Raman chemical imaging. *J. Raman Spectrosc.*, **2010**, *41*, 1632-1637.

[19] Pearman, W.F.; Lawrence-Snyder, M.; Angel, S. M.; Decho, A.W. Surface-Enhanced Raman Spectroscopy for in Situ Measurements of Signaling Molecules (Autoinducers) Relevant to Bacteria Quorum Sensing. *Appl. Spectrosc.*, **2007**, *61*, 1295-1300.

[20] Kim, J.; Kim, S.K.; Grégoire, G.; Manil, B.; Schermann, J.P. Infrared Study of the Bacterial Autoinducer *N*-Hexanoyl-Homoserine Lactone (C6-HSL) in the Gas-Phase, Water, and Octanol Solutions. *J. Phys. Chem A*, **2011**, *115*, 9199-9206

[21] Soulére, L.; Guiliani, N.; Queneau, Y.; Jerez, C.A; Doutheau, A. Molecular insights into quorum sensing in Acidithiobacillus ferrooxidans bacteria via molecular modelling of the transcriptional regulator AfeR and of the binding mode of long-chain acyl homoserine lactones. *J. Mol. Model*, **2008**, *14*, 599-606

[22] Decho, A.W.; Norman, R.S.; Visscher, P.T. Quorum sensing in natural environments: emerging views from microbial mats. *Trends in Microbiology*, **2010**, *18*, 73-80

[23] Decho, A.W.; Visscher, P.T.; Ferry, J.; Kawaguchi, T.; He, L.; Przekop, K.M.; Norman, R.S.; Reid, R.P. Autoinducers extracted from microbial mats reveal a surprising diversity of *N*-acylhomoserine lactones (AHLs) and abundance changes that may relate to diel pH. *Environmental Microbiology*, **2009**, *11*, 409-420.

[24] Clark, D.J.; Maaløe, O. DNA replication and the division cycle in Escherichia coli. *J. Mol. Biol.*, **1967**, *23*, 99-112

[25] Leopold, N.; Lendl, B. A New Method for Fast Preparation of Highly Surface-Enhanced Raman Scattering (SERS) Active Silver Colloids at Room Temperature by Reduction of Silver Nitrate with Hydroxylamine Hydrochloride. *Phys. Chem. B.*, **2003**, *107*, 5723-5727.

[26] Sharma, V.; Park, K.; Srinivasarao, M. Colloidal dispersion of gold nanorods: Historical background, optical properties, seed-mediated synthesis, shape separation and self-assembly. *Materials Science and Engineering R*, **2009**, *65*, 1-38.

[27] Link, S.; El-Sayad, M.A. Spectral Properties and Relaxation Dynamics of Surface Plasmon Electronic Oscillations in Gold and Silver Nanodots and Nanorods. *J. Phys. Chem. B*, **1999**, *103*, 8410-8426.

[28] Maiyalagan, T. Synthesis, characterization and electrocatalytic activity of silver nanorods towards the reduction of benzyl chloride. *Applied Catalysis A: General*, **2008**, *340*, 191-195.

[29] Mie, G. Beiträge zur optik trüber Medien, speziell kolloidaler Metallösungen. *Annalen der Physik.*, **1908**, *25*, 377-445.

[30] Chakraborty, P. Metal nanoclusters in glasses as non-linear photonic materials. *J. Mat. Sci*, **1998**, *33*, 2235-2249.

[31] Kapoor, S. Preparation, Characterization, and Surface Modification of Silver Particles. *Langmuir*, **1998**, *14*, 1021-1025.

[32] Henglein, A. Reactions of Organic Free Radicals at Cilloidal Silver in Aqueous Solution. Electron Pool Effect and Water Decomposition. *The Journal of Physical Chemistry*, **1979**, *83*, 2209-2216.

[33] Abdali, S.; Johannessen, C.; Nygaard, J.; Norbygaard, T. Resonance surface enhanced Raman optical activity of myoglobin as a result of optimized resonance surface enhanced Raman scattering conditions. *J. Phys. Condens. Matter.*, **2007**, *19*, 285205-213.

[34] Frisch, M. J.; Trucks, G. W.; Schlegel, H. B.; Scuseria, G. E.; Robb, M. A.; Cheeseman, J. R.; Scalmani, G.; Barone, V.; Mennucci, B.; Petersson, G. A.; Nakatsuji, H.; Caricato, M.; Li, X.; Hratchian, H. P.; Izmaylov, A. F.; Bloino, J.; Zheng, G.; Sonnenberg, J. L.; Hada, M.; Ehara, M.; Toyota, K.; Fukuda, R.; Hasegawa, J.; Ishida, M.; Nakajima, T.; Honda, Y.; Kitao, O.; Nakai, H.; Vreven, T.; Montgomery Jr., J. A.; Peralta, J. E.; Ogliaro, F.; Bearpark, M.; Heyd, J. J.; Brothers, E.; Kudin, K. N.; Staroverov, V. N.; Kobayashi, R.; Normand, J.; Raghavachari, K.; Rendell, A.; Burant, J. C.; Iyengar, S. S.; Tomasi, J.; Cossi, M.; Rega, N.; Millam, J. M.; Klene, M.; Knox, J. E.; Cross, J. B.; Bakken, V.; Adamo, C.; Jaramillo, J.; Gomperts, R.; Stratmann, R. E.; Yazyev, O.; Austin, A. J.; Cammi, R.; Pomelli, C.; Ochterski, J. W.; Martin, R. L.; Morokuma, K.; Zakrzewski, V. G.; Voth, G. A.; Salvador, P.; Dannenberg, J. J.; Dapprich, S.; Daniels, A. D.; Farkas, .; Foresman, J. B.; Ortiz, J. V.; Cioslowski, J.; Fox, D. J. Gaussian 09 Revision A.1. Gaussian Inc. Wallingford CT **2009**.

[35] Tawada, Y.; Tsuneda, T.; Yanagisawa, S. A long-range-corrected time-dependent density functional theory. *Journal of Chemical Physics*, **2004**, *120*, 8425-8433.

[36] Petersson,G. A. ; Bennett, A.; Tensfeldt, T. G.; AI-Laham, M. A.; Shirley, W. A. A complete basis set model chemistry. I. The total energies of closed-shell atoms and hydrides of the first-row elements. *Journal of Chemical Physics*, **1988**, *89*, 2193-2218.

[37] Petersson, G. A.; Al-Laham, M. A. A complete basis set model chemistry. II. *Journal of Chemical Physics*, **1991**, *94*, 6061-6090.

[38] Becke, A.D. Density-functional thermochemistry. III. The role of exact exchange. *J. Chem. Phys.*, **1993**, *98*, 5648-5652.

[39] Kneipp, K. Surface-enhanced Raman scattering. *Physics Today*, **2007**, *60*, 40-46.

[40] Sackmann, M.; Materny, A. Surface enhanced Raman scattering (SERS) - a quantitative analytical tool? *J. Raman Spectrosc.*, **2006**, *37*, 305-310.

[41] El Amri, C.; Baron, M.; Maurel, M. Adenine and RNA in mineral samples. Surface-enhanced Raman spectroscopy (SERS) for picomole detections. *Spectrochimica Acta Part A*, **2003**, *59*, 2645-2654.

[42] Shadii, I.T.; Chowdhry, B.Z.; Snowden, M.J.; Withnall, R. Semi-quantitative trace analysis of nuclear fast red by surface enhanced Raman scattering. *Analytica Chimica Acta*, **2001**, *450*, 115-122.

[43] Wigginton, N.S.; De Titta, A.; Piccapietra, F.; Dobias, J.; Nesatyv, V.J.; Suter, M.J.F.; Bernier-Latmani, R. Binding of silver nanoparticles to bacterial proteins depends on surface modifications and inhibits enzymatic activity. *Environ. Sci. Technol.*, **2010**, *44*, 2163-2168.

[44] Tripp, R.A.; Dluhy, R.A.; Zhao, Y. Novel nanostructures for SERS biosensing. *nanotoday*, **2008**, *3*, 31-37.

[45] Merrick, J.P.; Moran, D.; Radom, L. An Evaluation of Harmonic Vibrational Frequency Scale Factors. *J. Phys. Chem. A*, **2007**, *111*, 11683-11700.

[46] Socrates, G. Infrared and Raman Characteristic Group Frequencies: Tables and Charts. John Wiley & Sons Ltd, England. **2001**.

[47] Jakubczyk, D.; Barth, C.; Kubas, A.; Anastassacos, F.; Koelsch, P.; Fink, K.; Schepers, U.; Brenner-Weiss, G.; Bräse, S. Deuterium-labelled *N*-acyl-L-homoserine lactones (AHLs)-inter-kingdom signalling molecules-synthesis,structural studies, and interactions with model lipid membranes. *Anal Bioanal Chem*, **2012**, *403*, 473-482.

Appendix B

Paper II

The article describes the kinetics in the QS regulatory Las system in a combined data and modeling study. In the present in vitro study, we measure the response of the QS regulatory Las system in the monitor strain, MH155, to predetermined concentrations of OdDHL signal molecules. The kinetic model is seen to describe the data very well. Furthermore, the kinetic model is seen to explain data found in the literature as well. From this kinetic model we can conclude several behaviors of the Las system one of them being that OdDHL is not needed for the regulator LasR to fold to a stable dimer.
This is a first author article and I was involved in all aspects of the work.

Kinetic model for signal binding to the Quorum Sensing regulator LasR

Anetta Claussen[1,2], Tim Holm Jakobsen[2], Thomas Bjarnsholt[2], Michael Givskov[2,3], Martin Welch[4], Jesper Ferkinghoff-Borg[1], and Thomas Sams[1]
[1] Biomedical Engineering, Dept. of Electrical Eng., Ørsteds Plads 349, Technical University of Denmark, DK-2800, Denmark
[2] Department of International Health, Immunology, and Microbiology, Panum Institute, Blegdamsvej 3B, DK-2200, Denmark
[3] Singapore Centre on Environmental Life Sciences Engineering, Nanyang Technological University, Singapore 637551
[4] Department of Biochemistry, University of Cambridge, Hopkins Bldg., Downing Site, Cambridge CB2 1QW, United Kingdom

DRAFT, November 16, 2012

Abstract

We propose a conventional kinetic model for the activation of the *las* regulon in the opportunistic pathogen *Pseudomonas aeruginosa*. The model is based on new and recent *in vitro* data on the kinetics of regulator activation and deactivation. The model describes the activation of LasR through dimerization and consecutive activation by binding of two OdDHL signal molecules. The regulator monomer has a rapid proteolytic turnover while the dimerized regulator is protected against proteases and remains protected as it is activated through fully cooperative binding of two signal molecules.

Experimentally, the production of the active LasR quorum sensing regulator was studied in an *Escherichia coli* background as a function of signal molecule concentration at different growth rates. The functional activity of the regulator was monitored via a GFP reporter fusion to *lasB* expressed from the native, quorum sensing responsive *lasB* promoter.

The model describes the observed response to introduction of signal molecules at predetermined concentrations independent of growth rate. The model explains new data showing that the LasR dimer binds two signal molecules cooperatively and that the time scale for reaching saturation is independent of the signal molecule concentration.

In absence of signal molecules, the dimerized regulator can dissociate and degrade through the monomer channel. This resolves the apparent contradiction between our data and recent reports that the fully protected dimer is able to "degrade" when the induction of LasR ceases.

Keywords

quorum sensing, LasR, Pseudomonas aeruginosa, OdDHL, signal molecule

Introduction

Quorum sensing (QS) relies on a cell-cell signaling system by which bacteria keep track of the density of the population. The quorum sensors, which also function as regulators of gene expression, enable the bacteria to control gene expression in relation to the population cell density and accordingly undergo collective phenotypic changes [1, 2]. In Gram negative bacteria the quorum sensing regulatory system consists of a signal molecule synthase and a transcriptional regulator,

referred to as LuxI and LuxR homologues, respectively. At low population density signal molecules are present at concomitantly low levels. The signal molecules are acyl homoserine lactones (AHL). However, as the population density increases, the signal molecules accumulate and bind to the cognate transcriptional regulator inducing further transcription of the *luxI* homologue. This results in a rapid amplification of the signal [3–6].

Many LuxR homologues, including LasR of *Pseudomonas aeruginosa*, share the property that dimerization of the protein, necessary for transcriptional activation of target promoters, leads to significant protection against proteolytic degradation [7–15]. However, there has been considerable confusion concerning the detailed understanding the kinetics of the regulatory processes. Inspired by the study of TraR by Zhu *et al.* Schuster *et al.* found that, outside the cellular environment, LasR requires the presence of its cognate signal OdDHL (3-oxo-C_{12}-HSL) to stabilize [7, 15]. The confusion has largely been caused by the failure to purify the respective regulators in non-aggregated form outside the cellular environment [16].

Contrary to this Sappington *et al.* conclude that, in the cellular environment, the activated LasR-OdDHL complex is fully protected and that LasR and OdDHL readily dissociate and that LasR can remain in a conformation which is capable of reassociating with signal molecules [16]. We shall take this observation as the starting point for our kinetic modeling by assuming that the active forms of the regulator are in quasistatic equilibrium.

Here we study the properties of LasR binding to predetermined concentrations of the signal molecule OdDHL in the *Escherichia coli* strain MH155 hosting pMHLAS [17]. This plasmid encodes *lasR* under the control of P_{lac} and the LasR-responsive P_{lasB} driving expression of *lasB-gfp*(ASV). The strain (Fig. 1) constitutes an experimental playground for examining the dimerization of LasR and the binding of the regulator to predetermined levels of OdDHL.

The new data shows that the response to introduction of signal molecules follows second order cooperative kinetics. This suggests that the regulator dimerizes prior to signal binding. This is quite distinct from the kinetics when the dimerization follows the ligand binding. In addition, we observe identical fast response time to different levels of OdDHL. Were the two dimer forms not both long-lived, we would have observed a fast response for low levels of signal molecule and a slower response for high levels of signal molecule.

However, Sappington *et al.* also observe that when the production of regulator is stopped, in the absence signal molecules, the active form of the regulator disappears in around 20 minutes. At first sight, this appears in contradiction with our finding, i. e. that the dimer form of the regulator is protected against proteases. We demonstrate that this apparent contradiction can be resolved in our conventional kinetic model: When production of regulator is turned off, the condition for transient monomer is no longer satisfied. The dimerized regulators are then free to disappear through disassociation into monomers followed by degradation at the faster monomer degradation rate.

We therefore propose a very conventional picture of the LasR regulator: The regulator monomer has a rapid proteolytic turnover, the dimerized regulator is protected against proteases, and remains protected against proteases as it is activated through cooperative binding of two signal molecules. Below the threshold for transient monomer, the $(LasR)_2$ dimer "degrades" rapidly through the monomer channel.

We shall see in the "Kinetic model" that getting access to see these properties of the LasR regulator function relies on being in the limit of transient monomer where the timescale from monomer degradation does not occlude the picture. Therefore one cannot expect to observe the underlying cooperative kinetics and the response time invariance as clearly with the weaker native P_{lasR} promoter in single copy in the chromosome at exponential growth in the *P. aeruginosa*.

Results and discussion

When preparing a series of *in vitro* experiments to investigate the binding of LasR to OdDHL (reported as activation of *lasB-gfp* expression) we observed that cultures brought to exponential growth directly from overnight inocula had a much larger response to the introduction of OdDHL

than inocula that had been growing exponentially for a long time. Only after many generations in exponential growth does this "memory" fade. (Figures 2a,c and 2b,d summarize.) It was not clear whether the memory of the initial condition reflected an elevated dimer level or was due to an accumulation of plasmids. In fact, plasmid concentration as well as transcription rates can be strongly dependent on growth rates [18, 19]. On top of this there are significant uncertainties in interpretation of the GFP(ASV) reporter scaling when growth rate changes. We shall therefore not attempt to make conclusions concerning a possible accumulation of dimers versus accumulation of plasmids in the quasistatic mode based on the absolute scale of the responses at different growth conditions.

Instead, we analyzed the detailed shape and scaling of the response at three different growth rates ($\lambda_c = 0.34\,\mathrm{h}^{-1}$, $0.54\,\mathrm{h}^{-1}$, and $1.7\,\mathrm{h}^{-1}$). In these experiments the cultures were maintained at exponential growth for many generations prior to introduction of the signal molecules.

A model of the function of the monitor strain is illustrated in Fig. 1. Here we shall briefly summarize the properties of the model while the details are given in "Kinetic model". The model is based on a few observations from Fig. 4 and on a the recent findings by Sappington *et al.* [16]. a) Inside the living cell, the active conformation of lasR readily associates and dissociates from the ligand [16]. This means that we can assume quasistatic equilibrium between the active conformation of lasR and the lasR-OdDHL complex. b) The activated (ligand bound) regulator is fully protected against proteases [16]. c) From the data collapses in Figure 4 we see that the response to introduction of signal molecules follows second order cooperative kinetics $s^2/(K_d^2+s^2)$, $s = [\mathrm{OdDHL}]$. This suggests that the active form is a dimer and that it binds two signal molecules cooperatively, i. e. dimerization drives ligand binding. (This is quite distinct from the $s^2/(K_d+s)^2$ kinetics when ligand binding drives dimerization.) d) From the same figure we see that the response time is independent of ligand concentration. This leads to the conclusion that the active conformation has the same halflife as the ligand bound regulator. (In fact, we shall see that the shape of the response is fully accounted for by the properties of the GFP(ASV) reporter alone. This means that, within the resolution of the experiment, the response of *lasB* to introduction of signal molecules is instantaneous.) e) When LasR production is switched off, the active conformation survives in the cell for 20 minutes in absence of OdDHL [16]. This fairly rapid disappearance in combination with the stability of the active confirmation suggests that the disappearance goes through the monomer channel. In the "Kinetics" section we shall see that this leads us to conclude that the monomer is transient. When the production is switched off, the condition for transient monomer breaks down, and the degradation through the monomer channel opens up.

We shall make rough summary of the model. After many generations at constant growth rate, λ_c, steady state is reached for the total dimerized regulator level, r_d,

$$r_d = [\mathrm{R}_2] + [\mathrm{R}_2\mathrm{S}] + [\mathrm{R}_2\mathrm{S}_2] = \frac{b_1 R_t}{2\lambda_c} \tag{1}$$

This is a product of half the monomer production rate b_1 and the plasmid concentration R_t diluted by the growth rate λ_c.

When no signal molecules are present all dimers are in the free form, R_2. When signal molecules are added at concentration $s = [\mathrm{OdDHL}]$ the concentration of dimerized activated regulator quickly adjusts to

$$r_4 = r_d \, \frac{s^2}{K_d^2 + s^2} = \frac{b_1 R_t}{2\lambda_c} \, \frac{s^2}{K_d^2 + s^2} \tag{2}$$

This is a product of the maximal dimer level and the switch in the signal molecule concentration s at the effective dissociation constant K_d.

Following a change in the signal molecule concentration the activated dimer concentration adjusts rapidly. When the growth rate, transcription rate, or plasmid density changes the dimer concentration exponentially changes to its new value at rate λ_c (as will be described below, (20)).

The activated dimer level may be written as a sum of a static growth term and a "memory" term

$$r_4 = \frac{b_1 R_t}{2\lambda_c}\,(1 + m_d\,\mathrm{e}^{-(\lambda_c+\lambda_d)t})\,\frac{s^2}{K_d^2+s^2} \tag{3}$$

where m_d is the initial condition resulting from past growth conditions. The memory term describes the elevated response for overnight cultures as well as the "overshoot" observed in cultures that have not been kept in exponential growth mode sufficiently long to bring the plasmid and dimer concentrations to equilibrium. If the dimer/plasmid level achieved in stationary phase is much larger than the new asymptotic dimer level it may take many generations to "forget" the stationary phase level. The s-dependence is accounted for by the fully cooperative Hill-factor and the t-dependence is described by the exponential plus memory terms in (3) convolved with the impulse responses for GFP(ASV) production and maturation.

A detailed comparison with the experimental data, which requires a description of the properties of the GFP probe as well, is shown in Fig. 4. Here we see that the measured responses for exponential inocula are well accounted for by the model.

Conclusions

We established a conservative kinetic model for the regulator production and ligand binding in the *las* regulon of *Pseudomonas aeruginosa*. In the model, the regulator monomer has a rapid proteolytic turnover, the dimerized regulator is protected against proteases, and remains protected against proteases as it is activated through cooperative binding of two signal molecules.

We presented new data favoring this picture of the *las* regulon and resolved apparent contradictions between our data and other available data.

Methods

Kinetic model

The kinetic equations for the model in Fig. 1 are now established. The constitutive transcription of regulator molecules R with concentration r_1 is given by equation (4) and is proportional to the concentration R_t of *lasR* sites and the lasR transcription rate b_1. This results in a steady production of LasR regulator which rapidly decays at rate λ_1 or forms dimers. Cell division is included through addition of the growth rate λ_c to the proteolytic decay.

The observed second order cooperative response indicates that LasR dimerizes (5) before binding OdDHL. In the activation of the regulator through binding of two signal molecules (6)-(7) quasistatic equilibrium.

In all, the regulator formation and binding to the ligand is described by the kinetic equations

$$\frac{dr_1}{dt} = b_1 R_t + 2k_2^- r_2 - 2k_2^+ r_1^2 - (\lambda_1+\lambda_c) r_1 \tag{4}$$

$$\frac{dr_2}{dt} = k_2^+ r_1^2 + k_3^- r_3 - 2k_3^+ r_2 s - (k_2^- + \lambda_2 + \lambda_c) r_2 \tag{5}$$

$$\frac{dr_3}{dt} = 2k_3^+ r_2 s + 2k_4^- r_4 - k_4^+ r_3 s - (k_3^- + \lambda_3 + \lambda_c) r_3 \tag{6}$$

$$\frac{dr_4}{dt} = k_4^+ r_3 s - (2k_4^- + \lambda_4 + \lambda_c) r_4 \tag{7}$$

The sensor for the activated dimer level is the *lasB-gfp*(ASV) translational fusion depicted Fig. 1 (rhs). The rate of binding R_2S_2 to the *lasB* promoter site is proportional to the concentration of free sites $S_f = S_t - S_a$ and the concentration of activated dimers (8). The dissociation rate is proportional to the number of occupied sites S_a. The production (9) of non-mature GFP(ASV) is the sum of a small background production proportional to the number of free sites and an induced

production proportional to the number of occupied promoter sites. The maturation of GFP into its fluorescent form is described by equation (10). In all

$$\frac{dS_a}{dt} = k_S^+ r_4(S_t - S_a) - (k_S^- + \lambda_c)S_a \tag{8}$$

$$\frac{dn}{dt} = b_n S_t + (k_n - b_n)S_a - (k_g + \lambda_n + \lambda_c)n \tag{9}$$

$$\frac{dg}{dt} = k_g n - (\lambda_g + \lambda_c)g \tag{10}$$

In order to emphasize its role, the growth rate λ_c is explicitly included throughout.

Leveau *et al.* find that the proteolytic decay of GFP is Michaelis-Menten limited [20] for some of the very short lived variants introduced by Andersen *et al.* [21] but not important in GFP(ASV). We have therefore used the linear description in (9)-(10) in our model.

Driven systems

The signal sensor of the driven system in Fig. 1 consists of an input channel and four regulatory units with concentrations $r_1 = [\mathrm{R}]$, $r_2 = [\mathrm{R}_2]$, $r_3 = [\mathrm{R}_2\mathrm{S}]$, and $r_4 = [\mathrm{R}_2\mathrm{S}_2]$. Now, what comes in must go out. The entry channel is the production of monomer regulator at rate $b_1 R_t$, i.e. the product of the production rate per plasmid and the plasmid concentration. The exit channels are the dilution λ_c from cell growth and the proteolytic degradation $\lambda_i, i = 1, ..., 4$, of each form of the regulator. The total regulator balance is then

$$\frac{dr}{dt} = b_1 R_t - \lambda r \tag{11}$$

$$r = r_1 + 2r_2 + 2r_3 + 2r_4 \tag{12}$$

$$\lambda = \frac{r_1}{r}(\lambda_1 + \lambda_c) + \frac{2r_2}{r}(\lambda_2 + \lambda_c) + \frac{2r_3}{r}(\lambda_3 + \lambda_c) + \frac{2r_4}{r}(\lambda_4 + \lambda_c) \tag{13}$$

Since we know that the activated regulator $\mathrm{R}_2\mathrm{S}_2$ is well protected against proteases, we have $\lambda_4 = 0$. Further, the equilibration between the three dimer forms is rapid [16] and controlled by the signal molecule concentration. Finally, in figure 4a-c we observe that response time to changes in signal molecule concentration is independent of its concentration. If the non-activated forms of the regulator, R_2 and $\mathrm{R}_2\mathrm{S}$, had faster degradation that the active $\mathrm{R}_2\mathrm{S}_2$ this would lead to a faster time scale at lower concentrations of S. We therefore conclude that the proteolytic degradation rate of all dimer forms are identical, i.e. $\lambda_2 = \lambda_3 = \lambda_4 = 0$.

In absence of signal molecules, the active conformation of the regulator was observed to disappear in around 20 minutes after the production was turned off [16]. We are therefore in need for a fast degradation channel. This means that the monomer degradation is large and that the active conformation degrades only through disassociation followed by monomer degradation. Both the dissociation and degradation need be sufficiently large to account for the fast disappearance of the dimer. The dissociation constant for the ligand free dimer is therefore large. Now an apparent conflict appears: The higher degradation rate for the monomer should lead to shorter response time for lower signal molecule concentrations. Since this is not observed in our experiment, the influence of λ_1 in the weighed average (13) must be small. This means that the monomer is transient, $r_1\lambda_1 \ll (r_2+r_3+r_4)\lambda_c$, in our experiment and that this condition is not satisfied in the experiment of Sappington *et al.* where the monomer production is switched off. We shall see that the detailed kinetics reveals an accelerated degradation of the regulator through the monomer channel as the concentration decreases. This is in excellent agreement with the reported experiment [16].

In all, we are faced with a very "normal" regulator protein: a rapidly degrading monomer with dimerization into a protected but unstable active form prior to fully cooperative ligand binding. All on/off rates are fast.

Ligand binding

During build-up the balance between dimer forms can be assumed in quasistatic equilibrium. Equations (6) and (7) then lead to

$$r_4 = \frac{s^2}{s^2 + 2K_4 s + K_3 K_4}\, r_d \tag{14}$$

In the limit of highly cooperative ligand binding ($K_4 \ll K_3$)

$$r_4 = \frac{s^2}{s^2 + K_d^2}\, r_d \tag{15}$$

$$K_d^2 = K_3 K_4 \tag{16}$$

i. e. cooperative binding with Hill coefficient 2. As can be seen from the data collapses in Fig. 4 this gives gives an excellent description of the s-dependence of the data.

Turnover of dimer variants

In order to determine whether R_2 with no ligand bound could be shortlived, we will again consider what would happen if the turnover of the dimer R_2 was significantly faster than the turnover of the activated dimer R_2S_2. Since we know already that the ligand binding is cooperative binding we get

$$\lambda_d = \frac{r_2}{r_d}\lambda_2 + \frac{r_3}{r_d}\lambda_3 + \frac{r_4}{r_d}\lambda_4 \tag{17}$$

$$= \frac{K_d^2}{K_d^2 + s^2}\ \lambda_2 + \frac{s^2}{K_d^2 + s^2}\ \lambda_4 \tag{18}$$

We already know that R_2S_2 is stable. If λ_2 were much larger than the growth rate (18) would cause the response time to be fast when only small amounts of signal molecules were added and slower when large amounts were added. Since the data collapses in Fig. 4 show that the response time is independent of the signal molecule concentration, we conclude that the two dimer variants are both well protected against proteases, i. e. $\lambda_2 = \lambda_4 = 0$.

Regulator formation

Due to the fast production and turnover, the monomer formation (4) is to a good approximation in quasistatic equilibrium. This leads to

$$r_1 = \frac{\lambda_1}{4k_2^+}\left(\sqrt{1 + \frac{8k_2^+(b_1 R_t + 2k_2^- r_2)}{\lambda_1^2}} - 1\right) \tag{19}$$

where we have used that $\lambda_c \ll \lambda_1$.

We get the dimer build-up by adding up equations (5)-(7) describing the formation of the dimer variants

$$\frac{dr_d}{dt} = k_2^+ r_1^2 - k_2^- r_2 - \lambda_c r_d \tag{20}$$

$$r_d = r_2 + r_3 + r_4 \tag{21}$$

where used that all dimer forms are well protected against proteases.

In the limit of transient monomer, $8k_2^+ b_1 R_t \gg \lambda_1^2$, equations (19) and (20) result in

$$\frac{dr_d}{dt} = \frac{b_1 R_t}{2} - \lambda_c r_d \tag{22}$$

describing the population of the dimer states. When the growth conditions change the static dimer concentration

$$r_d = \frac{b_1 R_t}{2\lambda_c} \tag{23}$$

is approached exponentially at rate λ_c.

Notably the total dimer concentration r_d is independent of the signal molecule concentration. When signal molecules are added the dimer distributes quickly between the active form R_2 and the activated form R_2S_2 quickly. This results in Equation (3). The slow λ_c is not involved since the total dimer level does not change.

The monitor

In order to connect to the experiment the monitor needs to be described. The binding of the activated dimer to the *lasB* promoter site (8) is solved in the quasistatic limit. This results in

$$S_a = \frac{r_4}{r_4 + K_S} S_t \overset{r_4 \ll K_S}{\approx} \frac{r_4}{K_S} S_t \tag{24}$$

$$K_S = \frac{k_S^- + \lambda_c}{k_S^+} \tag{25}$$

Since the highest responses for exponential inocula (Fig. 2b) are much smaller than the maximal response observed (Fig. 2d), we may assume that $r_4 \ll K_S$. This results in linear scaling with the activated dimer concentration.

The induced GFP production described by (9) and (10) is linear in the activated operator concentration S_a

$$g(t) - g_0 = h_g(t) * h_n(t) * S_a(t) \tag{26}$$

$$h_n(t) = (k_n - b_n)\exp(-\Lambda_n t) \tag{27}$$

$$h_g(t) = k_g \exp(-\Lambda_g t) \tag{28}$$

$$\Lambda_n = k_g + \lambda_n + \lambda_c \tag{29}$$

$$\Lambda_g = \lambda_g + \lambda_c \tag{30}$$

where '$*$' denotes convolution with the impulse responses h_n and h_g. This introduces a delay and further suppression of the response at high growth rates.

The measured response

In experiments where the culture is kept at fixed growth rate for many generations before adding signal molecules the measured, OD-normalized, response is proportional to

$$g(t) - g_0 = \frac{S_t}{K_S} \frac{k_n - b_n}{\Lambda_n} \frac{k_g}{\Lambda_g} \frac{b_1 R_t}{2\lambda_c} \frac{s^2}{K_d^2 + s^2} f(t) \tag{31}$$

The time structure lies in the step response for the GFP monitor defined as

$$f(t) = 1 - \frac{\Lambda_n}{\Lambda_n - \Lambda_g}\exp(-\Lambda_g t) + \frac{\Lambda_g}{\Lambda_n - \Lambda_g}\exp(-\Lambda_n t) \tag{32}$$

conveniently normalized to unity at large t. This results in an OD-normalized induced response

$$\frac{G(t) - G_0(t)}{\mathrm{OD}} = A \frac{1}{\Lambda_n} \frac{1}{\Lambda_g} \frac{1}{\lambda_c} \frac{s^2}{K_d^2 + s^2} f(t) \tag{33}$$

to be compared to data. The normalization constant A contains the (arbitrary) fluorescence counter normalization and the remaining (growth rate dependent) constants.

The memory term has the same form, except, with a different form factor

$$f_m(t) = \frac{\Lambda_n \Lambda_g}{(\Lambda_n - \lambda_c)(\Lambda_n - \Lambda_g)(\Lambda_g - \lambda_c)} \\ ((\Lambda_n - \Lambda_g)\mathrm{e}^{-\lambda_c t} + (\Lambda_g - \lambda_c)\mathrm{e}^{-\Lambda_n t} + (\Lambda_c - \lambda_n)\mathrm{e}^{-\Lambda_g t}) \tag{34}$$

which accounts for the decay of the memory (initial condition) in (3).

The K_d dependence can be fitted separately and leads to the data collapse in Fig. 4. This leaves $\lambda_n + k_g$, λ_g, A, and m_d to be fitted to the collapsed data sets in Fig. 4a-c. The resulting parameters are given in Table 1.

Materials

Cultures of MH155 [pMHLAS] [17] were grown in fresh ABT minimal medium (B medium (Clark & Maaloe, 1967), containing 2.5 mg/l thiamine, 10 % A10 (Clark & Maaloe, 1967)), 0.5 % glucose, and 0.5 % casamino acids. This resulted in an exponential growth rate of $\lambda_c = 1.7\mathrm{h}^{-1}$. A lower growth rate of $\lambda_c = 0.54\mathrm{h}^{-1}$ was obtained by replacing the casamino acids by 0.5 % L-Leucine (Sigma Aldrich). A very low growth rate $\lambda_c = 0.34\mathrm{h}^{-1}$ was obtained by further replacing glucose by glycerol.

Experiments starting at exponential growth: While growing exponentially at 37 °C and 200 rpm the MH155 culture was diluted in fresh medium to $\mathrm{OD}_{450\mathrm{nm}} = 0.01$ measured on Shimadzu UV-1800 and distributed to preheated (37°C) 100 ml flasks containing 50 ml two-fold dilution rows of OdDHL (Sigma Aldrich, BioChemika Fluka) starting at 100 nM and leaving one flask without signal molecules for baseline determination.

Experiments starting at quasistationary: The culture was left to grow until an almost complete stop, i. e. $\mathrm{OD}_{450\mathrm{nm}} = 3.4$ and 2.9 for the casamino growth respectively the L-Leucine growth. At this stage the culture was rapidly diluted to $\mathrm{OD}_{450\mathrm{nm}} = 0.01$ and distributed to the two-fold dilution row flasks of OdDHL. Note that, if the culture is brought to complete static state it looses the ability to express GFP(ASV). It is thus critical to the usefulness of the GFP(ASV) reporter fusion that the culture be brought only to a quasistationary state ($\sim 0.9\,\mathrm{OD}_{\mathrm{max}}$).

Fluorescence from GFP(ASV) was measured using a Shimadzu RF-5301PC fluorimeter in quantitative raw data mode at $\lambda_{\mathrm{ex}} = 475\mathrm{nm} \pm 5\mathrm{nm}$, $\lambda_{\mathrm{em}} = 515\mathrm{nm} \pm 5\mathrm{nm}$, 4s integration time, and amplification set to high. The induced response is the measured OD-weighted background subtracted response, $(G - G_0)/\mathrm{OD} = \mathrm{GFP}/\mathrm{OD} - \mathrm{GFP}_0/\mathrm{OD}_0$, where GFP and GFP_0 are raw GFP counts with respectively without signal molecules.

Plasmid concentration, transcription rate, translation rate

The plasmid pMHLAS [17] used in this study has the same plasmid copy control as pUC18 is a *rom*$^-$ derivative of pBR322 with a further point mutation causing an increased temperature dependence. The physiological response of pBR322 has been extensively studied in *E. coli* by Lin-Chao and Bremer [22]. They found that the plasmid concentration is inversely proportional to the growth rate in the interval from 20-80 min. generation time (specific growth rates $\lambda_c = 0.5 - 2\mathrm{h}^{-1}$). Atlung *et al.* extended these results to include a *rom*$^-$ derivative of pBR322 and also extended the range of generation time well above 80 minutes [19]. In the overlapping region they confirm that *rom*$^+$ as well as *rom*$^-$ display $\mathrm{OD}_{450\mathrm{nm}}$ normalized plasmid concentration proportional to the generation time. At longer generation times the plasmid concentration is constant. The *rom*$^-$ derivative has plasmid concentration about 2-3 times higher than the *rom*$^+$ pBR322 and shares the property that the plasmid concentration is constant at specific growth rates below $0.5\mathrm{h}^{-1}$. The further point mutation in the pUC series leads to increased plasmid concentration and an increased sensitivity to temperature [23]. We have not been able to locate any reports on the growth rate dependence of this plasmids. Thus, while the high plasmid density of the pUC series have enabled us to enter the realm of transient monomer, they have, at the same time added complexity to the interpretation of the growth rate dependencies.

The growth rate dependence of transcription, and to a lesser extent the mRNA turnover and translation rates, of constitutively expressed chromosomal genes has been extensively studied [18]. These dependencies qualitatively compensate the growth rate dependence of the chromosomal gene density in the region where data are available, i.e. at growth rates $\lambda_c = 0.5 - 2\mathrm{h}^{-1}$.

Since we have two consecutive constructs on our plasmid (figure 1) effects of this sort enter squared. In addition significant uncertainties in the description of the absolute scale in the GFP(ASV) description are to be expected. We shall therefore not ascribe significance to the growth rate dependence of the data presented here.

Sappington "decay"

Sappington *et al.* recently pointed out that in the cellular environment the active form of the regulator readily binds to and dissociates from the signal molecule [16].

Further, in a monitor strain where induction of LasR can be switched off, they demonstrate that LasR is able to survive in its active form without the presence of OdDHL, though not for more than 20 minutes.

Our findings show that the active form is a dimer, R_2, which cooperatively binds two ligand molecules forming R_2S_2 require both forms to have vanishing proteolytic degradation rate. How can we understand the apparent contradiction that, at the same time, R_2 is not subject to proteolytic degradation and yet disappears in 20 minutes?

Within the conventional model the answer is surprisingly straight forward: When there are no signal molecules present the R_2 dimers are free to dissociate into monomers which are targeted for rapid proteolytic degradation. Due to the second order nature of the dimer formation this process speeds up as the production of regulator is switched off. Thus, in the absence of signal molecules, the dimers appear to be degrading even though they are disassociating and only subsequently degraded at the monomer degradation rate. At high signal molecule concentration the dimers are all in the R_2S_2 form and do not have access to the monomer channel.

Let us write this down formally. When the production of regulator is switched off we have

$$\frac{dr_1}{dt} = 2k_2^- r2 - 2k_2^+ r_1^2 - (\lambda_1 + \lambda_c) r_1 \tag{35}$$

$$\frac{dr_2}{dt} = k_2^+ r_1^2 - (k_2^- + \lambda_2 + \lambda_c) r_2 \tag{36}$$

in the absence of signal molecules. In the quasistatic limit of either of these equations we get

$$\begin{aligned} \frac{dr_1}{dt} &= -\frac{\frac{1}{4}\frac{2(\lambda_1+\lambda_c)}{\lambda_2+\lambda_c}K_2 + r_1}{\frac{1}{4}K_2 + r_1} \quad \frac{\lambda_2+\lambda_c}{2} \quad r_1 \\ &\approx \begin{cases} \dfrac{\lambda_2+\lambda_c}{2} & , \; r_1 > \frac{1}{4}\frac{2(\lambda_1+\lambda_c)}{\lambda_2+\lambda_c}K_2 \\ \lambda_1+\lambda_c & , \; r_1 < \frac{1}{4}K_2 \end{cases} \end{aligned} \tag{37}$$

and similarly

$$\begin{aligned} \frac{dr_2}{dt} &= -\frac{\frac{1}{4}\frac{2(\lambda_1+\lambda_c)}{\lambda_2+\lambda_c}\sqrt{K_2} + \sqrt{r_2}}{\frac{1}{4}\sqrt{K_2} + \sqrt{r_2}} \quad \frac{\lambda_2+\lambda_c}{2} \quad r_2 \\ &\approx \begin{cases} -(\lambda_2+\lambda_c) & , \; r_2 > \frac{1}{16}(\frac{2(\lambda_1+\lambda_c)}{\lambda_2+\lambda_c})^2 K_2 \\ -2(\lambda_1+\lambda_c) & , \; r_2 < \frac{1}{16}K_2 \end{cases} \end{aligned} \tag{38}$$

This shows that the dimer R_2 dissociates and subsequently degrades through the open monomer channel at rate $2(\lambda_1 + \lambda_c)$ when the concentration is low. In figure 5 the solution to r_2 is plotted with the asymptotes for $(\lambda_1 + \lambda_c)/(\lambda_2 + \lambda_c) = 20$. We clearly see the transition from slow degradation through the dimer channel to fast degradation through the monomer channel.

In the experiment by Sappington *et al.* it is observed that the active conformation of non-ligand-bound LasR disappears at accelerated rate over time. This may well correspond to moving down the shoulder of the r_2 curve in figure 5.

Acknowledgements

AC was supported by Radiometer Ltd. TS was supported by the Otto Mønsted Foundation. We are grateful to Mathew Scott, Steen Pedersen, and Stefan Klumpp for sharing their knowledge on plasmid copy number control.

References

[1] Fuqua C, Winans SC, Greenberg EP: **Census and Consensus in Bacterial Ecosystems: The LuxR-LuxI Family of Quorum-Sensing Transcriptional Regulators**. *Annual Review of Microbiology* 1996, **50**:727–753.

[2] Williams P: **Quorum Sensing: an emerging target for antibacterial chemotherapy?** *Expert Opin. Ther. Targets* 2000, **6**:257.

[3] Eberhard A: **Inhibition and activation of bacterial luciferase synthesis**. *J. Bacteriology* 1972, **109**:1101.

[4] Nealson KH, Platt T, Hastings JW: **Cellular control of the synthesis and activity of the bacterial luminescence system**. *J. Bacteriol.* 1970, **104**:313–322.

[5] Choi SH, Greenberg EP: **Genetic dissection of DNA binding and luminescence gene activation by the *Vibrio fischeri* LuxR protein**. *J. Bacteriology* 1992, **174**:4064–69.

[6] Hanzelka BL, Greenberg EP: **Evidence that the N-terminal region of the *Vibrio fischeri* LuxR protein constitutes an autoinducer-binding domain**. *J. Bacteriology* 1995, **177**(3):815–17.

[7] Zhu J, Winans SC: **Autoinducer binding by the quorum-sensing regulator TraR increases affinity for target promoters** *in vitro* **and decreases TraR turnover rates in whole cells**. *Proc. Natl. Acad. Sci. USA* 1999, **96**:4832–37.

[8] Welch M, Todd DE, Whitehead NA, McGowan SJ, Bycroft BW, Salmond GP: ***N*-acyl homoserine lactone binding to the CarR receptor determines quorum-sensing specificity in *Erwinia***. *The EMBO journal* 2000, **19**(4):631–641.

[9] Zhu J, Winans SC: **The quorum-sensing transcriptional regulator TraR requires its cognate signaling ligand for protein folding, protease resistance, and dimerization**. *Proc. Natl. Acad. Sci. USA* 2001, **98**:1507–12.

[10] Ventre I, Ledgham F, Prima V, Lazdunski A, Foglino M, Sturgis JN: **Dimerization of the quorum sensing regulator RhlR: development of a method using EGFP fluorescence anisotropy**. *Molecular Microbiology* 2003, **48**:187–198.

[11] Liu HB, Koh KP, Lee JH, Kim JS, Park S: **Characterization of LasR protein involved in bacterial quorum sensing mechanism of *Pseudomonas aeruginosa***. *Biotechnology and Bioprocess Engineering* 2009, **14**(2):146–154.

[12] Gonzalez JE, Keshavan ND: **Messing with Bacterial Quorum Sensing.** *Microbiology & Molecular Biology Reviews* 2006, **70**(4):1.

[13] Yang M, Giel JL, Cai T, Zhong Z, Zhu J: **The LuxR Family Quorum-Sensing Activator MrtR Requires Its Cognate Autoinducer for Dimerization and Activation but Not for Protein Folding**. *Journal of Bacteriology* 2009, **191**:434–438.

[14] Pinto UM, Winans SC: **Dimerization of the quorum-sensing transcription factor TraR enhances resistance to cytoplasmic proteolysis**. *Molecular Microbiology* 2009, **73**:32–42.

[15] Schuster M, Urbanowski ML, Greenberg EP: **Promoter Specificity in *Pseudomonas aeruginosa* Quorum Sensing Revealed by DNA Binding of Purified LasR**. *Proceedings of the National Academy of Sciences of the United States of America* 2004, **101**(45):15833–15839 and 3373727.

[16] Sappington KJ, Dandekar AA, Oinuma KI, Greenberg EP: **Reversible Signal Binding by the *Pseudomonas aeruginosa* Quorum-Sensing Signal Receptor LasR**. *mBio* 2011, **2**:e00011–11.

[17] Hentzer M, Riedel K, Rasmussen TB, Heydorn A, Andersen JB, Parsek MR, Rice SA, Eberl L, Molin S, Hoiby N, Kjelleberg S, Givskov M: **Inhibition of quorum sensing in *Pseudomonas aeruginosa* biofilm bacteria by a halogenated furanone compound**. *Microbiology (Reading)* 2002, **148**:87–102.

[18] Klumpp S, Zhang Z, Hwa T: **Growth Rate-Dependent Global Effects on Gene Expression in Bacteria**. *Cell* 2009, **139**(7):1366–1375.

[19] Tove A, Christensen BB, Hansen FG: **Role of Rom protein in copy number control of plasmid pBR322 at different growth rates in Escherichia coli K-12**. *Plasmid* 1999, **41**:110–119.

[20] Leveau JHJ, Lindow SE: **Predictive and interpretive simulation of green fluorescent protein expression in reporter bacteria**. *Journal of Bacteriology* 2001, **183**(23):6752–62.

[21] Andersen JB, Sternberg C, Poulsen LK, Bjorn SP, Givskov M, Molin S: **New Unstable Variants of Green Fluorescent Protein for Studies of Transient Gene Expression in Bacteria**. *Applied and Environmental Microbiology* 1998, **64**:2240–46.

[22] Lin-Chao S, Bremer H: **Effect of the bacterial growth rate on replication control of plasmid pBR322 in Escherichia coli**. *Molecular and General Genetics MGG* 1986, **203**:143–149.

[23] Lin-Chao S, Chen W, Wong T: **High copy number of the pUC plasmid results from a Rom/Rop-suppressible point mutation in RNA-II**. *Molecular Microbiology* 1992, **6**(22):3385–3393.

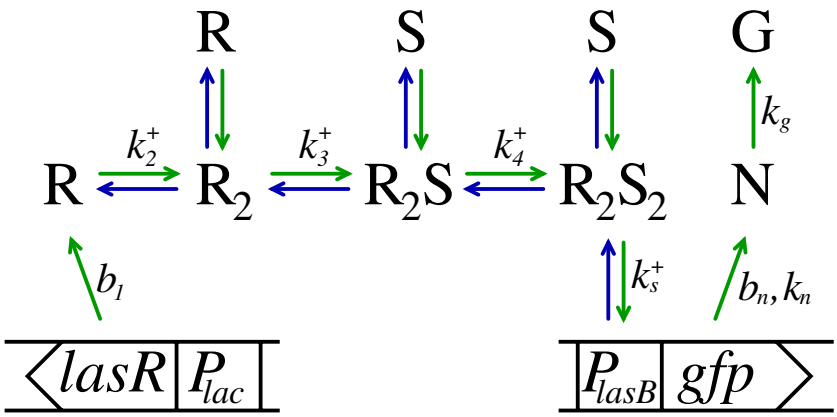

Figure 1: Schematic diagram of the functional components of the monitor strain used to measure the LasR - OdDHL kinetic response. In the diagram the LasR regulator is denoted R and the signal molecule OdDHL is denoted S. On-rate constants for each process are indicated in the figure. The *lac-lasR* translational fusion ensures constitutive production of LasR at rate b_1. The regulator decays rapidly at rate λ_1 or binds another R forming a slowly decaying dimer R_2. When signal molecules are present two signal molecules bind cooperatively to the dimer which retains the slow proteolytic decay rate. The *lasB-gfp*(ASV) reporter fusion is used to monitor the R_2S_2 concentration and leads induction of the reporter GFP(ASV) which matures into its measurable fluorescent form at rate k_g.

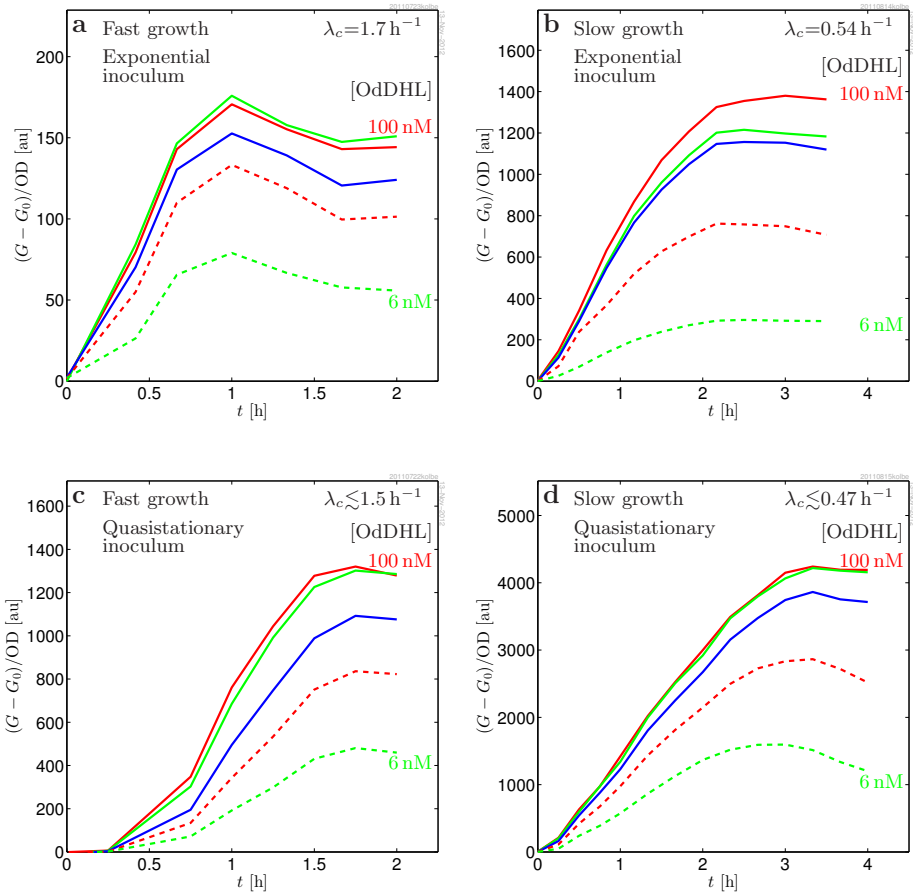

Figure 2: Induced response of MH155 [*Plac-lasR PlasB-gfp*(ASV)] to predetermined concentrations of signal molecules $s = [\text{OdDHL}] = 100\text{nM}/2^i,\ i = 0, ..., 4$. The response is normalized to the $\text{OD}_{450\text{nm}}$ shown in Fig. 3 and baseline subtracted. **a**, **b**: Response of exponentially growing cultures from exponentially growing inocula at two different growth rates. The fast growth is obtained using Casamino acids as amino acid source. The slow growth is obtained with L-Leucine as sole amino acid source. **c**, **d**: Response of exponentially growing cultures from quasistationary inocula ($\text{OD}_{450\text{nm}}$ of 3.4 and 2.9 respectively).

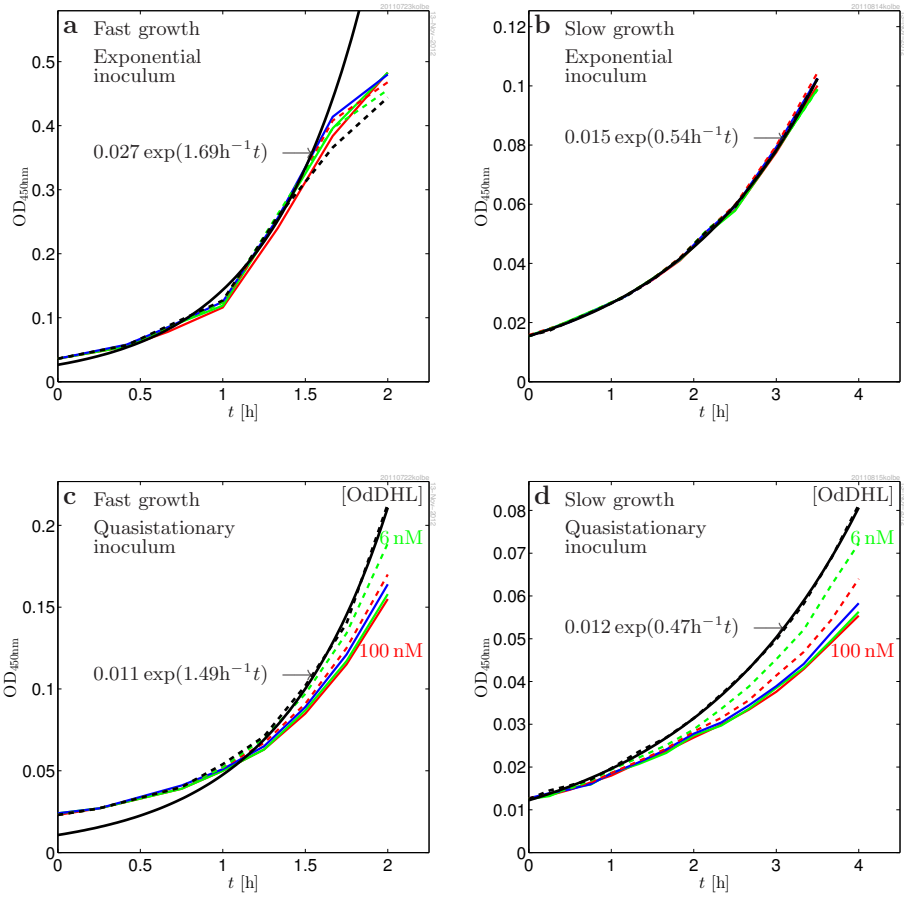

Figure 3: OD_{450nm} used for normalization of the fluorescence data. The deduced exponential growth rates are used when modeling the data. **a**: High growth rate obtained with Casamino acids in the nutrient. **b**: Low growth rate obtained with L-Leucine as the only amino acid source. **c,d**: Growth curves from quasistatic inocula, i. e. where the signal molecules were added at the same time as the dilution from almost saturated growth. The exponential shown fits the data with no signal molecules added at large t. The growth is slowed down when a high concentrations of signal molecules are added.

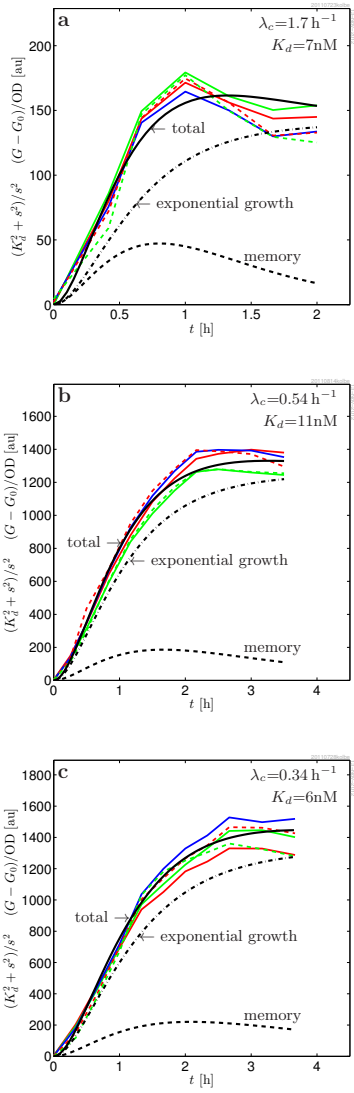

Figure 4: Data collapse of the induced response of MH155 [*Plac-lasR PlasB-gfp*(ASV)] to predetermined concentrations of signal molecules $s = 100\mathrm{nM}/2^i,\ i = 0, ..., 4$, at three different growth rates. The data collapse is obtained by dividing out the signal molecule switch $s^2/(K_d^2 + s^2)$ as indicated in the ordinate label. The time structure is completely determined by the properties of the GFP(ASV) production and maturation. and is independent of the signal molecule concentration. This shows that the regulator dimerization occurs before its binding to the signal molecules, that the kinetics is fully cooperative, and that the LasR dimer is fully protected already before ligand binding. The model curves are produced with the parameters in Table 1.

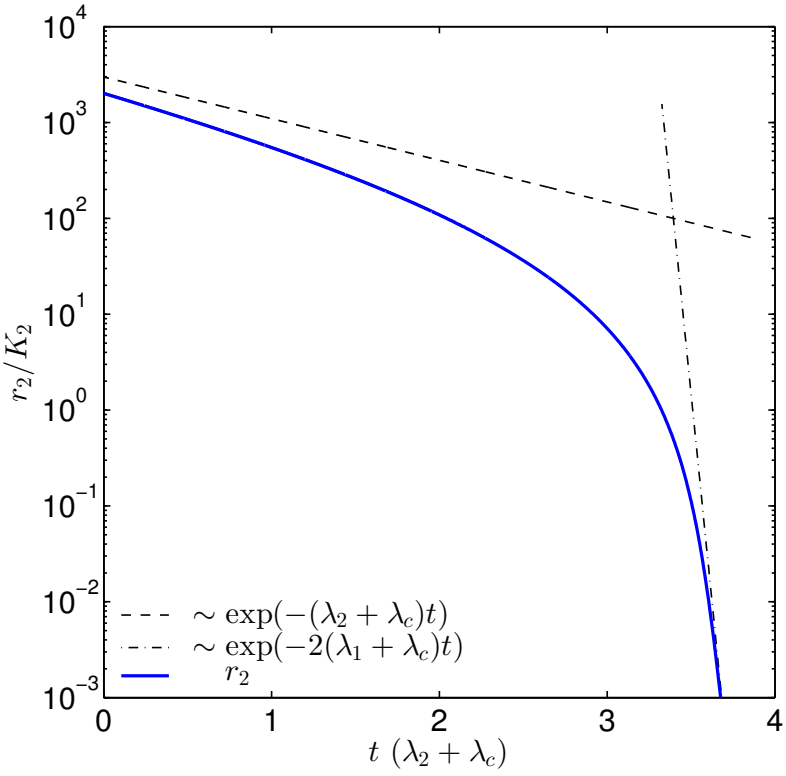

Figure 5: Plot showing the transition from direct degradation of the dimer to degradation through dissociation into rapidly degrading monomers as shown in equation (38). The $(\lambda_1 + \lambda_c)/(\lambda_2 + \lambda_c)$ ratio which determines the concentration at the transition was set to 20.

Table 1: Parameters used in the model in the kinetic model

Parameter	Value	
$\lambda_n + k_g$	$(2.1 \pm 0.3)\,\mathrm{h}^{-1}$	degradation plus maturation (consistent with [20, 21])
λ_g, λ_n	$(0.7 \pm 0.3)\,\mathrm{h}^{-1}$	proteolytic decay for GFP (consistent with [21])
K_d	$(8 \pm 2)\,\mathrm{nM}$	dissociation constant (agrees with [17])
A	$2170 \pm 200\,[\mathrm{a.u.}]$	amplitude (Glucose, Casamino)
	$2170 \pm 200\,[\mathrm{a.u.}]$	amplitude (Glucose, Casamino)
	$1200 \pm 200\,[\mathrm{a.u.}]$	amplitude (Glycerol, L-Leucine)
m_d	0.9 ± 0.2	memory (Glucose, Casamino)
	0.3 ± 0.1	memory (Glucose, L-Leucine)
	0.3 ± 0.1	memory (Glycerol, L-Leucine)
λ_c	$(1.69 \pm 0.04)\,\mathrm{h}^{-1}$	growth rate (Glucose, Casamino)
	$(0.54 \pm 0.03)\,\mathrm{h}^{-1}$	growth rate (Glucose, L-Leucine)
	$(0.34 \pm 0.03)\,\mathrm{h}^{-1}$	growth rate (Glycerol, L-Leucine)
$g(t)$		density normalized GFP response
g_0		density normalized GFP response at $s = 0$
$G(t)$		measured fluorescence response
$G_0(t)$		measured fluorescence response at $s = 0$
$\mathrm{OD}(t)$		optical density at 450nm
$h_n(t)$, $h_g(t)$		impulse response for GFP production and maturation
$k_2^{\pm}$		on/off rates for dimer formation
$k_3^{\pm}$, $k_4^{\pm}$		on/off rates for ligand binding
K_2		dimer dissociation constant
K_3, K_4		ligand-dimer dissociation constants
K_d	$\sqrt{K_3 K_4}$	dissociation constant for cooperative ligand binding
b_1	$\sim 1000\mathrm{h}^{-1}$	production rate of LasR per plasmid copy [18]
b_n		background production of GFP(ASV)
k_n	$\sim 1000\mathrm{h}^{-1}$	induced production rate of GFP per plasmid copy
k_g	$\sim 1.5\mathrm{h}^{-1}$	maturation rate of GFP [20]
λ_1	$\sim 20\mathrm{h}^{-1}$	R monomer degradation, [7]
λ_2	$\sim 0\mathrm{h}^{-1}$	R_2 degradation (this study)
λ_3		R_2S degradation, insensitive to this value
λ_4	$\sim 0\mathrm{h}^{-1}$	degradation of R_2S_2 [16]
λ_d		averaged dimer degradation rate
Λ_n	$k_g + \lambda_n + \lambda_c$	GFP parameter
Λ_g	$\lambda_g + \lambda_c$	GFP parameter
R_t		*lac* promoter density (plasmid density)
S_t		*lasB* promoter density (plasmid density)
S_a		active *lasB* promoter density (plasmid density)
S_f		free *lasB* promoter density (plasmid density)
r_1, r_2, r_3, r_4	[R], [R_2], [R_2S], [R_2S_2]	LasR monomer and dimer concentrations
s	[S]	Signal molecule concentration
t		time since addition of signal molecules

Appendix C

Paper III

The article describes the kinetics in the QS regulatory ahyRI system in a combined data and modeling study. In the present in vitro study, we measure the response of the QS regulatory ahyRI locus in the monitor strain, MH205, to predetermined concentrations of C4-HSL signal molecules. A minimal kinetic model describes the data well.
Although I was not involved in the main experiments leading to the article I contributed with experiments determining the decay of C4-HSL, see Appendix G for the protocol of the experiments.

doi:10.1016/j.jmb.2010.01.002 J. Mol. Biol. (2010) 396, 849–857

JMB

Available online at www.sciencedirect.com

ScienceDirect

ELSEVIER

Quorum Sensing Regulation in *Aeromonas hydrophila*

Christian Garde[1], Thomas Bjarnsholt[2], Michael Givskov[2], Tim Holm Jakobsen[2], Morten Hentzer[2], Anetta Claussen[1], Kim Sneppen[3], Jesper Ferkinghoff-Borg[1] and Thomas Sams[1]*

[1]*Elektro, Technical University of Denmark, DK-2800 Lyngby, Denmark*

[2]*Department of International Health, Immunology, and Microbiology, Panum Institute, Blegdamsvej 3B, DK-2200 Copenhagen, Denmark*

[3]*Niels Bohr Institute, Blegdamsvej 17, DK-2100 Copenhagen, Denmark*

Received 30 July 2009; received in revised form 6 December 2009; accepted 5 January 2010
Available online 11 January 2010

Edited by J. Karn

We present detailed results on the C4-HSL-mediated quorum sensing (QS) regulatory system of the opportunistic Gram-negative bacterium *Aeromonas hydrophila*. This bacterium contains a particularly simple QS system that allows for a detailed modeling of kinetics. In a model system (i.e., the *Escherichia coli* monitor strain MH205), the C4-HSL production of *A. hydrophila* is interrupted by fusion of *gfp*(ASV). In the present *in vitro* study, we measure the response of the QS regulatory *ahyRI* locus in the monitor strain to predetermined concentrations of C4-HSL signal molecules. A minimal kinetic model describes the data well. It can be solved analytically, providing substantial insight into the QS mechanism: at high concentrations of signal molecules, a slow decay of the activated regulator sets the timescale for the QS regulation loop. Slow saturation ensures that, in an *A. hydrophila* cell, the QS system is activated only by signal molecules produced by other *A. hydrophila* cells. Separate information on the *ahyR* and *ahyI* loci can be extracted, thus allowing the probe to be used in identifying the target when testing QS inhibitors.

Keywords: quorum sensing; *Aeromonas hydrophila*; Michaelis–Menten; *E. coli*; signal molecules

Introduction

Quorum sensing (QS) is an intercellular communication system by which bacterial cells are capable of indirectly monitoring their own population density through production and exchange of diffusible signal molecules. This enables bacteria to control gene expression dependent on population size and thereby perform coordinated phenotypic changes in a multicellular fashion.[1,2]

The first evidence of the social behavior of QS was observed in the marine bacterium *Vibrio fischeri*. *V. fischeri* colonizes "light organs" of certain fish and starts to produce visible light when a threshold density of bacteria has amassed. At present, QS regulatory systems have been reported for Gram-positive and Gram-negative bacteria.[3,4]

For both types of bacteria, regulation depends on the concentration of signal molecules, which are small peptides for Gram positives and acyl homoserine lactones for Gram negatives. For Gram negatives, the regulatory system consists of a signal molecule synthetase and a transcriptional regulator, and constituents of QS regulation are referred to as Lux homologues, derived from the luciferase of *V. fischeri* (LuxR for the regulator and LuxI for the signal molecule synthetase). At low population densities, the production and secretion of QS signal molecules proceed at a basal level. As population density increases, the signal molecules accumulate above the threshold and fuse with the transcriptional regulator to induce transcription of *luxI* and other target genes. This results in a positive feedback loop, which ensures a rapid amplification of the signal.[5–8]

Aeromonas hydrophila is a motile Gram-negative bacillus found in water sources, and it is a known pathogen for both humans and animals. Its pathogenicity typically includes minor skin infections or gastroenteritis in humans. The *A. hydrophila* QS sensor consists of an AhyRI monitor system homologous to the LuxRI system.[2,9–13]

In order to investigate the kinetics governing the QS activation loop, we broke the *ahyRI* locus into its constituents and measured its response to the

*Corresponding author. E-mail address: ts@elektro.dtu.dk.

Abbreviation used: QS, quorum sensing.

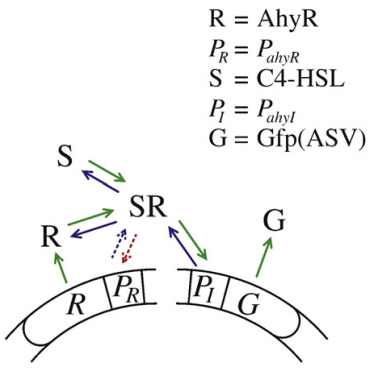

Fig. 1. Diagram of the AhyRI sensor system in the *E. coli* monitor strain MH205. The QS regulatory system, termed the AhyRI system, consists of a signal molecule synthetase (AhyI) and a transcriptional regulator (AhyR).

introduction of predetermined concentrations of C4-HSL signal molecules. To limit the investigation to AhyRI sensor components, we cloned the sensor components into *Escherichia coli*. Knowledge about corresponding input and output levels is acquired by the construction of an *E. coli* monitor strain MH205 representing the *ahyRI* locus (cf. Construction of the AhyRI Sensor System in MH205). As depicted in Fig. 1, *ahyR* is oriented in the reverse direction of *ahyI*, which has been interrupted by fusion of *gfp*(ASV). The *E. coli* strain responds to C4-HSL through synthesis of the unstable green fluorescence protein Gfp(ASV), with a degradation rate on the order of 0.4 h^{-1} [14,15] and a maturation constant of 1.5 h^{-1}.[16] Henceforth, Gfp(ASV) will be referred to as Gfp. Thus, MH205 is capable of responding to the signal molecules in a measurable way while lacking the ability to produce the signal molecules itself. This permits measurement of the response of the simulated AhyRI system to predetermined signal molecule concentrations.

Model

Below we describe a simple model of Gfp production in the MH205 *E. coli* monitor strain. The variables and parameters used in the model are listed in Table 1. The AhyRI construct of MH205 and the main processes of interest are illustrated in Fig. 1.

The model separates into two: (1) the production of the RS monomer r_1, and (2) the activation of the *ahyI* promoter and the production of mature Gfp. This is a valid separation, since the concentration of activated *ahyI* operator sites (I_a ~nanomolars) is much smaller than the concentration of the RS monomer (r_1 ~micromolars).

The production of regulator molecules is controlled by the *ahyR* site (i.e., proportional to the concentration of the carrier plasmid indicated in the production term in Eq. (1)). (R_t is the density of *ahyR* sites, which is equal to the plasmid copy number divided by the volume of the cell.)

The activation of the regulator through binding to a signal molecule is a slow process described by Eq. (2). While the free regulator R decays rapidly ($\lambda_0 \sim 20\ h^{-1}$), the RS complex is protected against proteases and has a much slower decay rate ($\lambda_1 \sim 0.6\ h^{-1}$).[19] In RS formation, details on how the different timescales come into play are discussed.

The RS complex activates a free operator site (I_f) for Gfp production, forming an activated operator

Table 1. Variables and constants used in the model

Parameter/variable		Magnitude	Reference
s, [S], [C4-HSL]	Signal molecule concentration	<10 μM	Current study
r_0, [R], [AhyR]	Free regulator concentration	<1 μM	Current study[a]
r_1, [RS]	Concentration of RS complex	<10 μM	Current study[a]
r_{1sat}	Saturated concentration of RS complex	~10 μM	Current study[a]
n, [N]	Concentration of nonmature Gfp in cell	(1–100) μM	Current study[a]
g, [G]	Concentration of mature Gfp in cell	(1–100) μM	Current study[a]
R_t, [*ahyR*]	Concentration of *ahyR* sites in cell	~10 nM	Current study
I_t, [*ahyI*]	Concentration of *ahyI* sites in cell	~10 nM	Current study
I_a	Concentration of activated *ahyI* sites in the cell	$<I_t$	Current study
λ_s	Decay of C4-HSL	<0.05 h^{-1}	Decay of Signal Molecules
λ_c	Growth rate for cells	(0.58±0.02) h^{-1}	Fig. 2
b_0	AhyR transcription rate per plasmid	~1000 h^{-1}	Fagerlind *et al.*[18]
λ_0	Degradation rate for AhyR	~20 h^{-1}	Zhu and Winans[19]
k_1^+	Production rate for RS complex	~600 $\mu M^{-1}\ h^{-1}$	Fagerlind *et al.*[18]
k_1^-	Dissociation rate for RS complex	~1000 h^{-1}	Fagerlind *et al.*[18]
λ_1	Degradation rate for RS complex	~0.6 s^{-1}	Zhu and Winans[19,20]
k_I^+	On-rate for RS complex binding to *ahyI*	~200 $\mu M^{-1}\ h^{-1}$	Fagerlind *et al.*[18]
k_I^-	Off-rate for RS complex binding to *ahyI*	~300 h^{-1}	Fagerlind *et al.*[18]
b_n	Spontaneous Gfp transcription rate	~1000 h^{-1}	Fagerlind *et al.*[18]
k_n^+	Induced nonmature Gfp production rate	~20b_n	Current study
λ_n	Degradation rate for nonmature Gfp	~0.4 h^{-1}	Andersen *et al.*[14] and Hentzer *et al.*[15]
k_g^+	Maturation rate for Gfp	~1.5 h^{-1}	Leveau and Lindow[16]
λ_g	Degradation rate for mature Gfp	~0.4 h^{-1}	Andersen *et al.*[14] and Hentzer *et al.*[15]

Numbers are given as order-of-magnitude estimates.
[a]Current study based on values from Leveau and Lindow[16] and Fagerlind *et al.*[18]

site (I_a) described by Eq. (3). This, in turn, initiates the production of nonmature Gfp (n) (Eq. (4)), subsequently maturating into fluorescent Gfp (g) (Eq. (5)).[14–16] In parallel, there is a spontaneous production of Gfp proportional to the number of free operator sites. Estimates of decay constants are on the order of $\lambda_{n,g} \sim 0.4\ h^{-1}$.[14–16] The introduction of such a long timescale from Gfp maturation and decay reduces the sensitivity of the measured response to rapid changes in underlying processes.

By normalizing data to spontaneous Gfp production, we directly measure the enhancement factor caused by the added signal molecules. Since, from Fig. 2, we can assume exponential growth, this leads to the simplification that all calculations can be performed "per plasmid copy" by augmenting the decay rate of all intracellular concentrations by the growth rate λ_c:

$$\frac{dr_0}{dt} = b_0 R_t + k_1^- r_1 - k_1^+ r_0 s - (\lambda_0 + \lambda_c) r_0 \quad (1)$$

$$\frac{dr_1}{dt} = k_1^+ r_0 s - \left(k_1^- + \lambda_1 + \lambda_c\right) r_1 \quad (2)$$

$$\frac{dI_a}{dt} = k_I^+ r_1 (I_t - I_a) - \left(k_I^- + \lambda_c\right) I_a \quad (3)$$

$$\frac{dn}{dt} = b_n I_t + \left(k_n^+ - b_n\right) I_a - \left(\lambda_n + \lambda_c + k_g^+\right) n \quad (4)$$

$$\frac{dg}{dt} = k_g^+ n - \left(\lambda_c + \lambda_g\right) g \quad (5)$$

$$I_t = I_a + I_f. \quad (6)$$

This description assumes a number of simplifications. First, the possible decay of the signal molecules has been omitted from the model, since as described in Decay of Signal Molecules, it has been measured to be negligible. Second, since the signal molecules diffuse rapidly through the cell membrane, they are assumed to be in transmembrane equilibrium.[18] Third, the possible feedback mechanism in the regulator production indicated in Fig. 1 has been ignored, since we find no need for this mechanism in the description of our data. Finally, we limit the description to the formation of monomer RS complexes. The possibility of RS complexes forming multimers has not been discussed explicitly for *A. hydrophila*. For similar QS subsystems, it has been considered by Ventre *et al.*,[21] but has been omitted by, Fagerlind *et al.*[18] In the present work the measured response function is well described without an explicit inclusion of multimer formation.

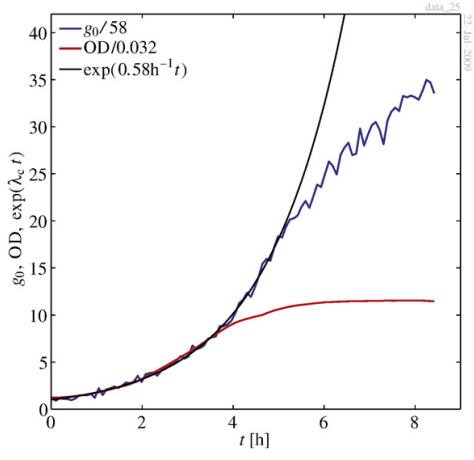

Fig. 2. Spontaneous Gfp production for MH205 measured on a Wallac 1420 VICTOR^2. Growth is exponential for 5 h, with a growth rate of $\lambda_c = 0.58\ h^{-1}$. As control, optical density is shown and follows the same exponential for about 3 h, whereafter rescattering causes the OD measurement to underestimate the number of cells.[17]

Results

In order to investigate the kinetics of the QS activation loop, we measured the response to predetermined concentrations of signal molecules, $s = 12\ \mu M/2^i$ (where $i = 0, 1, \ldots, 8$). The culture was in exponential growth phase when signal molecules were added (Fig. 2; Growth Assays and Normalization).

After subtraction of spontaneous Gfp production, the concentration of Gfp per plasmid copy is the response induced (see Background Subtraction for details). The data are shown in Fig. 3 and compared

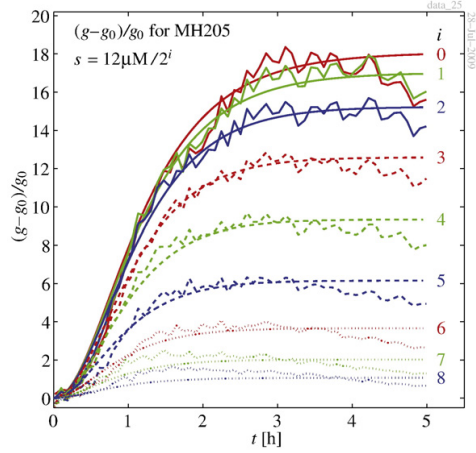

Fig. 3. The measured Gfp level expressing the activation of the AhyRI system for selected initial C4-HSL concentrations. The maximal initial C4-HSL concentration used is 12 μM in the data curve labeled $i = 0$. For each $i = 1, \ldots, 8$, the signal molecule concentration is divided by 2. Spontaneous Gfp production g_0 (i.e., Gfp production without signal molecules) has been subtracted and divided to obtain the normalized $(g-g_0)/g_0$. The model curves are fits with parameters given in Table 2. Only $t < 4$ h and $s > 12/2^6$ μM are included in the fit.

with the minimal model of the AhyRI system (to be discussed below).

At this point, we note that the response saturates as a function of the signal molecule concentration: the response to $s=6$ μM does not differ from the response to $s=12$ μM. Furthermore, the maximal response seems to be reached earlier at lower signal molecule concentrations. Finally, the response is a higher-order response (i.e., the underlying kinetics is at least second order in time). These observations will be illuminated in the discussion of results in light of the analytical solution of the model.

RS formation

Since the signal molecules do not decay (Decay of Signal Molecules) and the on/off rates for RS formation are large (Table 1), RS formation may be solved in the quasi-static limit. This is obtained by adding Eqs. (1) and (2) and setting $\mathrm{d}r_1/\mathrm{d}t=0$ in Eq. (2). The resulting solution is:

$$r_1 = b_0 R_t \left(\frac{1}{\lambda_0 + \lambda_c} \frac{s}{K_1 + s} e^{-\lambda t} + \frac{1}{\lambda_1 + \lambda_c} \frac{s}{\tilde{K}_1 + s} \left(1 - e^{-\lambda t}\right) \right) \tag{7}$$

with

$$K_1 = \frac{k_1^- + \lambda_1 + \lambda_c}{k_1^+} \tag{8}$$

$$\tilde{K}_1 = K_1 \frac{\lambda_0 + \lambda_c}{\lambda_1 + \lambda_c} \tag{9}$$

$$\lambda = \frac{K_1}{K_1 + s}(\lambda_0 + \lambda_c) + \frac{s}{K_1 + s}(\lambda_1 + \lambda_c) = \begin{cases} \lambda_0 + \lambda_c, & s \ll K_1 \\ \lambda_1 + \lambda_c, & s \gg K_1 \end{cases}. \tag{10}$$

From these equations, we read two important features. First, λ in Eq. (10) sets the timescale for reaching steady state of r_1. At $s \gg K_1$, this timescale is $1/(\lambda_1+\lambda_c)$. In conjunction with rapid diffusion (~5 s) out of the cell, this ensures that at high concentrations of signal molecules, only intercellular activation is permitted in *A. hydrophila*, whereas autoinduction is suppressed. With diffusion constant $D \sim 10^4$ mm^2/s and typical $\lambda_1+\lambda_c \sim 1$ h^{-1}, the signal molecules activating the QS system have traveled $\gtrsim 1$ mm upon binding to a regulator. Second, the rescaled dissociation constant $\tilde{K}_1 \sim 3\mu$m acts as the cutoff in the equilibrium r_1 concentration at $t \gtrsim 1/(\lambda_1+\lambda_c)$, thus enhancing the dynamic range of sensitivity to s. To our knowledge, this rescaling of the dissociation constant has not been reported in the literature. Thus, the slow decay of the AhyR/C4-HSL complex has two important effects: it suppresses autoinduction of QS and ensures an enhanced dynamic range in sensitivity to signal molecule concentration.

The solution in Eq. (7) is an excellent approximation even when allowing for a slow decay of the signal molecules as compared to the decay of the RS complex.

ahyI promoter activation

The role of the RS complex is to activate the *ahyI* site. (In *A. hydrophila in vivo*, the RS complex also plays the role of activating virulence factors in the attack system.) This is a fast process compared to neighboring processes, and it can be solved in the static limit:

$$I_a = I_t \frac{r_1}{K_I + r_1} \tag{11}$$

$$K_I = \frac{k_I^- + \lambda_c}{k_I^+}. \tag{12}$$

This Michaelis–Menten-limited process is responsible for the saturation of Gfp production in the monitor strain MH205 and thereby for the cutoff in C4-HSL production in *A. hydrophila*.

Gfp production and maturation

Induced Gfp production and maturation are linear in the activated operator concentration I_a and may be described as a convolution (∗) with the impulse response $Ah_g(t)$ of strength $A=(k_n^+/b_n-1)$:

$$g(t) - g_0 = A g_0 \left(h_g * \frac{I_a}{I_t} \right)(t) \tag{13}$$

$$h_g(t) = \frac{\Lambda_n \Lambda_g}{\Lambda_n - \Lambda_g} \left(e^{-\Lambda_g t} - e^{-\Lambda_n t} \right) \tag{14}$$

$$g_0 = \frac{k_g^+ b_n}{\Lambda_n \Lambda_g} I_t \tag{15}$$

$$\Lambda_n = \lambda_n + \lambda_c + k_g^+ \tag{16}$$

$$\Lambda_g = \lambda_g + \lambda_c \tag{17}$$

$$A = \frac{k_n^+}{b_n} - 1. \tag{18}$$

This effectively introduces a delay in the response and is responsible for the initial t^2 behavior of the induced response (cf. Fig. 4c and d).

Leveau and Lindow found that the proteolytic decay of Gfp is Michaelis–Menten limited.[16] This is the case for some of the short-lived variants introduced by Andersen *et al.*, but is found to be less important in Gfp(ASV).[14]

Variable reduction

While fitting, it is convenient to measure r_1 and K_I in units of the saturated r_1 level, $r_{1sat}=b_0R_t/(\lambda_1+\lambda_c)$.

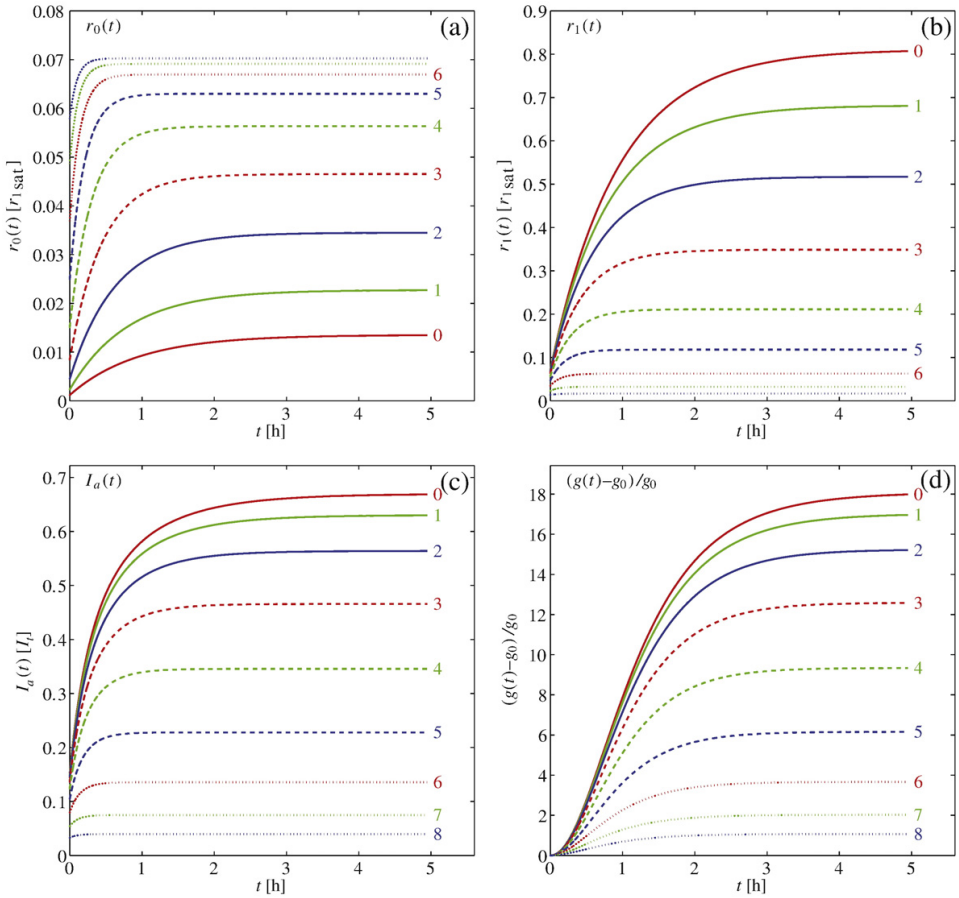

Fig. 4. Concentration of (a) the regulator [AhyR]=r_0 and (b) the activated regulator complex in units of r_{1sat}. (c) Activated *ahyI* operator (I_a) in units of I_t. (d) Mature Gfp(ASV) $(g-g_0)/g_0$ as a function of time after the introduction of signal molecules. The index at the end of each curve indicates the concentration of signal molecules $s=12\,\mu M/2^i$ (where $i=0,\ldots,8$).

Choosing the independent parameters as λ_1, K_1, $\tilde{K}_1$, Λ_n, Λ_g, K_I, and A, we express the induced response as:

$$\frac{g(t)-g_0}{g_0} = A\left(h_g * \frac{r_1}{K_I + r_1}\right)(t) \tag{19}$$

where

$$r_1(t) = \frac{K_1}{\tilde{K}_1}\frac{s}{K_1+s}e^{-\lambda t} + \frac{s}{\tilde{K}_1+s}\left(1-e^{-\lambda t}\right) \tag{20}$$

and

$$\lambda = \frac{\tilde{K}_1+s}{K_1+s}(\lambda_1+\lambda_c). \tag{21}$$

Scaling relations

After a time on the order of $1/(\lambda_1+\lambda_c)$, the system reaches steady state. Still in units of the saturated level, r_1 in Eq. (20) may then be expressed as:

$$r_1 \simeq \frac{s}{\tilde{K}_1+s}. \tag{22}$$

At steady state, the convolution in Eq. (19) reduces to the identity, and we get:

$$\frac{g(t)-g_0}{g_0} \simeq A\frac{r_1}{K_I+r_1} \simeq \frac{A}{K_I+1}\frac{s}{K_I\tilde{K}_1/(K_I+1)+s}. \tag{23}$$

Thus, we expect $A/(K_I+1)$ and $K_I\tilde{K}_1/(K_I+1)$ to be well-defined constants.

Numerical results

A comparison of the model with the measured response to the introduction of signal molecules is shown in Fig. 3. With the parameters listed in Table 2, the model reproduces the data well. Parameter estimation is detailed in Estimation of Parameters. Given the model, we are able to follow the response for each step in the QS regulatory system.

Table 2. Estimated model parameters as described in Variable Reduction, Scaling Relations, and Estimation of Parameters

Fitting parameters		
$A/(1+K_I)$	19.3±0.3	Saturated response (Eq. (24))
$\tilde{K}_1 / (1 + 1 / K_I)$	(0.80±0.05) μM	Effective cutoff (Eq. (25))
K_I	0.4±0.2	Dissociation constant for the binding of RS complex to the AhyI site (in units of r_{1sat})
λ_1	(0.3±0.2) h^{-1}	Degradation rate for RS complex
K_1	$\left(0.20 \pm \begin{smallmatrix} 0.20 \\ 0.05 \end{smallmatrix}\right)\mu$M	Dissociation constant for RS complex
Λ_n	(2.5±0.3) h^{-1}	Effective decay for nonmature Gfp (Eq. (16))
Λ_g	(2.0±0.3) h^{-1}	Effective decay for mature Gfp (Eq. (17))
Fixed parameters during fit		
λ_c	(0.58±0.02) h^{-1}	Cell growth rate
λ_s	0 h^{-1}	Decay of signal molecules

This set of parameters has been used in the comparison between model and data in Fig. 3.

As expected, fits to data reveal narrow bounds on the steady-state relations:

$$\frac{A}{K_I + 1} = 19.3 \pm 0.3 \qquad (24)$$

$$\frac{K_I \tilde{K}_1}{K_I + 1} = (0.80 \pm 0.05)\mu\text{M} \qquad (25)$$

between the parameters derived from Eq. (23).

As the signal molecule concentration is lowered, the maximal response occurs earlier. This reflects the change towards large λ in Eq. (10): the QS system is sensitive to the transition from fast ($\lambda \simeq 12\ h^{-1}$) RS saturation at low signal molecule concentration to slow ($\lambda \simeq 0.9\ h^{-1}$) RS saturation at high signal molecule concentration.

In Fig. 4a–c, the concentrations of the free regulator r_0 and the activated regulator r_1, and the activation of the *ahyI* operator site I_a are shown. The concentration of the free regulator r_0 starts at a high equilibrium level. The addition of signal molecules results in a rapid drop in r_0, expressing that R + S ⇆ RS is in static equilibrium ($r_0 s = K_1 r_1$). Hereafter, r_1 builds up at a timescale given by $1/\lambda$ in Eq. (10). At high signal molecule concentration, where λ is small, the equilibrium concentration of r_0 and r_1 is reached only slowly. The plots of r_0 and r_1 confirm the understanding that this timescale is on the order of 1 h when the signal molecule concentration is much larger than K_1. As noted earlier, this serves to suppress autoinduction of the QS system in *A. hydrophila in vivo*.

The large value of $\tilde{K}_1$ in Eqs. (7) and (9) ensures a large dynamic range in the sensitivity of r_1 to s. Even at the highest tested concentrations of signal molecules, r_1 is still sensitive to s, thus allowing for virulence factors at other sites in *A. hydrophila* to turn on at s higher than the cutoff for signal molecule production. In *A. hydrophila in vivo*, this ensures a large dynamic range in sensitivity to colony size for QS-controlled virulence factors.

In Fig. 4d, the concentration of mature Gfp (g) is shown. The slow production and maturation of the Gfp are limiting factors in the time resolution of the experiment, preventing direct access to the activation of the *ahyI* locus. We have considered an unfolding of the linear production and maturation of Gfp. However, this involves effectively differentiating twice the data and is not possible given the experimental uncertainties.

Discussion

We have presented a detailed experimental study of the C4-HSL-mediated QS regulatory system from *A. hydrophila* in the *E. coli* monitor strain MH205. The experimental data were presented in conjunction with a minimal mathematical model that provides remarkable insight into the QS mechanism reaching beyond the description of the MH205 monitor system.

The analytical solution of the formation of the AhyR/C4-HSL complex demonstrates how the dramatic difference between the decay rate of the free regulator and the decay rate of the activated regulator reported in the literature[19,20] plays its role: first, it ensures that only intercellular activation of the QS process is allowed, and, second, it ensures an enhanced dynamic range of sensitivity to the signal molecule concentration.

The large timescale is only activated at high signal molecule concentrations. In the experiment, this shows up as a delay in the maximal response, making our experiment sensitive to the *ahyR* locus. Furthermore, the overall saturation in the response to signal molecule concentration is predominantly determined by the dissociation constant K_I controlling the dissociation of the AhyR/C4-HSL complex from the *ahyI* site and is less sensitive to the cutoff $\tilde{K}_1$ for the binding of the regulator to the signal molecule. This makes our experiment sensitive to the *ahyI* locus. (In *A. hydrophila*, this ensures that, at a signal molecule concentration beyond the saturation of the regulatory loop, the concentration of AhyR/C4-HSL complexes is a measure of the size of the *A. hydrophila* colony.) Together, this makes the experiment sensitive to the *ahyR* and the *ahyI* loci

individually, thus making the monitor strain a sensitive probe for identifying targets for QS inhibitors.

Materials and Methods

Construction of the AhyRI sensor system in MH205

ahyR and P*ahyI* (promoter region) from *A. hydrophila* were isolated as a 2601 bp BamHI-EcoRI fragment and inserted into pMH391.[15] The vector pMH391 contains an unstable version of the green fluorescent protein Gfp (ASV) inserted between the NotI sites of pUCP22Not ($Ap^R Gm^R$). The fusion point between P*ahyI* and *gfp*(ASV) is located between the BamHI terminal point of the *ahyI* sequence and XbaI (originating from pJBA113[14]). The resulting plasmid, termed pMHRHL, contains divergently transcribed P*ahyR–ahyR* and P*ahyI–gfp*(ASV) transcriptional fusions flanked by NotI restriction sites (Fig. 5a). The plasmid was introduced by electroporation into *E. coli* MT102.[22] The resulting monitor strain is named MH205.

Growth assays

An overnight culture of MH205 was diluted in fresh ABT minimal medium [B medium[23] plus 2.5 mg/l thiamine and 10% A10[23]] supplemented with 0.5% glucose and 0.5% casa amino acids and grown to exponential phase at 37 °C and 200 rpm. The growing culture was diluted to $OD_{450\ nm} = 0.1$ measured on Genesys 10 UV USA and distributed to a heated (37 °C) 96-well microtiter plate (black PolyBase; Nunc USA) containing 2-fold dilution rows of C4-HSL (09945; Sigma Aldrich, BioChemika Fluka) starting at 12 μM. The microtiter plate was placed in a Wallac 1420 VICTOR^2 (Perkin-Elmer, Waltham, MA, USA) set to measure $OD_{450\ nm}$ and fluorescence (excitation, 485 nm; emission, 535 nm) every fifth minute,

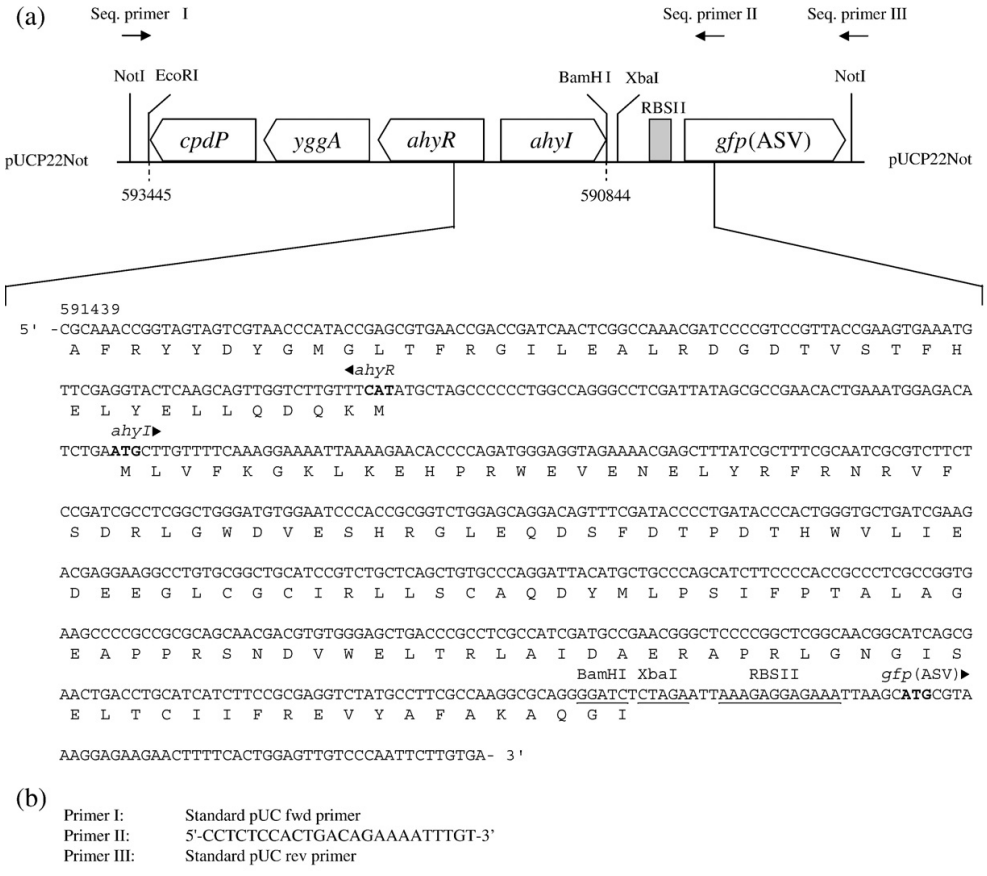

Fig. 5. (a) Schematic drawing of the AhyRI sensor system and the nucleotide sequence of the fusion point between *ahyRI* and the unstable green fluorescence protein *gfp*(ASV). Relevant restriction sites are shown, and primers used to sequence the insertion are indicated by arrows. On the nucleotide sequence, the direction of gene transcription is indicated by arrows, and start codons are shown in bold letters. RBSII refers to the synthetic ribosome binding site carried by pJBA113; 593445 and 590844 refer to nucleotide numbers of the *A. hydrophila* genome. (b) Primers used to generate sequence information.

with 99 repetitions in total. Additionally, corresponding measurements of $OD_{450\ nm}$ and fluorescence offsets were performed and subtracted from the data to obtain the growth curve (Fig. 2) and the active response of the monitor strain to the exogenous C4-HSL. All throughout, data are normalized to spontaneous Gfp production deduced from an exponential fit (Fig. 2) to the fluorescence offset experiments after subtraction of Gfp from a nutrient-only offset measurement.

Decay of signal molecules

The decay of exogenous C4-HSL was established by measuring the GFP response of the MH205 culture to a 1 μM C4-HSL solution having already aged 1, 2, 4, and 8 h in ABT minimal medium. With identical responses at all ages, the decay of C4-HSL is negligible ($\lambda_s < 0.05\ h^{-1}$).

Background subtraction

The spontaneous Gfp production shown in Fig. 2 is extracted from data by subtraction of an ABT-medium-only from a sample with MH205 cells (C) growing exponentially in medium (M), $g_0(t) = g_{C+M}(t) - g_M(t)$. The signal (induced + spontaneous) at a finite concentration of signal molecules (S) is $g(t) = g_{S+C+M}(t) - g_M(t)$. The induced signal is then $g(t) - g_0(t) = g_{S+C+M}(t) - g_{C+M}(t)$. The interpretation of this as an induced signal relies on the linearity of the production and the maturation of Gfp with respect to I_a and I_f.

Normalization

In order to simplify the comparison with the mathematical model, we normalized the Gfp "per plasmid". Traditionally, this is performed by normalization of the Gfp signal to the optical density. However, we use the fluorescent response from the spontaneous Gfp production for normalization. The advantage of this is that the light paths for excitation and emission are the same in normalization measurements and in induced excitation measurements, thus ensuring correct normalization of the response "per plasmid." In Fig. 2, the exponential normalization divisor is shown. Exponential growth is observed up until $t = 5$ h. Beyond this time, we refrain from interpreting the data, since knowledge of the growth rate λ_c entering in the model description is lost.

Estimation of parameters

The estimation of the model parameters is obtained by minimizing a chi-square measure $\chi^2 = \sum_{s,t}((g(s,t) - g_0(t))/g_0(t) - \text{model}(s,t))^2/\sigma^2(s,t)$, where summations are over signal concentrations and time. The variance $\sigma^2(s,t)$ consists of two contributions: the variance between six repetitions of the experiment and the variance of rapid fluctuations in the data. Only data for $t < 4$ h and $s > 12/2^6$ μM were included in the fit. The uncertainties of the estimates in Table 2 reflect the variations obtained with the simplex minimization procedure from random initial parameter seeds.[24] The resulting chi-square is on the order of $\chi^2 = 0.9$–1.2. During the parameter search, we have restricted ourselves to $K_1 > 0.15$ to obtain values in reasonable agreement with the literature.[18] We find that, when restricting the search to values of Λ_g in accordance with Leveau and Lindow, only values of K_I smaller than 0.4 are acceptable.[16] The scaling relations discussed in Materials and Methods are excellently reproduced by all possible parameter sets.

Acknowledgements

We are grateful to Anne Kathrine Nielsen for assistance in the laboratory.

References

1. Fuqua, C., Winans, S. C. & Greenberg, E. P. (1996). Census and consensus in bacterial ecosystems: the LuxR–LuxI family of quorum-sensing transcriptional regulators. *Annu. Rev. Microbiol.* **50**, 727–753.
2. Williams, P. (2000). Quorum sensing: an emerging target for antibacterial chemotherapy? *Expert Opin. Ther. Targets*, **6**, 257.
3. Parsek, M. R. & Greenberg, E. P. (2000). Acyl-homoserine lactone quorum sensing in Gram-negative bacteria: a signaling mechanism involved in associations with higher organisms. *Proc. Natl Acad. Sci. USA*, **97**, 8789–8793.
4. Dunny, G. & Leonard, B. (1997). Cell–cell communication in Gram-positive bacteria. *Annu. Rev. Microbiol.* **51**, 527–564.
5. Eberhard, A. (1972). Inhibition and activation of bacterial luciferase synthesis. *J. Bacteriol.* **109**, 1101.
6. Nealson, K. H., Platt, T. & Hastings, J. W. (1970). Cellular control of the synthesis and activity of the bacterial luminescence system. *J. Bacteriol.* **104**, 313–322.
7. Choi, S. H. & Greenberg, E. P. (1992). Genetic dissection of DNA binding and luminescence gene activation by the *Vibrio fischeri* LuxR protein. *J. Bacteriol.* **174**, 4064–4069.
8. Hanzelka, B. L. & Greenberg, E. P. (1995). Evidence that the N-terminal region of the *Vibrio fischeri* LuxR protein constitutes an autoinducer-binding domain. *J. Bacteriol.* **177**, 815–817.
9. Kirke, D. F., Swift, S., Lynch, M. J. & Williams, P. (2004). The *Aeromonas hydrophila* LuxR homologue AhyR regulates the *N*-acyl homoserine lactone synthase, AhyI positively and negatively in a growth phase-dependent manner. *FEMS Microbiol. Lett.* **241**, 109–117.
10. Lynch, M. J., Swift, S., Kirke, D. F., Keevil, C. W., Dodd, C. E. R. & Williams, P. (2002). The regulation of biofilm development by quorum sensing in *Aeromonas hydrophila*. *Environ. Microbiol.* **4**, 18–28.
11. Swift, S., Karlyshev, A. V., Durant, E. L., Winson, M. K., Chhabra, S. R., Williams, P. *et al.* (1997). Quorum sensing in *Aeromonas hydrophila* and *Aeromonas salmonicida*: identification of the LuxRI homologues AhyRI and AsaRI and their cognate signal molecules. *J. Bacteriol.* **179**, 5271–5282.
12. Swift, S., Lynch, M. J., Fish, L., Kirke, D. F., Tomás, J. M., Stewart, G. S. & Williams, P. (1999). Quorum sensing-dependent regulation and blockade of exoprotease production in *Aeromonas hydrophila*. *Infect. Immun.* **67**, 5192–5199.
13. Bi, Z. X., Liu, Y. J. & Lu, C. P. (2007). Contribution of AhyR to virulence of *Aeromonas hydrophila* J-1. *Res. Vet. Sci.* **83**, 150–156.
14. Andersen, J. B., Sternberg, C., Poulsen, L. K., Bjorn, S. P., Givskov, M. & Molin, S. (1998). New unstable variants of green fluorescent protein for studies of

transient gene expression in bacteria. *Appl. Environ. Microbiol.* **64**, 2240–2246.
15. Hentzer, M., Riedel, K., Rasmussen, T. B., Heydorn, A., Andersen, J. B., Parsek, M. R *et al.* (2002). Inhibition of quorum sensing in *Pseudomonas aeruginosa* biofilm bacteria by a halogenated furanone compound. *Microbiology*, **148**, 87–102.
16. Leveau, J. H. J. & Lindow, S. E. (2001). Predictive and interpretive simulation of green fluorescent protein expression in reporter bacteria. *J. Bacteriol.* **183**, 6752–6762.
17. Walstra, P. (1965). Discussion of errors in turbidimetry. *Br. J. Appl. Phys.* **16**, 1187–1192.
18. Fagerlind, M. G., Nilsson, P., Harlén, M., Karlsson, S., Rice, S. A. & Kjelleberg, S. (2005). Modeling the effect of acylated homoserine lactone antagonists in *Pseudomonas aeruginosa*. *BioSystems*, **80**, 201–213.
19. Zhu, J. & Winans, S. C. (1999). Autoinducer binding by the quorum-sensing regulator TraR increases affinity for target promoters *in vitro* and decreases TraR turnover rates in whole cells. *Proc. Natl Acad. Sci. USA*, **96**, 4832–4837.
20. Zhu, J. & Winans, S. C. (2001). The quorum-sensing transcriptional regulator TraR requires its cognate signaling ligand for protein folding, protease resistance, and dimerization. *Proc. Natl Acad. Sci. USA*, **98**, 1507–1512.
21. Ventre, I., Ledgham, F., Prima, V., Lazdunski, A., Foglino, M. & Sturgis, J. N. (2003). Dimerization of the quorum sensing regulator RhlR: development of a method using EGFP fluorescence anisotropy. *Mol. Microbiol.* **48**, 187–198.
22. Emborg, C., Jepsen, P. K. & Biedermann, K. (1989). Two-level factorial screening of new plasmid/strain combinations for production of recombinant-DNA products. *Biotechnol. Bioeng.* **33**, 1393–1399.
23. Clark, D. J. & Maaløe, O. (1967). DNA Replication and the Division Cycle in *Escherichia coli*. *J. Mol. Biol.* **23**, 99–112.
24. Lagarias, J. C., Reeds, J. A., Wright, M. H. & Wright, P. E. (1998). Convergence properties of the Nelder–Mead simplex method in low dimensions. SIAM J. *Optimization*, **9**, 112–117.

Appendix D

Raman Theory

D.1 Vibrations

A molecule has various electronic states that each contains a large number of vibrational and rotational sub-states [7]. The energy of a molecule is quantified and the molecule can only exist in one of these energy states [7, 2]. The energy difference between the electronic states is larger than between the vibrational states, which again is larger than the energy difference between the rotational states.
When light interacts with a molecule it can be absorbed or scattered. The process of absorption, where an electron is excited from the ground state to a higher state, requires that the energy of the incident photon must correspond to the energy gap between the ground state of a molecule and the excited state. In contrast, scattering can occur whether or not the energy of the incident photon corresponds to the energy gap between two states [2]. As the energy difference between vibrational levels is low, light with low energy is needed to excite a molecule from the ground state to an excited state.
From quantum mechanics it is known that only certain vibrations are allowed. These are known as the normal modes of vibration of the molecule and are determined by the symmetry of the molecule. To work out the possible number of vibrations that occurs it is necessary to consider the degree of freedom of each atom. Each atom has three degrees of freedom and can move independently

along each of the three axes of a Cartesian coordinate system. If a molecule consists of N atoms, there are 3N degrees of motional freedom. Three degrees of freedom describe the translation of the molecule, and another three the rotations. The last 3N-6 degrees describe the vibrational motion, which changes the distances between atoms. Linear molecules have 3N-5 vibrations [4].
Since these bonds are elastic, periodic motions occur and the energy of the vibrational levels can be calculated by using the harmonic approximation. A diatomic molecule is considered as two masses connected by a vibrating spring. When considered this way, Hooke's law gives the relationship between frequency, the mass of the atoms involved in the vibration and the bond strength for a diatomic molecule [2]:

$$\nu = \frac{1}{2pic}\sqrt{\frac{K}{\mu}} \tag{D.1}$$

where c is the velocity of light, K is the force constant of the bond between the two atoms A and B, and μ is the reduced mass of A and B of masses M_A and M_B:

$$\mu = \frac{M_A M_B}{M_A + M_B} \tag{D.2}$$

These equations show that the frequency is higher for lighter atoms, e.g. C-H vibrations will have a higher frequency than C-C vibrations.

The harmonic approximation predicts that the separation between two successive vibrational levels is always the same, i.e. hν, but in reality there is a departure from harmonicity in a real system. The energy, E_ν , of a vibrational level when this anharmonicity is included can be calculated by [7]:

$$E^\nu = hc\omega_\varepsilon(\nu + \frac{1}{2})hc\chi_\varepsilon\omega_\varepsilon(\nu + \frac{1}{2})^2 \tag{D.3}$$

where h is Plancks constant, ν is the vibrational quantum number, ω_ε is the wavenumber corrected for anharmonicity and $\chi_\varepsilon\omega_\varepsilon$ indicates the magnitude of anharmonicity [7]. The wavenumber, ν , is defined as:

$$\hat{\nu} = \frac{1}{\lambda} \tag{D.4}$$

Equation D.3 shows that the energy levels are not equally spaced, but that the separation decreases with higher energies or as increases. As previously mentioned, according to quantum mechanics not all transitions are allowed, thus only a change of one is allowed in the harmonic case, while transitions of more than one is allowed in the anharmonic case [7].

D.2 Raman Scattering

Infrared (IR) and Raman spectra are both vibrational spectroscopy techniques and vibrational transitions are observed in both, but different things are measured. In IR the absorption of infrared light by the sample is measured as a function of frequency. The molecule absorbs the energy $\Delta E = h\nu$ from the light. In IR the intensity I of the light from the IR source is known and a frequency is chosen, so absorption will take place. The majority of the molecules will be in the ground state and will be excited to a higher energy level. The intensity of the IR absorption follows the Beer-Lambart law [7]:

$$I = I_0 e^{\varepsilon cd} \tag{D.5}$$

where I_0 and I are the intensities of the incident and transmitted beams, respectively, ε is the molecular absorption coefficient, and c and d are the concentrations of the sample and the cell length, respectively. The intensity of I will be smaller than I_0 due to absorption. In Raman spectroscopy the sample is irradiated by laser beams and the scattered light is measured in the direction either perpendicular or parallel to the incident beam. Two types of scattered light are identified, the Rayleigh scattering and the Raman scattering. The Raman scattering is 10^3 weaker than the Rayleigh scattering [3].

To explain this effect, it is necessary to consider what happens when light interacts with the molecule. Light is considered as a propagating oscillating dipole that can interact and distort the cloud of electrons around the nuclei and cause the electrons to polarize and go to a higher energy state. This process differs from an absorption process. This interaction, which can be considered as a formation of a complex between the light and the molecule, is often called the virtual state of the molecule. This state is not stabile and the light is released as scattered radiation before the nuclei can respond and reach a new equilibrium geometry to fit the distorted electron arrangement. The shape of the polarized cloud of electrons and the energy of the virtual state depends on the amount of energy that is transferred to the molecule and therefore the frequency of the laser [2].

The majority of the light that is sent through a sample will scatter elastically, i.e. it will not lose or gain any energy and have the same wavelength, ν_0, as the incident photon. This is Rayleigh scattering. A small part of the light is inelastically scattered i.e. it has lost or gained energy. The inelastic scattering is Raman scattering. This occurs when there is a change in the molecules vibration due to the absorption of photons. Raman scattering can happen in two ways called Stokes scattering and anti-Stokes scattering. Stokes scattering occurs when the molecule in a ground state gains energy and ends in an excited vibrational level. The scattered photon will therefore lose energy and have a

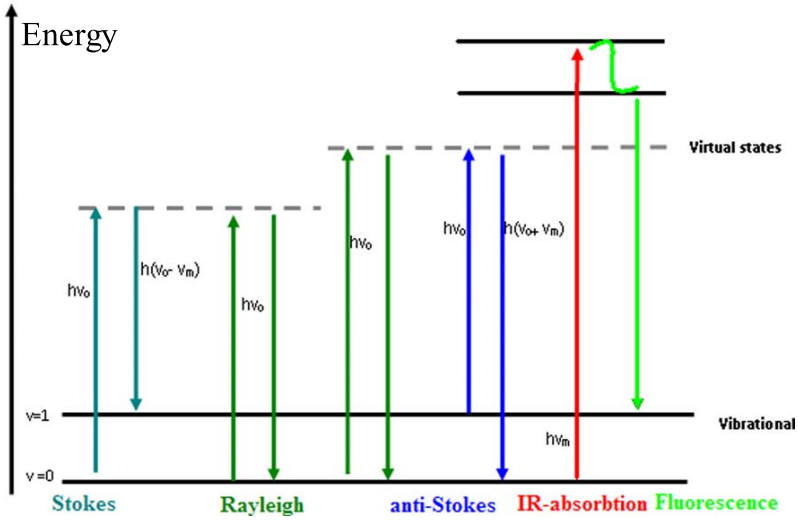

Figure D.1: Energy level diagram showing Stokes scattering, Anti-Stokes scattering, Rayleigh scattering, IR absorption and fluorescence.

frequency $\nu_0 - \nu_m$, where vm is the vibrational frequency of a molecule. On the other hand, anti-Stokes scattering occurs when the molecule starts in a vibrationally excited state and relaxes to the ground state releasing a photon with the frequency v_0+v_m [3]. Figure D.1 illustrates an energy level diagram showing Rayleigh and Raman scattering. In Raman spectroscopy, the vibrational frequency is measured as a shift from the incident beam frequency typically as a wavenumber. The Stokes and anti-Stokes scattering will lie symmetrically around the Rayleigh scattering. The majority of the Raman scattering will be Stokes scattering and the intensity of the Stokes scattering is therefore greater than the anti-Stokes scattering. The reason for this is that most of the molecules will be in the ground vibrational state. The ratio of molecules in the ground state and excited state is given by the Boltzmann equation [2]:

$$\frac{N_n}{N_m} = \frac{g_n}{g_m} e^{\frac{-(E_n - E_m)}{kT}} \tag{D.6}$$

where N_n is the number of molecules in the excited vibrational energy level (n), N_m is the number of molecules in the ground vibrational energy level (m), g is the degeneracy of the levels n and m, $E_n - E_m$ is the difference in energy between the vibrational energy levels, and k is Boltzmann's constant. . The majority of the Raman scattering originates from transitions involving a change of one vibrational quantum number ($\Delta = \pm 1$). However, as previously mentioned, transitions involving $\Delta = \pm 2$ or more can happen, and these bands, called overtones, can be observed in a Raman spectrum [7]. These bands appear due

to the anharmonic nature of the vibration of the molecule.

D.3 Polarizability

As previously mentioned, light can be viewed as a propagating oscillating dipole. When light with the frequency vo interacts with a molecule, the molecule will be in an electric field where the electric field strength E, fluctuates with time [7]:

$$E = E_0 \cos(2\pi\nu_0 t) \tag{D.7}$$

where E_0 is the vibrational amplitude of the electric field and t is the time. When a molecule is placed in an electric field, the electron cloud is distorted, since the positively charged nuclei are attracted toward the negative pole and electrons to the positive pole, thereby inducing an electric dipole moment P [7]. The amount of distortion depends on the ability of the electrons to polarize - the polarizability α [2]. As mentioned earlier, when the molecule absorbs light with the frequency v_0 a short-lived complex is formed and thereafter the light is emitted. This interaction can result in the change of molecular vibration by Stokes or anti-Stokes scattering. The change in vibrations alters the distance between the atoms in the molecule thereby changing the polarizability of the molecule [4]. The dipole moment is dependent on the electric field and is thus a function of E and α [7]:

$$P = \alpha E \tag{D.8}$$

The nuclear displacement, q, for a molecule vibrating with a frequency v_m, is given by [7]:

$$q = q_0 \cos 2\pi\nu_m t \tag{D.9}$$

where q_0 is the vibrational amplitude. If the vibrational amplitude is small, α is a linear function of q [7]:

$$\alpha = \alpha_0 + \left(\frac{d\alpha}{dq}\right)_0 q \tag{D.10}$$

where α_0 is the polarizability at the equilibrium position, and $\left(\frac{d\alpha}{dq}\right)_0$ is the rate of change of α_0 with respect to the change in q, evaluated at the equilibrium position. Combining D.8 through D.10 and using trigonometric conversions ,P

can be written as [7]:

$$\begin{aligned} P &= \alpha E_0 \cos 2\pi\nu_0 t \\ &= \alpha_0 E_0 \cos 2\pi\nu_0 t + \left(\frac{d\alpha}{dq}\right)_0 q E_0 \cos 2\pi\nu_0 t \\ &= \alpha_0 E_0 \cos 2\pi\nu_0 t + \left(\frac{d\alpha}{dq}\right)_0 q_0 E_0 \cos 2\pi\nu_0 t \cos 2\pi\nu_m t \\ &= \alpha_0 E_0 \cos 2\pi\nu_0 t + \frac{1}{2}\left(\frac{d\alpha}{dq}\right)_0 q_0 E_0 \left(\cos 2\pi(\nu_0 + \nu_m)t\right) + \cos 2\pi(\nu_0 - \nu_m)t) \end{aligned} \tag{D.11}$$

Equation D.11 shows how the different terms describe the different scattering processes. The first term represents an oscillating dipole with the frequency v_0, which correspond to Rayleigh scattering. The second term describes scattering of light with the frequency $v_0 - v_m$ which corresponds to Stokes scattering, while the third term corresponds to anti-Stokes scattering with frequency $v_0 + v_m$. Equation D.11 shows that if $\left(\frac{d\alpha}{dq}\right)_0$ is zero, the vibration is not Raman-active and only Rayleigh scattering is observed. The vibration is Raman active if the polarizability is changed during the vibration resulting in the observation of both Stokes and anti-Stokes scattering [7, 3].

In actual molecules, P and E are vectors consisting of three components in the x, y, z directions of a Cartesian coordinate system. Equation D.8 is therefore [7, 2]:

$$\begin{bmatrix} P_x \\ P_y \\ P_z \end{bmatrix} = \begin{bmatrix} a_{xx} & a_{xy} & a_{xz} \\ a_{yx} & a_{yy} & a_{yz} \\ a_{zx} & a_{zy} & a_{zz} \end{bmatrix} \begin{bmatrix} E_x \\ E_y \\ E_z \end{bmatrix} \tag{D.12}$$

The matrix to the right of the equality sign is called the polarizability tensor. This tensor is symmetric in normal Raman scattering, i.e. αxy = αyx, αxz = αzx and αyz = αzy, which means that there are maximum 6 different components in the tensor [3]. The molecule will be Raman active if just one of these components is changed during the vibration. To see whether or not the polarizability of a molecule changes during the vibration $\frac{1}{\sqrt{\alpha_i}}$ (α in the i-direction) is plotted from the centre of gravity in all directions resulting in a polarizability ellipsoid. The vibration is Raman active if the size, shape or orientation changes during the vibration [7]. Consider a molecule as H_2O. Water has three normal vibrations, v_1, v_2 and v_3. Figure D.2, a illustrates the changes in the polarizability ellipsoid during the normal vibrations of H_2O when looking at q = 0 and ± q. The v_1 and v_2 vibrations are Raman active because the size (v_1) and the shape (v_2) of the ellipsoid is different at +q and -q. The v_3 vibration is Raman active because the orientation of the ellipsoid changes during the vibration. In this example

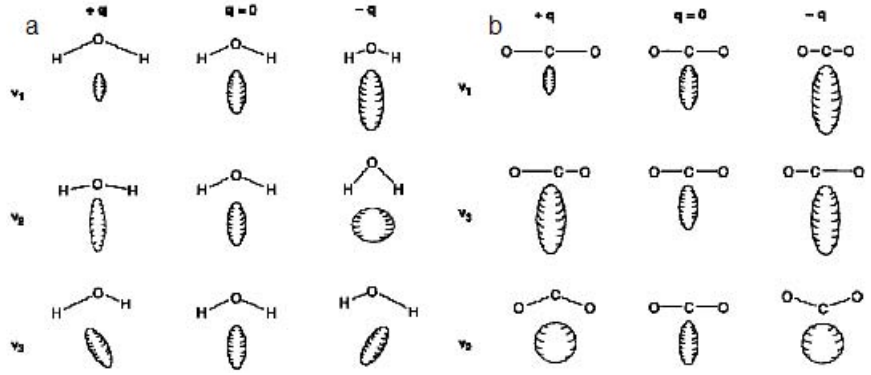

Figure D.2: Changes in polararizability ellipsoid during normal vibrations of a. H_2O, b. CO_2.*Source: [7]*

all of the normal vibrations are Raman active, but even in the case where only one of the normal vibrations is Raman active, the molecule will still be Raman active. Figure D.2, b shows the vibrations in CO_2 where only one vibration (v_1) is Raman active. In contrast to Raman activity, a vibration is IR active if the dipole moment changes during the vibration. Thus all the vibrations in H_2O and v_2 and v_3 vibrations of CO_2 are IR active. At a very simple level, this means that asymmetric rather than symmetric vibrations will give intense IR activity while symmetric vibrations will give intense Raman activity [2]. Some vibrations are weak in IR and strong in Raman spectra. Some of these are the stretching vibrations of C≡C, C=C and S-S. In general, vibrations are strong in Raman if the bond is covalent, and strong in IR if the bond is ionic (e.g. O-H, N-H) [7].

D.4 Depolarization Ratio

The polarization and intensity of the Raman scattered light also contains useful information. When plane polarized light interacts with a sample it will be scattered and some fraction of the scattered light will have been polarized in a direction perpendicular to the incident light. This component is called the perpendicular component. The light where polarization has not been changed is called the parallel component. The ratio between these two components is described by the depolarization ratio ρ, defined as:

$$\rho = \frac{I_\perp}{I_\parallel} \tag{D.13}$$

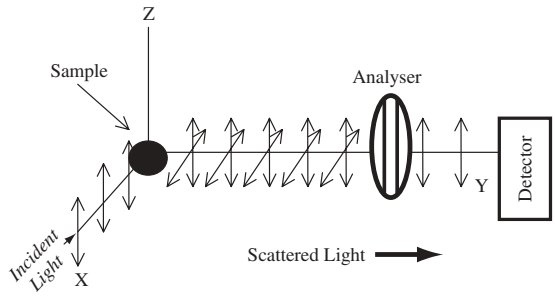

Figure D.3: Measuring the parallel scattered light and perpendicular scattered light. *Source: [2]*

The depolarization ratio can be measured using plane polarized light and a polarization analyzer. The analyzer is set to measure the light that is perpendicular to the incident light and subsequently the parallel scattered light, see Figure D.3. The depolarization ratio depends on the symmetry of the molecule and the vibration. ρ is lowest when the vibrations are symmetric [2], thus for totally symmetric vibrations $0 < \rho > 3/4$, while for non-totally symmetric vibrations ρ is 0.75. If non-plane polarized light is used, $0 < \rho > 6/7$ for totally symmetric vibrations and ρ is 6/7 for non-totally symmetric vibrations [3]. It is therefore possible to obtain information about the symmetry of a molecular vibration by measuring the depolarization ratio. Furthermore, measurements of the depolarization ratio can be used for assignment of molecular vibrations, distinguishing between fundamentals and overtones etc. [33].

D.5 Advantages and Disadvantages of Raman Spectroscopy

IR and Raman spectroscopy are the most important tools for observing vibrational spectra and there are advantages and disadvantages to each technique, some of them are mentioned here. Both techniques are applicable to the solid states, gaseous and solution state of a sample and both spectra can usually be recorded non-destructively. A major advantage of Raman spectroscopy is the minimum of sample handling and preparation that is required. Raman spectra can be taken in situ on samples inside packages and only a small amount of sample is needed. Another advantage of Raman spectroscopy is that it is possible to get Raman spectra of samples in aqueous solutions without major interference from water, since water is a weak Raman scatterer. In contrast, IR

spectroscopy has strong absorption of water. Similarly, it is possible to place a sample in sealed glass tubing and obtain Raman spectra, while this is not possible with IR, since glass tubing absorbs IR radiation [7].

A major disadvantage with Raman spectroscopy is fluorescence. If a powerful beam is used, light can be absorbed into the sample of some compounds (e.g. some colored molecules) and cause fluorescence. The fluorescence signal will mask the Raman spectrum. This is not an issue in IR. It should however be noted that IR and Raman spectroscopy provide complementary images of molecular vibrations, but in many instances, vibrational modes that are not observed by IR absorption can be studied by Raman spectroscopy [4].

D.6 Gaussian

The program Gaussian uses the law of quantum mechanics rather than classical physics in its calculations. Quantum mechanics states that the energy and other properties of a molecule may be obtained by solving the Schrödinger equation:

$$H\Psi = E\Psi \tag{D.14}$$

However, exact solutions to the Schrödinger equation are not computationally convenient for any but the smallest systems. Thus, mathematical approximations to its solution are used. There are three classes: Semi-empirial methods, ab initio methods, and density functional methods (DFT).

Semi-empirial methods use parameters derived from experimental data to simplify the computation, while ab initio methods only use the values of some physical constants (the speed of light, masses/charges, Planck's constant). DFT methods are similar to the ab initio methods in accuracy of result and require about the same amount of computer resources (in contrast, semi-empirical calculations are relatively inexpensive). DFT includes the electron correlation (interactions between electrons) while e.g. Hartree-Fock calculations (ab initio) only consider electron interactions in an average sense (electron density). Thus, Hartree-Fock calculations will in some cases be less accurate than the DFT method. An example of a DFT method is the B3LYP (Becke 3-Parameter density functional theory using the Lee, Yang and Parr correlation functional).

When a method has been chosen, a basis set has to be specified. A basis set is a model of the molecular orbitals within a molecule. The models differ by the amount of space they allow each electron to have. Larger basis sets impose fewer constraints on electrons and approximate the exact molecular orbitals more accurately, but then they require more computational resources.

As a last thing before running the Gaussian program one has to decide whether to use a restricted or an unrestricted option. The restricted option sets the system in closed shell mode, which forces each electron pair into a single spatial orbital. This is default when there is an even number of electrons. Unrestricted, closed shell calculations use separate spatial orbitals for the spin up and spin down electrons and this option is default for the case with molecules with odd numbers of electrons. As job types we have concentrated on the geometry optimization (Opt) and the frequency and thermochemical analysis (Freq) [6].

Appendix E

Colloids

As part of my phD I visited Professor Duncan Graham's research group, The Centre for Molecular Nanometrology at the University of Strathclyde, Glasgow. Here I was taught how to produce silver and gold colloids. In the following I will describe the procedure.

E.1 Ag Nanoparticles (The Citrate Method 1)

Materials:

- Glass flask (round bottom, d=20cm) with 3 straight bottlenecks.
- Thermometer.
- Gasket for thermometer.
- Bunsen burner (must be moved during heating).
- Tripod.
- Stirer (a la drill) "RW16basics KIKA LABORTECHNIK".
- Glass stirrer (with two "chicken little" at the end).
- Silver foil.
- Aqua regia (3HCL:HNO3) - hydrochloric acid 37% and nitric acid 65%.
- Sodium carbonate VWR 27766.292.
- 500 mL destilled water.

- 90 mg silver nitrate (204390-10G) dissolved in 10 mL distilled water.
- 110 mg sodium citrate (4641-500G) dissolved in 10 mL distilled water.

Prepare:
Everything involving Aqua Regia is made in the extraction facility on a metal tray with sodium carbonate at the bottom (neutralizes any spillage)

- Glass flask, tip of the thermometer and the glass stirrer are placed in Agua Regia for 1-2 hours (if fresh solution, 15 min). Remember special acid-gloves.

Procedure:

- Aqua regia is reused (for approx. 1 month in Glasgow until bright orange). Rinse the residue of Aqua Regia out with tap water. First rinse is neutralized with sodium carbonate (just enough so it precipitates a bit), then it can be poured into the sink. Let tap water run down into the glass flask.
- While water flows the silver nitrate and sodium citrate is measured. Both are dissolved in 10 mL of distilled water.
- The flask is rinsed in distilled water.
- The flask is placed on the tripod and the stirrer is placed with the chicken rings nearly reaching the bottom. 500 mL distilled water is poured into the flask and all openings are sealed with aluminum foil. Stir at 3/10 and heated by means of the Bunsen burner at low/medium heat[1].
- Heated up to 45∘C (2 min), silver nitrate is added. The color is transparent (otherwise start again).
- Heated to 98∘C, add sodium citrate. The color is transparent. Keep the temperature as constant as possible at 98∘C for 75 min. Do not boil!
- Stir until it cools down (finished when it can be touched).
- The color will change to yellow (the longer it takes to change color to yellow the better) -¿ rust red / green -¿ darker. The more milk white the worse.

E.2 Ag Nanoparticles (The Citrate Method 2)

Materials:

- 3L round glass bulb with a flat bottom.

[1]Not too high and not too low. The flame (Bunsen burner) must get oxygen from the bottom (not fully open). Visually there should not be any or very little orange color in the flame. Furthermore, it should not be turned up so high that there is a blue peak inside the flame. The strength must be screwed up by sound - a gentle brrr. Move the Bunsen. Focal point of the flame must be inside the liquid.

- Two Thermometers (also for the oil).
- Gasket for thermometer.
- Magnetic stirrer + electric heat in one.
- Magnetic ball for the stirring.
- Round bowl with flat bottom for the paraffin oil.
- Condensation equipment with 2 hoses (for cooling).
- Glass stopper for neck.
- Paraffin oil.
- Aqua regia (3HCL:HNO3) - hydrochloric acid 37% and nitric acid 65%.
- Sodium carbonate VWR 27766.292.
- 500 mL destilled water.
- 90 mg silver nitrate (204390-10G) dissolved in 10 mL distilled water.
- 110 mg sodium citrate (4641-500G) dissolved in 10 mL distilled water.

Prepare:
Everything involving Aqua Regia is made in the extraction facility on a metal tray with sodium carbonate at the bottom (neutralizes any spillage).

- Glass flask, tip of the thermometer and the magnetic ball are placed in Agua Regia for 1-2 hours (if fresh solution, 15 min). Remember special acid-gloves.

Procedure:

- Aqua regia is reused (for approx. 1 month in Glasgow until bright orange). Rinse the residue of Aqua Regia out with tap water. First rinse is neutralized with sodium carbonate (just enough so it precipitates a bit), then it can be poured into the sink. Let tap water run down into the glass flask.
- While water flows the silver nitrate and sodium citrate is measured. Both are dissolved in 10 mL of distilled water.
- The flask is rinsed in distilled water.
- The flask is placed in the oil-bath (the bulb should not touch the bottom). The condensation equipment is connected - everything has to be closed tight. The bottom tube is connected to the water tap and the water is turned on. The thermometer is placed in the oil. 500 mL distilled water + the silver nitrate is poured in the bulb and the glass stopper is put in the bottle neck. Stirring at upper-medium and heated at max.
- At reflux (condensation in the bottle neck, (droplets are formed at app. 100∘C) sodium citrate is poured gently in (little at a time).
- Keep it at reflux (temp app. constant). Keep the oil under 120∘C. Watch out not to get water in the oil. Is kept here for 1 hour.
- Stirred while it is cooling down (finished when it can be touched).

E.3 Ag Nanoparticles (The EDTA Method)

Materials:

- 3L round glass bulb with a flat bottom.
- Electric heat.
- Glass stirrer with some sort of a glass "bow/loop".
- Silver foil.
- Aqua regia (3HCL:HNO3) - hydrochloric acid 37% and nitric acid 65%.
- Sodium carbonate VWR 27766.292.
- 2L distilled water.
- 94.7 mg EDTA (431788-25mg) dissolved in 10 mL distilled water.
- 0.32 g NaOH (VWR 28245.265) in 10mL distilled water.
- 0.088 g silver nitrate in 20 mL distilled water.

Prepare:
Everything involving Aqua Regia is made in the extraction facility on a metal tray with sodium carbonate at the bottom (neutralizes any spillage)

- Glass flask and the glass stirrer are placed in Agua Regia for 1-2 hours (if fresh solution, 15 min). Remember special acid-gloves.

Procedure:

- Aqua regia is reused (for approx. 1 month in Glasgow until bright orange). Rinse the residue of Aqua Regia out with tap water. First rinse is neutralized with sodium carbonate (just enough so it precipitates a bit), then it can be poured into the sink. Let tap water run down into the glass flask.
- The flask is rinsed in distilled water.
- Add 2L distilled water.
- Turn on the heat (max). Measure EDTA, NaOH and silver nitrate and dissolve in 10, 10 and 20mL distilled water respectively.
- Add NaOH and EDTA to the bulb. Can be added together or one at a time as long as they are added a long time before the boiling point.
- At the boiling point (app. 65 min after start): add the silver nitrate 5mL at a time. The effect looks like a brown cloud - wait until the cloud is fully distributed before more is added.
- Boil for 15min.
- Stir, while it cools down (finished when it can be touched).

E.4 Au Nanoparticles (The Citrate Method) dia=16nm, λ=600-700nm

Materials:

- Glass flask (round bottom, d=20cm) with 3 straight bottlenecks.
- Thermometer.
- Gasket for thermometer.
- Bunsen burner (must be moved during heating).
- Tripod.
- Stirer (a la drill) "RW16basics KIKA LABORTECHNIK".
- Glass stirrer (with two "chicken little" at the end).
- Silver foil.
- Aqua regia (3HCL:HNO3) - hydrochloric acid 37% and nitric acid 65%.
- Sodium carbonate VWR 27766.292.
- 500 mL destilled water.
- 50mg sodium tetrachloroaurate (aldrich 298174-1g) dissolved in 10 mL distilled water.
- 0.075g sodium citrate (S4641-500G) dissolved in 10mL distilled water.

Prepare:
Everything involving Aqua Regia is made in the extraction facility on a metal tray with sodium carbonate at the bottom (neutralizes any spillage).

- Glass flask, tip of the thermometer and the glass stirrer are placed in Agua Regia for 1-2 hours (if fresh solution, 15 min). Remember special acid-gloves.

Procedure:

- Aqua regia is reused (for approx. 1 month in Glasgow until bright orange). Rinse the residue of Aqua Regia out with tap water. First rinse is neutralized with sodium carbonate (just enough so it precipitates a bit), then it can be poured into the sink. Let tap water run down into the glass flask.
- While water flows the sodium tetrachloroaurate and sodium citrate is measured. Both are dissolved in 10 mL of distilled water.
- The flask is rinsed in distilled water.
- The flask is placed on the tripod and the stirrer is placed with the chicken rings nearly reaching the bottom. 500 mL distilled water and sodium tetrachloroaurate is poured into the flask and all openings are sealed with aluminum foil. Stir at 3/10 and heated by means of the Bunsen burner at low/medium heat[1]
- When it starts to boil (after app. 15min) sodium citrate is added.
- Boiled for app. 15min - stirred while cooling down (finished when it can

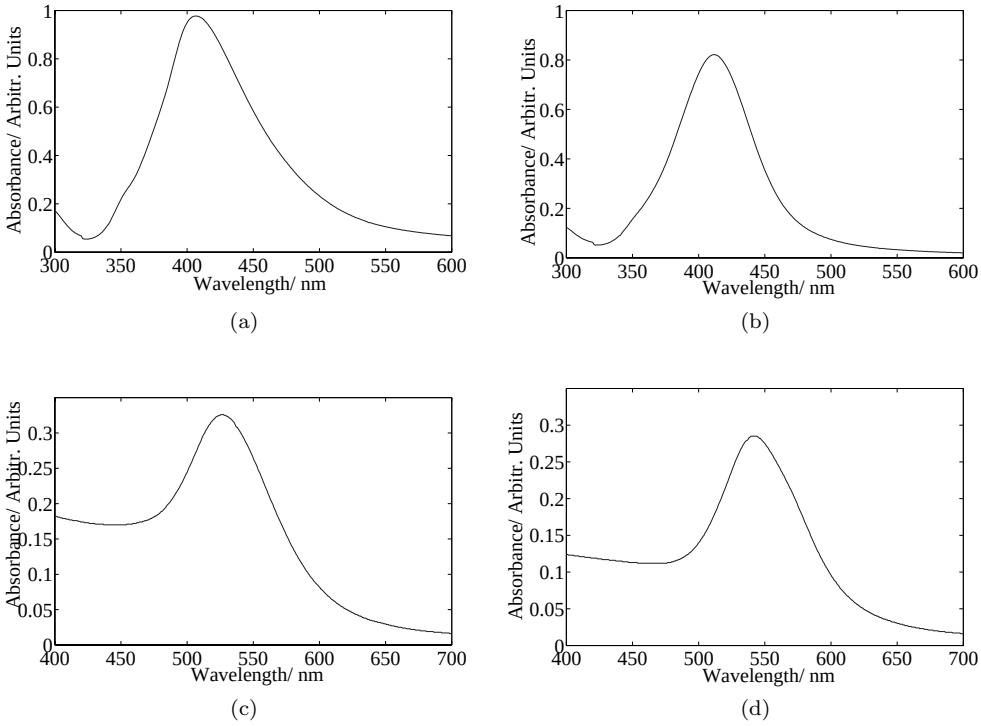

Figure E.1: UV-VIS, absorbance as a function of wavelength. (a) Ag colloids produced by the citrate method 1, diluted 11 times, (b) Ag colloids produced by the EDTA method, diluted 5 times, (c) Au colloids produced by the citrate method, diluted 4 times and (d) colloids bought at Strem Chemicals Inc. diluted 4 times.

be touched).

- The color should be cranberry-juice colored. Not dark red wine.

Appendix F

MH155 Protocols

F.1 MH155 Microtiter Protocol

Chemicals: LB medium, ABTGcasa minimal medium (225 mL BT, 25 mL A-10, 6,25 mL 20 %casa aminosyre, 12,5mL glucose and 625 μL thiamine)[19], ethanol 96%, OdDHL (Sigma Aldrich).
Equipment: wallac 1420 VICTOR2(Perkin Elmer), 96 welled microtiter plate (Nunc, black PolyBase, USA), incubator, and spectrophotometer (Genesys 10 uv, USA).

Exponential inoculum
Freeze stock was grown overnight in LB medium with $\approx$ 180 rpm at 37°C.
The day after grown to OD_{450nm} = 0.35 in ABTGcasa minimal medium at 37°C ($\approx$ 180 rpm) and then diluted in fresh, heated ABTGcasa minimal media to OD_{450nm} = 0.1 measured by the spectrophotometer.

Quasistationary inoculum
Freeze stock was grown overnight in LB medium with $\approx$ 180 rpm at 37°C.
The day after diluted in fresh, heated ABTGcasa minimal media to $OD_{450nm}450$ = 0.1 measured by the spectrophotometer.

Preparation of the microtiter plate, Tables F.1, F.2 and F.3 (for C_0 = 500nM):

1. The OdDHL was diluted in ethanol 96% to a concentration of 10 mM then in milliQ water to 5 μM.
2. An ethanol/water solution was made with the exact concentration of ethanol as the OdDHL 5 μM concentration.
3. 30 μL of 5 μM OdDHL was added to each of the wells C_0.
4. 30 μL of ethanol/water solution was added to each of the wells C_0, GFP_{ref} and OD_{ref}.
5. Two-fold dilutions were made from C_0, $2^{-1}C_0$,...$2^{-n}C_0$. Pipette tips were changed after each dilution in order to avoid contamination.
6. 300 μL of ABTGcasa minimal medium was added to each of the wells OD_ref.
7. The microtiter plate and the petri dishes were placed in an incubator at 37∘C. Additionally, a lid was put on the microtiter plate to minimize evaporation.
8. The bacteria diluted to $OD_{450nm} = 0.1$, a portion of it was poured into a heated petri dishes.
9. From the petri dish 270 μL of batch culture was added to GFP_{ref} and to the dilution rows, starting from low concentration $2^{-n}C_0$ to high C_0
10. The microtiter plate was placed in wallac 1420 VICTOR2 set to perform OD_{450nm} and fluorescence excitation: 485 nm, emission: 535nm measurements every fifth minutes at 37°C, 99 times in total and with shake.

GFP_{ref} (GFP reference): 270 μL *E. coli* bacteria in ABTGcasa media, added 30 μL ethanol/water.
OD_{ref} (OD reference): 270 μL ABTGcasa media and added 30 μL ethanol/water.
C_0: Max concentration of OdDHL.

F.2 Protocol for the Growth Experiments

Chemicals: ABTGcasa minimal medium (225 mL BT, 25 mL A-10, 6,25 mL 20 %casa aminosyre, 12,5mL glucose and 625 μL thiamine)[19] and for low growth casa amino acid was replaced with L-leucine (Sigma Aldrich) (also 0.5% L-leucine), henceforth called ABTGleu. OdDHL (Sigma Aldrich, Biochemika Fluka).
Equipment: Spectrophotometer (Shimadzu RF-5301PC), quantitative raw data

	1	2 6	7	8 12
A	C_0	$2^{-1}C_0$ .... $2^{-5}C_0$	$2^{-6}C_0$	$2^{-7}C_0$ .... $2^{-11}C_0$
B	C_0	$2^{-1}C_0$ .... $2^{-5}C_0$	$2^{-6}C_0$	$2^{-7}C_0$ .... $2^{-11}C_0$
C	C_0	$2^{-1}C_0$ .... $2^{-5}C_0$	$2^{-6}C_0$	$2^{-7}C_0$ .... $2^{-11}C_0$
D	C_0	$2^{-1}C_0$ .... $2^{-5}C_0$	$2^{-6}C_0$	$2^{-7}C_0$ .... $2^{-11}C_0$
E	C_0	$2^{-1}C_0$ .... $2^{-5}C_0$	$2^{-6}C_0$	$2^{-7}C_0$ .... $2^{-11}C_0$
F	C_0	$2^{-1}C_0$ .... $2^{-5}C_0$	$2^{-6}C_0$	$2^{-7}C_0$ .... $2^{-11}C_0$
G	C_0	$2^{-1}C_0$ .... $2^{-5}C_0$	$2^{-6}C_0$	$2^{-7}C_0$ .... $2^{-11}C_0$
H	OD_{ref}	OD_{ref} .... OD_{ref}	GFP_{ref}	GFP_{ref} .... GFP_{ref}

Table F.1: This microtiter design was used for the experiments in Figure 3.4.

	1 5	6 10	11	12
A	C_0 .... C_0	C_0 .... C_0	GFP_{ref}	OD_{ref}
B	C_0 .... C_0	C_0 .... C_0	GFP_{ref}	OD_{ref}
C	$2^{-1}C_0$ .... $2^{-1}C_0$	$2^{-1}C_0$ .... $2^{-1}C_0$	GFP_{ref}	OD_{ref}
D	$2^{-2}C_0$ .... $2^{-2}C_0$	$2^{-2}C_0$ .... $2^{-2}C_0$	GFP_{ref}	OD_{ref}
E	$2^{-3}C_0$ .... $2^{-3}C_0$	$2^{-3}C_0$ .... $2^{-3}C_0$	GFP_{ref}	OD_{ref}
F	$2^{-4}C_0$ .... $2^{-4}C_0$	$2^{-4}C_0$ .... $2^{-4}C_0$	GFP_{ref}	OD_{ref}
G	$2^{-5}C_0$ .... $2^{-5}C_0$	$2^{-5}C_0$ .... $2^{-5}C_0$	GFP_{ref}	OD_{ref}
H	$2^{-6}C_0$ .... $2^{-6}C_0$	$2^{-6}C_0$ .... $2^{-6}C_0$	GFP_{ref}	OD_{ref}

Table F.2: This microtiter design was used for the experiments in Figure 3.5.

	1	2 ... 10	11	12
A	C_0	$2^{-1}C_0$ .... $2^{-9}C_0$	GFP_{ref}	OD_{ref}
B	C_0	$2^{-1}C_0$ .... $2^{-9}C_0$	GFP_{ref}	OD_{ref}
C	C_0	$2^{-1}C_0$ .... $2^{-9}C_0$	GFP_{ref}	OD_{ref}
D	C_0	$2^{-1}C_0$ .... $2^{-9}C_0$	GFP_{ref}	OD_{ref}
E	C_0	$2^{-1}C_0$ .... $2^{-9}C_0$	GFP_{ref}	OD_{ref}
F	C_0	$2^{-1}C_0$ .... $2^{-9}C_0$	GFP_{ref}	OD_{ref}
G	C_0	$2^{-1}C_0$ .... $2^{-9}C_0$	GFP_{ref}	OD_{ref}
H	C_0	$2^{-1}C_0$ .... $2^{-9}C_0$	GFP_{ref}	OD_{ref}

Table F.3: This microtiter design was used for the experiments in Figure 3.6.

mode at λ_{ex}=475nm±5nm, λ_{em}=515nm±5nm, 4s integration time, and amplification set to high. Shimadzu UV-1800 for preliminary measurements.

Exponential inoculum
While growing exponentially at 37°C and 200rpm the MH155 culture was diluted in fresh medium to OD_{450nm} = 0.01 on the Shimadzu UV-1800 and distributed to preheated (37°C) 100ml flasks containing 50ml two-fold dilution rows of OdDHL starting at 100 nM and leaving one flask without signal molecules for baseline detection.

Quasistationary inoculum
The culture was left to grow until an almost complete stop, i.e. OD_{450nm} =3.4 and 2.9 for the casa amino growth and the L-leucine growth, respectively. At this stage the culture was rapidly diluted to OD_{450nm} = 0.01 and distributed to the two-fold dilution row flasks of OdDHL. Note that, if the culture is brought to complete static state it looses the ability to express GFP(ASV). It is thus critical to the usefulness of the GFP(ASV) reporter fusion that the culture be brought only to a quasistationary state ($\approx 0.9 OD_{max}$).

Fluorescence from GFP(ASV) was measured using the Shimadzu RF-5301PC flurimeter. The induced response is the measured OD-weighted background subtracted response, $(G\text{-}G_0)/OD = GFP/OD - GFP_0/OD_0$ where GFP and GFP_0 are raw GFP counts with and without signal molecules, respectively.

Appendix G

Experimental Determination of the Decay of C4-HSL

Day 1

- ABT minimal media (ABT) is made (kept at 5°C):
  - 225mL BT media
  - 25 mL A-10 buffer
  - 6,25 mL 20% Casa amino acid
  - 625 μL Thiamine (1mg/mL)
  - 12,5 mL glucose (10%), sterile
- The ABT (ABT-0.8%) is mixed with 2.16 mL ethanol (96 %)- gives a 0.8 vol% ethanol content (5∘C).
- Signal molecule solution: 5μL C4-HSL (100 mM) for 995 μL ethanol (96 %), which is equivalent to a signal molecule solution of 0.5 mM. Frozen until needed.
- Signal molecule solution: 60 μL C4-HSL (100 mM) for 940 μL ethanol (96%), which corresponds to a signal molecule concentration of 6 mM. Frozen until needed.
- Overnight culture is made by adding 5 mL LB medie to a tube and adding a small amount of bacteria from the frozen stock MH205. Afterwards incubation at 37∘C at constant shakings (180 rpm overnight).
- **6:03** (32h) - 1488 μL ABT-0.8% is mixed with 12 μL C4-HSL (0.5 mM) and incubated at 37∘C under constant shakings (180 rpm).
- **22:06** (16h) - 1488 μL ABT-0.8% is mixed with 12 μL C4-HSL(0.5 mM) and incubated at 37∘C under constant shakings (180 rpm).

Figure G.1: A sketch of the micro titer plate. Blue is the GFP reference, red is the OD reference. Max concentrationis C. Right side is dilution rows for 0 delay time and left side is max concentration, C added 0, 1, 2, ...32 hours ago.

Day 2

- BakABT: The overnight culture is diluted (with tempered ABT) to an OD at 0.1, determined by:
  $x = T_{ML} \frac{0.1}{OD_{measured}}$,
  where x is mL overnight culture and (T_{ML}-x) is mL ABT. The culture is incubated at 37∘C and is shaken at 180 rpm. In order to be able to follow the growth of the bacteria the OD is measured every half hour. At an OD of 0.5 the culture is again diluted to an OD of 0.05. The OD is allowed to grow to 0.1 (the final OD in the finished micro titter essay will be 0.05 because of the dilution in the procedure).

- **6:06** (8h) - 1488 μL ABT-0.8% is mixed with 12 μL C4-HSL (0.5 mM) and incubated at 37∘C under constant shakings (180rpm).
- **10:05** (4h) - 1488 μL ABT-0.8% is mixed with 12 μL C4-HSL (0.5 mM) and incubated at 37∘C under constant shakings (180 rpm).
- **12:00** (2h) - 1488 μL ABT-0.8% is mixed with 12 μL C4-HSL (0.5 mM) and incubated at 37∘C under constant shakings (180 rpm).
- **13:00** (1h) - 1488 μL ABT-0.8% is mixed with 12 μL C4-HSL (0.5 mM) and incubated at 37∘C under constant shakings (180 rpm).
- **14:00** - The micro titter tray is made as shown in Figure G.1. The micro titter tray is divided in a left and right side. For both left and right sides every row has 6 repititions.
  - **Left**: The first 7 (A-G) rows contain C4-HSL in ABT added BakABt, with different delay (time since C4-HSL was added, 0-32 hours). The last row, H contains ABT and BakABT, and is the reference for GFP.
  - **Right**: The first 7 (A-G) rows contain dilution-rows of C4-HSL in ABT (no delay time) with added BakABT. The last row, H only contains ABT and is the reference for OD.

Bibliography

[1] *Gaussian 09 Revision A.1.* Gaussian Inc. Wallingford CT 2009.

[2] *Modern Raman Spectroscopy - A Practical Approach.* Wiley.

[3] *Noter: Spektroskopi og Struktur.*

[4] *Infrared and Raman Spectroscopy - Methods and Applications.* Wiley VCH, 1995.

[5] *Escherichia coli and Salmonella: Cellular and Molecular Biology*, chapter 97: Modulation of chemical composition and other parameters of the cell by growth rate. ASM Press, Washington DC, 1996.

[6] *Exploring Chemistry With Electronic Structure Methods: A Guide to Using Gaussian.* Gaussian, 1996.

[7] *Introductory Raman Spectroscopy.* Academic Press Limeted, 2003.

[8] *Surface-Enhanced Raman Scattering.* Springer, 2006.

[9] *Handbook of Surface Plasmon Resonance.* RSC Publishing, 2008.

[10] S. Abdali, B. De Laere, M. Poulsen, M. Grigorian, E. Lukanidin, and J. Klingelh"ofer. Toward methodology for detection of cancer-promoting s100a4 protein conformations in subnanomolar concentrations using raman and sers. *J. Phys. Chem. C*, 114:7274–7279, 2010.

[11] M.G. Albrecht and J.A. Creighton. Anomalously intense raman spectra of pyridine at a silver electrode. *Journal of the American Chemical Society*, 1977.

[12] C. El Amri, M. Baron, and M. Maurel. Adenine and rna in mineral samples. surface-enhanced raman spectroscopy (sers) for picomole detections. *Spectrochimica Acta Part A*, 59:2645–2654, 2003.

[13] J.B. Andersen, C. Sternberg, L.K. Poulsen, S. Petersen Bjørn, M. Givskov, and S. Molin. New unstable variants of green fluorescent protein for studies of transient gene expression in bacteria. *Appl. Environ. Microbiol.*, 64:2240–2246, 1998.

[14] T. Atlung, B.B. Christensen, and F.G. Hansen. Role of the rom protein in copy number control of plasmid pbr322 at different growth rates in *Escherichia coli* k-12. *Plasmid*, 41:110–119, 1999.

[15] L. Baia and S. Simon. Uv-vis and tem assesment of morphological features of silver nanoparticles from phosphate glass matrices. *Modern Research and Educational Topics in Microscopy*, 2007.

[16] A.D. Becke. Density-functional thermochemistry. iii. the role of exact exchange. *Journal of Chemical Physics*, 98:5648–5652, 1993.

[17] S.E.J. Bell and N.M.S. Sirimuthu. Quantitative surface-enhanced raman spectroscopy. *Chem. Soc. Rev.*, 2008.

[18] M.J. Bottomley, E. Muraglia, R. Bazzo, and A. Carfi. Molecular insights into quorum sensing in the human pathogen pseudomonas aeruginosa from the structure of the virulence regulator lasr bound to its autoinducer. *The Journal of Biological Chemistry*, 2007.

[19] D.J. Clark and O. Malløe. Dna replication and the devision cycle in escherichia coli. *J. Mol. Biol.*, 23:99–112, 1967.

[20] A.W. Decho, R.L. Frey, and J.L. Ferry. Chemical challenges to bacterial ahl signalling in the environment. *Chem. Rev.*, 111:86–99, 2011.

[21] A.W. Decho, R.S. Norman, and P.T. Visscher. Quorum sensing in natural environments: emerging views from microbial mats. *Trends in Microbiology*, 19:73–80, 2010.

[22] S. Efrima and L. Zeiri. Understanding sers of bacteria. *Raman Spectrosc.*, 2008.

[23] C. Gera and S. Srivastava. Quorum-sensing: The phenomenon of microbial communication. *Current Science*, 2006.

[24] L. Guerrini and D. Graham. Molecularly-mediated assemblies of plasmonic nanoparticles for surface-enhanced raman spectroscopy applications. *Chem. Soc. Rev.*, 2012.

[25] J. Guicheteau, S. Christesen, and D. Emge A. Tripathi. Bacterial mixture identification using raman and surface-enhanced raman chemical imaging. *J. Raman Spectrosc.*, 2010.

[26] M. Hentzer, K. Riedel, T. B. Rasmussen, A Heydorn, J. B. Andersen, M. R. Parsek, S. A. Rice, L. Eberl, S. Molin, N. Høiby, S. Kjelleberg, and M. Givskov. Inhibition of quorum sensing in pseudomonas aeruginosa biofilm bacteria by a halogenated furanone compound. *Microbiology*, 148:87–102, 2002.

[27] M. Hentzer, H. Wu, J.B. Andersen, K. Riedel, T.B. Rasmussen, N. Bagge, N. Kumar, M.A. Schembri, Z. Song, P. Kristoffersen, M. Manefield, J.W. Costerton, S. Molin, L. Eberl, P. Steinberg, S. Kjelleberg, N. Høiby, and M. Givskov. Attenuation of pseudomonas aeruginosa virulence by quorum sensing inhibitors. *The EMBO Journal*, 2003.

[28] K. Hering, D. Cialla, K. Ackermann, T. Dörfer, R. Möller, H. Schneidewind, R. Mattheis, W. Fritzsche, P. Rösch, and J. Popp. Sers: a versatile tool in chemical and biochemical diagnostics. *Anal. Bioanal. Chem.*, 2008.

[29] D. Jakubczyk, C. Barth, A. Kubas, F. Anastassacos, P. Koelsch, K. Fink, U. Schepers, G. Brenner-Weiss, and S. Br"ase. Deuterium-labelled *N*-acyl-l-homoserine lactones (ahls)-inter-kingdom signalling molecules-synthesis,structural studies, and interactions with model lipid membranes. *Anal Bioanal Chem*, 403:473–482, 2012.

[30] R.M. Jarvis, A. Brooker, and R. Goodacre. Surface-enhanced raman scattering for the rapid discrimination of bacteria. *Faraday Discuss.*, 2006.

[31] D.L. Jeanmaire and R.P. van Duyne. Surface raman spectroelectrochemistry: Part i. heterocyclic, aromatic, and aliphatic amines adsorbed on the anodized silver electrode. *J. Electroanal. Chem.*, 1977.

[32] S. Kapoor. Preparation, characterization, and surface modification of silver particles. *Langmuir*, 1998.

[33] S.A. Kirillov, A. Morresi, and M. Paolantoni. Recovery of the depolarization ratio of single lines from overlapping isotropic and anisotropic raman profiles and assignment of molecular vibrations, with special reference to toluene and toluene-d8. *Journal of Raman Spectroscopy*, 2007.

[34] S. Klumpp. Growth rate-dependence reveals design principles of plasmid copy control. *PLos ONE*, 6:e20403, 2011.

[35] S. Klumpp, Z. Zhang, and T. Hwa. Growth rate-dependent global effects on gene expression in bacteria. *Cell*, 139:1366–1375, 2009.

[36] K. Kneipp. Surface-enhanced raman scattering. *Physics Today*, 2007.

[37] J. Lee, Y. Lequette, and E.P. Greenberg. Activity of purified qscr, a pseudomonas aeruginosa orphan quorum-sensing transcription factor. *Molecular Microbiology*, 2006.

[38] J.H.J. Leveau and S.E. Lindow. Predictive and interpretive simulation of green fluorescent protein expression in reporter bacteria. *Journal of Bacteriology*, 183:6752–6762, 2001.

[39] S. Lin-Chao, W. Chen, and T. Wong. High copy number of the puc plasmid results from a rom/rop-suppressible point mutation in rna ii. *Molecular Microbiology*, 6:3385–3393, 1992.

[40] S. Link and M.A. El-Sayad. Spectral properties and relaxation dynamics of surface plasmon electronic oscillations in gold and silver nanodots and nanorods. *J. Phys. Chem.*, 1999.

[41] P.J. Hendra M. Fleischmann and A.J. McQuillan. Raman spectra of pyridine adsorbed at a silver electrode. *Chemical Physics Letters*, 1974.

[42] A. Macaskill, A.A. Chernonosov, V.V. Koval, E.A. Lukyanets, O.S. Fedorova, W.E. Smith, K. Faulds, and D. Graham. Quantitative surface-enhanced resonance raman scattering of phthalocyanine-labelled oligonucleotides. *Nucleic Acids Research*, 2007.

[43] F. McKenzie, V. Steven, A. Ingram, and D. Graham. Quantitation of biomolecules conjugated to nanoparticles by enzyme hydrolysis. *Chem. Commun.*, 2009.

[44] E.A. Meighen. Genetics of bacterial bioluminescence. *Annu. Rev Genet.*, 1994.

[45] J.P. Merrick, D. Moran, and L. Radom. An evaluation of harmonic vibrational frequency scale factors. *J. Phys. Chem. A*, 111:11683–11700, 2007.

[46] G. Mie. Beiträge zur optik trüber medien, speziell kolloidaler metallösungen. *Annalen der Physik*, 1908.

[47] L. Passador, K.D. Tucker, K.R. Guertin, M.P. Journet, A.S. Kende, and B.H. Iglewski. Functional analysis of the pseudomonas aeruginosa autoinducer pai. *Jounal of Bacteriology*, 178:5995–6000, 1996.

[48] W.F. Pearman, M. Lawrence-Snyder, S.M. Angel, and A.W. Decho. Surface-enhanced raman spectroscopy for in situ measurements of signaling molecules (autoinducers) relevant to bacteria quorum sensing. *Appl. Spectrosc.*, 61:1295–1300, 2007.

[49] J.P Pearson, C. Van Delden, and B.H. Iglewski. Active efflux and diffusion are involved in transport of pseudomonas aeruginosa cell-to-cell signals. *Journal of Bacteriology*, 1999.

[50] J.P Pearson, L. Passador, B.H. Iglewski, and E.P. Greenberg. A second *N*-acylhomoserine lactone signal produced by pseudomonas aeruginosa. *Proc. Natl. Acad. Sci. USA*, 1995.

[51] G. A. Petersson and M. A. AI-Laham. A complete basis set model chemistry. ii. *Journal of Chemical Physics*, 94:6061–6090, 1991.

[52] G. A. Petersson, A. Bennett, T. G Tensfeldt, M. A. AI-Laham, and W. A Shirley. A complete basis set model chemistry. i. the total energies of closed-shell atoms and hydrides of the first-row elements. *Journal of Chemical Physics*, 89:2193–2218, 1988.

[53] M Sackmann and A. Materny. Surface enhanced raman scattering (sers) - a quantitative analytical tool? *J. Raman Spectrosc.*, 2006.

[54] K.J. Sappington, A.A. Dandekar, K. Oinuma, and E.P. Greenberg. Reversible signal binding by the pseudomonas aeruginosa quorum-sensing signal receptor lasr. *mBio*, 2:e00011–11, 2011.

[55] H.P. Schweizer. Escherichia-pseudomonas shuttle vectors derived from puc18/19. *Gene*, 97:109–112, 1991.

[56] A. Sengupta, M. Mujacic, and E.J. Davis. Detection of bacteria by surface-enhanced raman spectroscopy. *Anal Bioanal Chem.*, 2006.

[57] I.T. Shadi, B.Z. Chowdhry, M.J. Snowden, and R. Withnall. Semi-quantitative trace analysis of nuclear fast red by surface enhanced resonance raman scattering. *Analytica Chimica Acta*, 2001.

[58] V. Sharma, K. Park, and M. Srinivasarao. Colloidal dispersion of gold nanorods: Historical background, optical properties, seed-mediated synthesis, shape and self-assembly. *Materials Science and Engineering R*, 2009.

[59] M. Shuster, C.P. Lostroh, T. Ogi, and E.P. Greenberg. Identification. timing, and signal specificity of pseudomonas aeruginosa quorum-controlled genes: a transcriptome analysis. *Journal of Bacteriology*, 2003.

[60] M. Shuster, M.L. Urbanowski, and E.P. Greenberg. Promoter specificity in pseudomonas aeruginosa quorum sensing reveales by dna binding of purified lasr. *PNAS*, 2004.

[61] Y. Tawada, T. Tsuneda, and S. Yanagisawa. A long-range-corrected time-dependent density functional theory. *Journal of Chemical Physics*, 120:8425–8433, 2004.

[62] R.A. Tripp, R.A. Dluhy, and Y. Zhao. Novel nanostructures for sers biosensing. *nanotoday*, 3:31–37, 2008.

[63] M. L. Urbanowski, C. P. Lostroh, and E. P. Greenberg. Reversible acyl-homoserine lactone binding to purified vibrio fischeri luxr protein. *Journal of Bacteriology*, 2004.

[64] P. Walstra. Discussion of errors in turbidimetry. *Brit. J. Appl. Phys.*, 16:1187–1192, 1965.

[65] C.M. Waters and B.L. Bassler. Quorum sensing: Cell-to-cell communication in bacteria. *Annu. Rev. Cell Dev. Biol.*, 2005.

[66] N.S. Wigginton, A. De Titta, F. Piccapietra, J. Dobias, V.J. Nesatyv, M.J.F. Suter, and R. Bernier-Latmani. Binding of silver nanoparticles to bacterial proteins depends on surface modifications and inhibits enzymatic activity. *Environ. Sci. Technol.*, 44:2163–2168, 2010.

[67] J. Zhu and S.C. Winans. Autoinducer binding by the quorum-sensing regulator trar increases affinity for target promoters in vitro and decreases trar turnover rates in whole cells. *PNAS*, 1999.

[68] J. Zhu and S.C. Winans. The quorum-sensing transcriptional regulator trar requires its cognate signaling ligand for protein folding, protease resistance, and dimerization. *PNAS*, 2001.